

Validation report of Level(s)
0, 1, 2, 3, 4, 5, A, W, O

I²PC Validation server

February 25, 2022
4:07pm

Abstract

The map seems to be well centered. There is no problem with the suggested threshold. There seems to be a problem with the map's background (see Sec. 2.3). The resolution does not seem to be uniform in all directions (see Sec. 4.6). The 2D classes provided by the user do not seem to correlate well with the reprojections of the map (see Sec. 6.1). It seems that the input particles cannot be easily aligned (see Sec. 9.2). It seems that the angular assignment given by the user does not match with the one produced by CryoSparc (see Sec. 9.5). It seems that the angular assignment produced by Relion does not match with the one produced by Cryosparc (see Sec. 9.6). This is probably a sign of the difficulty to align these particles. It seems that there is some problem with the CTF (see Sec. 9.11). According to phenix, it seems that there might be some mismatch between the map and its model (see Sec. 13.5). The EMRinger score is negative, it seems that the model side chains do not match the map (see Sec. 13.6). DAQ detects some mismatch between the map and its model (see Sec. 13.7).

The average resolution of the map estimated by various methods goes from 2.0Å to 4.6Å with an average of 3.3Å. The resolution provided by the user was 2.6Å. The resolution reported by the user may be overestimated.

The overall score (passing tests) of this report is 26 out of 36 evaluable items.

0.a Mass analysis	Sec. 2.1	OK
0.b Mask analysis	Sec. 2.2	OK
0.c Background analysis	Sec. 2.3	2 warnings
0.d B-factor analysis	Sec. 2.4	OK
0.e DeepRes	Sec. 2.5	1 warnings
0.f LocBfactor	Sec. 2.6	OK
0.g LocOccupancy	Sec. 2.7	OK
0.h DeepHand	Sec. 2.8	OK
1.a Global resolution	Sec. 4.1	OK
1.b FSC permutation	Sec. 4.2	OK
1.c Blocres	Sec. 4.3	OK
1.d Resmap	Sec. 4.4	1 warnings
1.e MonoRes	Sec. 4.5	OK
1.f MonoDir	Sec. 4.6	1 warnings
1.g FSO	Sec. 4.7	OK
1.h FSC3D	Sec. 6.1	OK
2.a Reprojection consistency	Sec. 6.1	OK
3.a Outlier detection	Sec. 9.1	OK
3.b 2D Classification internal consistency	Sec. 8.2	Cannot be automated
3.c 2D Classification external consistency	Sec. 8.3	OK
4.a Similarity criteria	Sec. 9.1	Cannot be automated
4.b Alignability smoothness	Sec. 9.2	1 warnings
4.c Alignability precision and accuracy	Sec. 9.3	OK
4.d1 Relion alignment	Sec. 9.4	OK
4.d2 CryoSparc alignment	Sec. 9.5	1 warnings
4.d3 Relion/CryoSparc alignments	Sec. 9.6	1 warnings
4.e Classification without alignment	Sec. 9.8	OK
4.f Overfitting detection	Sec. 9.8	OK
4.g Angular distribution efficiency	Sec. 9.9	OK
4.h SCF	Sec. 9.10	OK
4.i CTF stability	Sec. 9.11	1 warnings
5.a Micrograph cleaner	Sec. 11.1	OK
A.a MapQ	Sec. 13.1	OK
A.b FSC-Q	Sec. 13.2	OK
A.c Multimodel	Sec. 13.3	OK
A.d Map-Model Guinier	Sec. 13.4	OK
A.e Phenix validation	Sec. 13.5	1 warnings
A.f EMRinger	Sec. 13.6	1 warnings
A.g DAQ	Sec. 13.7	1 warnings
W Workflow	Sec. 14	Cannot be automated
O.b SAXS	Sec. 15.1	Cannot be automated

Summary of the warnings across sections.

If it is empty below this point, it means that there are no warnings.

Section 2.3 (0.c Background analysis)

1. **The null hypothesis that the background mean is 0 has been rejected because the p-value of the comparison is smaller than 0.001**
2. **There is a significant proportion of outlier values in the background (cdf5 ratio=2031.06)**

Section 2.5 (0.e DeepRes)

1. **The reported resolution, 2.60 Å, is particularly with respect to the local resolution distribution. It occupies the 0.00 percentile**

Section 4.4 (1.d Resmap)

1. **The reported resolution, 2.60 Å, is particularly with respect to the local resolution distribution. It occupies the 0.00 percentile**

Section 4.6 (1.f MonoDir)

1. **The distribution of best resolution is not uniform in all directions. The associated p-value is 0.000000.**

Section 9.2 (4.b Alignability smoothness)

1. **The percentage of images whose angular assignment is significantly away from the smoothed maximum is too high, 50.2%**

Section 9.5 (4.d2 CryoSparc alignment)

1. **The percentage of images with uncertain shift is larger than 20%**

Section 9.6 (4.d3 Relion/CryoSparc alignments)

1. **The percentage of images with uncertain shift is larger than 20%**

Section 9.11 (4.i CTF stability)

1. **The 95% confidence interval of scale factor is not centered.**

Section 13.5 (A.e Phenix validation)

1. **The resolution reported by the user, 2.6 Å, is significantly smaller than the resolution estimated between map and model (FSC=0.5), 4.4 Å**

Section 13.6 (A.f EMRinger)

1. **The EMRinger score is smaller than 1, it is 0.892.**

Section 13.7 (A.g DAQ)

1. The average DAQ is smaller than 0.5.

Contents

1	Input data	9
2	Level 0 analysis	12
2.1	Level 0.a Mass analysis	12
2.2	Level 0.b Mask analysis	13
2.3	Level 0.c Background analysis	15
2.4	Level 0.d B-factor analysis	17
2.5	Level 0.e Local resolution with DeepRes	18
2.6	Level 0.f Local B-factor	20
2.7	Level 0.g Local Occupancy	22
2.8	Level 0.h Hand correction	24
3	Half maps	24
4	Level 1 analysis	26
4.1	Level 1.a Global resolution	26
4.2	Level 1.b FSC permutation	29
4.3	Level 1.c Local resolution with Blocres	30
4.4	Level 1.d Local resolution with Resmap	32
4.5	Level 1.e Local resolution with MonoRes	33
4.6	Level 1.f Local and directional resolution with MonoDir	35
4.7	Level 1.g Fourier Shell Occupancy	38
4.8	Level 1.h Fourier Shell Correlation 3D	40
5	2D Classes	42
6	Level 2 analysis	43
6.1	Level 2.a Reprojection consistency	43
7	Particles	49
8	Level 3 analysis	49
8.1	Level 3.a Outlier detection	49
8.2	Level 3.b Classification internal consistency	56
8.3	Level 3.c Classification external consistency	57

9	Level 4 analysis	64
9.1	Level 4.a Similarity criteria	64
9.2	Level 4.b Alignability smoothness	65
9.3	Level 4.c Alignability precision and accuracy	66
9.4	Level 4.d1 Relion alignment	68
9.5	Level 4.d2 CryoSparc alignment	70
9.6	Level 4.d3 Relion/CryoSparc alignments	72
9.7	Level 4.e Classification without alignment	74
9.8	Level 4.f Overfitting detection	74
9.9	Level 4.g Angular distribution efficiency	75
9.10	Level 4.h Sampling compensation factor	76
9.11	Level 4.i CTF stability	77
10	Micrographs	81
11	Level 5 analysis	82
11.1	Level 5.a Micrograph cleaner	82
12	Atomic model	83
13	Level A analysis	84
13.1	Level A.a MapQ	84
13.2	Level A.b FSC-Q	85
13.3	Level A.c Multimodel stability	87
13.4	Level A.d Map-Model Guinier analysis	89
13.5	Level A.e Phenix validation	90
13.6	Level A.f EMRinger validation	97
13.7	Level A.g DAQ validation	104
14	Workflow	106
15	Other experimental techniques	107
15.1	O.b SAXS	107

1 Input data

Input map: /home/coss/ScipionUserData/projects/Example_10248_Scipion3/-
Runs/010948_XmippProtLocSharp/extra/sharpenedMap_1.mrc
SHA256 hash: 58f4d24dafbbf69aad9790730d8910d2fbbe0de545b17f28850bc2a1b4b5230b
Voxel size: 0.740000 (Å)
Visualization threshold: 0.002500
Resolution estimated by user: 2.600000

Orthogonal slices of the input map

Explanation:

In the orthogonal slices of the map, the noise outside the protein should not have any structure (stripes going out, small blobs, particularly high or low densities, ...)

Results:

See Fig. 1.

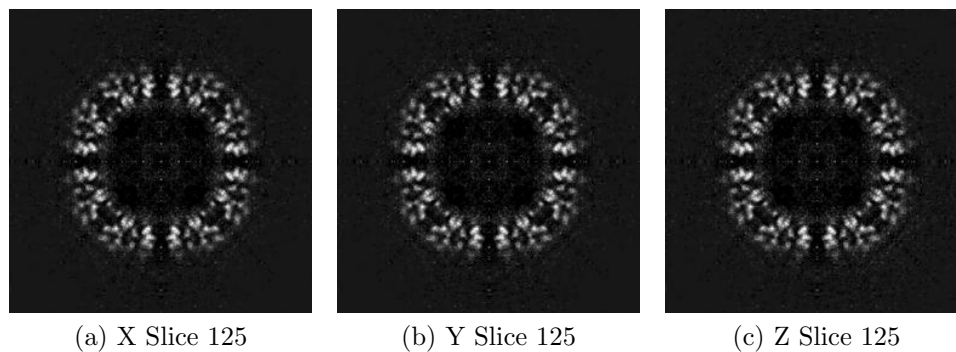


Figure 1: Central slices of the input map in the three dimensions

Orthogonal slices of maximum variance of the input map

Results:

See Fig. 2.

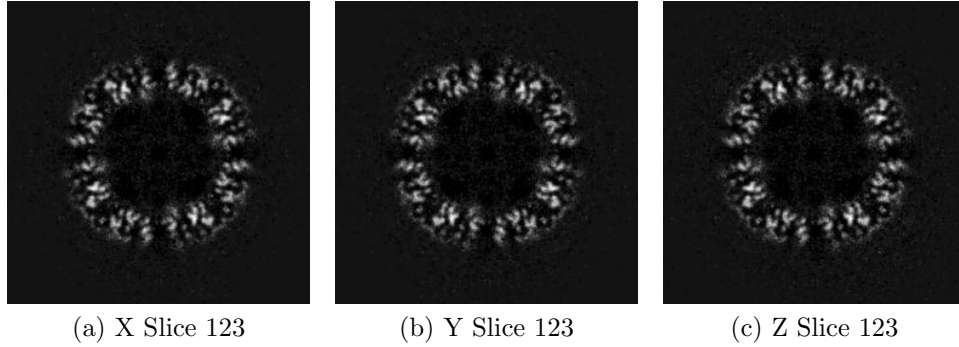


Figure 2: Slices of maximum variation in the three dimensions

Orthogonal projections of the input map

Explanation:

In the projections there should not be stripes (this is an indication of directional overweighting, or angular attraction), and there should not be a dark halo around or inside the structure (this is an indication of incorrect CTF correction or the reconstruction of a biased map).

Results:

See Fig. 3.

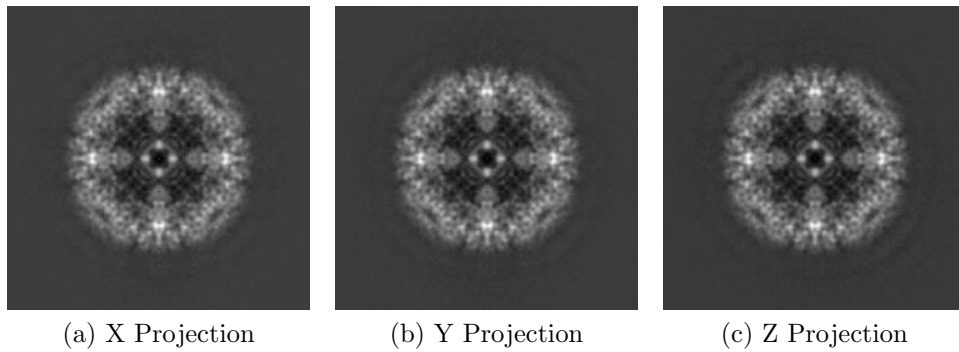


Figure 3: Projections in the three dimensions

Isosurface views of the input map

Explanation:

An isosurface is the surface of all points that have the same gray value. In these views there should not be many artifacts or noise blobs around the map.

Results:

See Fig. 4.

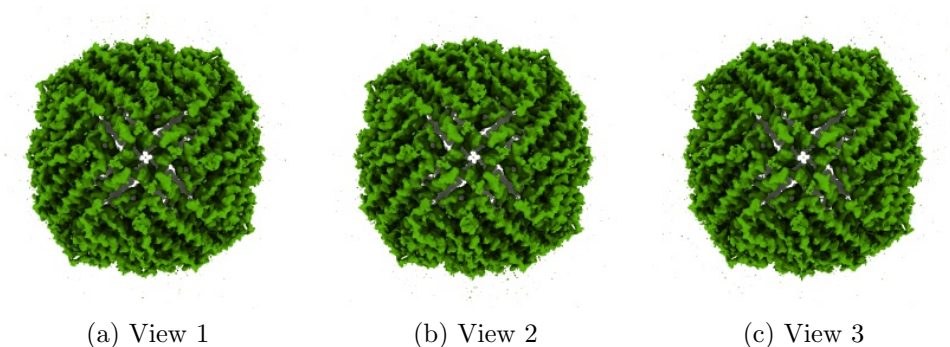


Figure 4: Isosurface at threshold=0.002500. Views generated by ChimeraX at a the following X, Y, Z angles: View 1 (0,0,0), View 2 (90, 0, 0), View 3 (0, 90, 0).

Orthogonal slices of maximum variance of the mask

Explanation:

The mask has been calculated at the suggested threshold 0.002500, the largest connected component was selected, and then dilated by 2Å.

Results:

See Fig. 5.

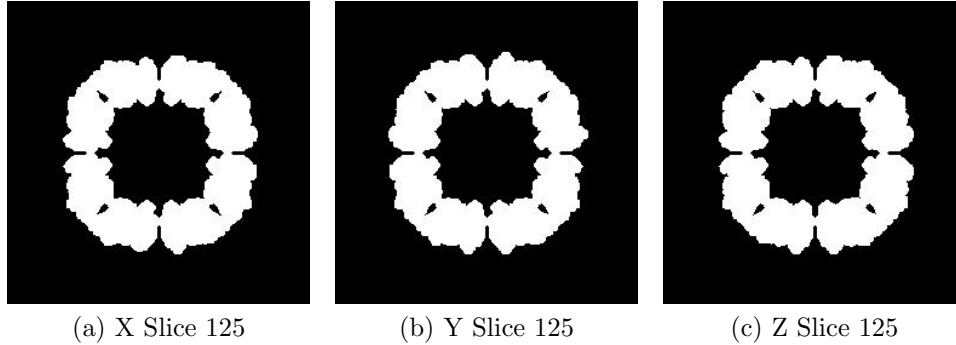


Figure 5: Slices of maximum variation in the three dimensions of the mask

2 Level 0 analysis

2.1 Level 0.a Mass analysis

Explanation:

The reconstructed map must be relatively well centered in the box, and there should be at least 30\AA (the exact size depends on the CTF) on each side to make sure that the CTF can be appropriately corrected.

Results:

The space from the left and right in X are 31.08 and 31.08 \AA , respectively. There is a decentering ratio $(\text{abs}(\text{Right-Left})/\text{Size})\%$ of 0.00%

The space from the left and right in Y are 33.30 and 31.08 \AA , respectively. There is a decentering ratio $(\text{abs}(\text{Right-Left})/\text{Size})\%$ of 1.20%

The space from the left and right in Z are 32.56 and 31.08 \AA , respectively. There is a decentering ratio $(\text{abs}(\text{Right-Left})/\text{Size})\%$ of 0.80%

The center of mass is at $(x,y,z)=(125.05,125.02,124.99)$. The decentering of the center of mass $(\text{abs}(\text{Center})/\text{Size})\%$ is 0.02, 0.01, and 0.01, respectively.%

Automatic criteria: The validation is OK if 1) the decentering and

center of mass less than 20% of the map dimensions in all directions, and 2) the extra space on each direction is more than 20% of the map dimensions.

STATUS: OK

2.2 Level 0.b Mask analysis

Explanation:

The map at the suggested threshold should have most of its mass concentrated in a single connected component. It is normal that after thresholding there are a few thousands of very small, disconnected noise blobs. However, their total mass should not exceed 10%. The raw mask (just thresholding) and the mask constructed for the analysis (thresholding + largest connected component + dilation) should significantly overlap. Overlap is defined by the overlapping coefficient ($\text{size}(\text{Raw AND Constructed})/\text{size}(\text{Raw})$) that is a number between 0 and 1, the closer to 1, the more they agree.

Results:

Raw mask: At threshold 0.002500, there are 2172 connected components with a total number of voxels of 357214 and a volume of 144751.69 \AA^3 (see Fig. 6). The size and percentage of the total number of voxels for the raw mask are listed below (up to 95% of the mass), the list contains (No. voxels (volume in \AA^3), percentage, cumulatedPercentage):

(353875 (143398.64), 99.07, 99.07)

Number of components to reach 95% of the mass: 1

The average size of the remaining 2171 components is 1.54 voxels (0.41 \AA^3). Their size goes from 72 voxels (29.18 \AA^3) to 1 voxel (0.41 \AA^3).

The slices of the raw mask can be seen in Fig. 6.

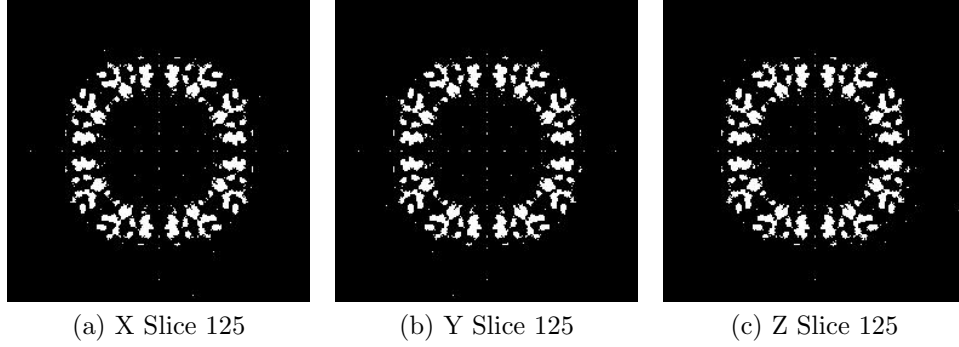


Figure 6: Maximum variance slices in the three dimensions of the raw mask

The following table shows the variation of the mass enclosed at different thresholds (see Fig. 7):

Threshold	Voxel mass	Molecular mass(kDa)	# Aminoacids
0.0006	934328.00	313.68	2851.64
0.0013	600420.00	201.58	1832.53
0.0019	448905.00	150.71	1370.09
0.0025	350635.00	117.72	1070.16
0.0032	279330.00	93.78	852.54
0.0038	223199.00	74.93	681.22
0.0045	179094.00	60.13	546.61
0.0051	143532.00	48.19	438.07
0.0057	114177.00	38.33	348.48
0.0064	89515.00	30.05	273.21
0.0070	69341.00	23.28	211.63
0.0076	52372.00	17.58	159.84
0.0083	38167.00	12.81	116.49
0.0089	26921.00	9.04	82.16
0.0096	18314.00	6.15	55.90
0.0102	12779.00	4.29	39.00
0.0108	7836.00	2.63	23.92
0.0115	4494.00	1.51	13.72
0.0121	2108.00	0.71	6.43
0.0127	1032.00	0.35	3.15
0.0134	534.00	0.18	1.63
0.0140	241.00	0.08	0.74
0.0147	96.00	0.03	0.29
0.0153	30.00	0.01	0.09

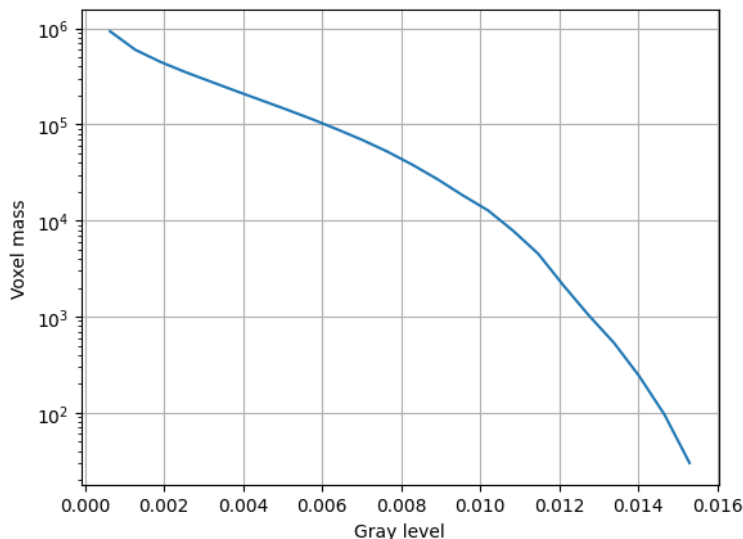


Figure 7: Voxel mass as a function of the gray level.

Constructed mask: After keeping the largest component of the previous mask and dilating it by 2\AA , there is a total number of voxels of 1730415 and a volume of 701205.69\AA^3 . The overlap between the raw and constructed mask is 1.00.

Automatic criteria: The validation is OK if 1) to keep 95% of the mass we need to keep at most 5 connected components; and 2) the average volume of the blobs outside the given threshold has a size smaller than 5\AA^3 ; and 3) the overlap between the raw mask and the mask constructed for the analysis is larger than 75%.

STATUS: OK

2.3 Level 0.c Background analysis

Explanation:

Background is defined as the region outside the macromolecule mask. The background mean should be zero, and the number of voxels with a very low or very high value (below 5 standard deviations of the noise) should be very small and they should be randomly distributed without any specific structure.

Sometimes, you can see some structure due to the symmetry of the structure.

Results:

The null hypothesis that the background mean is 0 was tested with a one-sample Student's t-test. The resulting t-statistic and p-value were -666.91 and 0.000000, respectively.

The mean and standard deviation of the background were -0.000050 and 0.000279. The percentage of background voxels whose absolute value is larger than 5 times the standard deviation is 0.12 % (see Fig. 8). The same percentage from a Gaussian would be 0.000057% (ratio between the two percentages: 2031.055410).

Slices of the background beyond 5*sigma can be seen in Fig. 8.

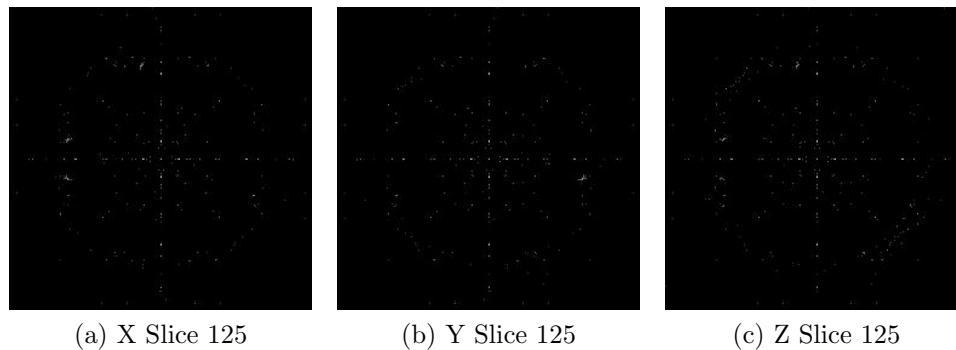


Figure 8: Maximum variance slices in the three dimensions of the parts of the background beyond 5*sigma

Automatic criteria: The validation is OK if 1) the p-value of the null hypothesis that the background has 0 mean is larger than 0.001; and 2) the number of voxels above or below 5 sigma is smaller than 20 times the amount expected for a Gaussian with the same standard deviation whose mean is 0.

WARNINGS: 2 warnings

1. **The null hypothesis that the background mean is 0 has been rejected because the p-value of the comparison is smaller than 0.001**
2. **There is a significant proportion of outlier values in the background (cdf5 ratio=2031.06)**

2.4 Level 0.d B-factor analysis

Explanation:

The B-factor line [Rosenthal and Henderson, 2003] fitted between 15Å and the resolution reported should have a slope that is between 0 and 300 Å².

Results:

Fig. 9 shows the logarithm (in natural units) of the structure factor (the module squared of the Fourier transform) of the experimental map, its fitted line, and the corrected map. The estimated B-factor was -93.3. The fitted line was $\log(|F|^2) = -23.3/R^2 + (-13.2)$.

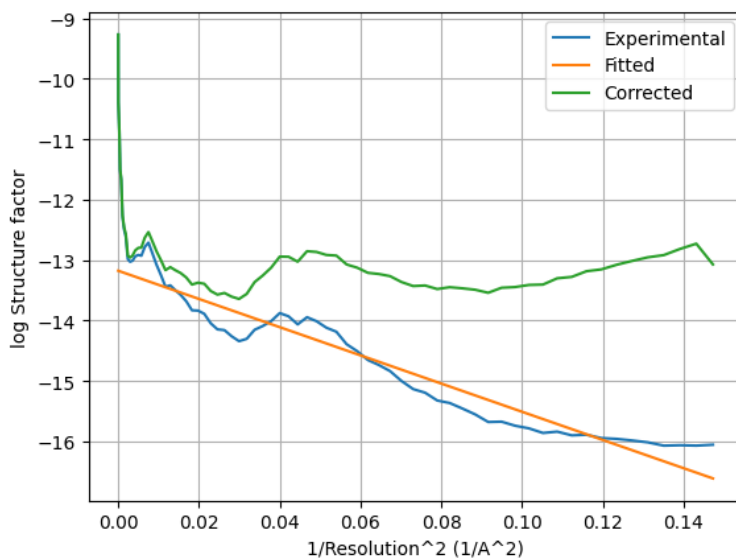


Figure 9: Guinier plot. The X-axis is the square of the inverse of the resolution in Å.

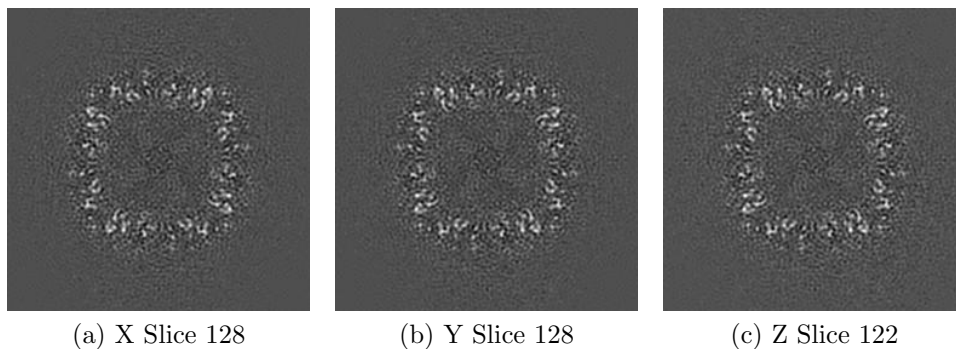


Figure 10: Slices of maximum variation in the three dimensions of the B-factor corrected map

Automatic criteria: The validation is OK if the B-factor is in the range $[-300,0]$.

STATUS: OK

2.5 Level 0.e Local resolution with DeepRes

Explanation:

DeepRes [Ramírez-Aportela et al., 2019] measures the local resolution using a neural network that has been trained on the appearance of atomic structures at different resolutions. Then, by comparing the local appearance of the input map to the appearance of the atomic structures a local resolution label can be assigned.

Results:

Fig. 11 shows the histogram of the local resolution according to DeepRes. Some representative percentiles are:

Percentile	Resolution(\AA)
2.5%	3.41
25%	3.84
50%	4.09
75%	4.35
97.5%	4.90

The reported resolution, 2.60 \AA , is at the percentile 0.0. Fig. 12 shows some representative views of the local resolution.

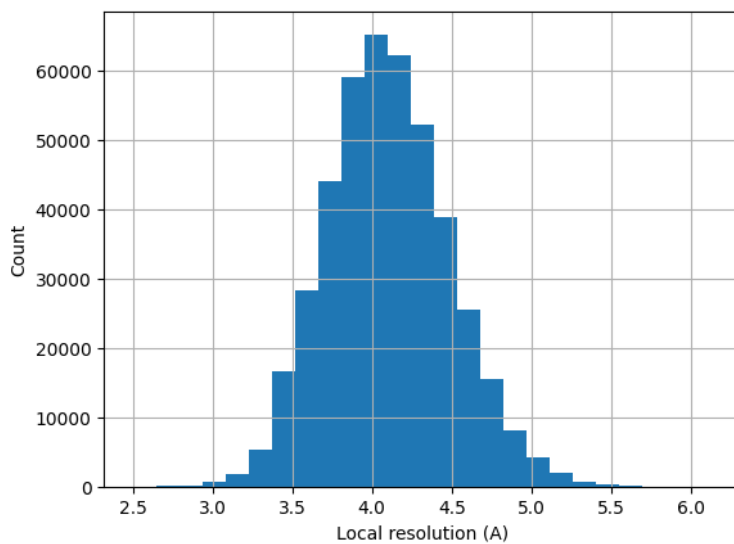


Figure 11: Histogram of the local resolution according to deepres.

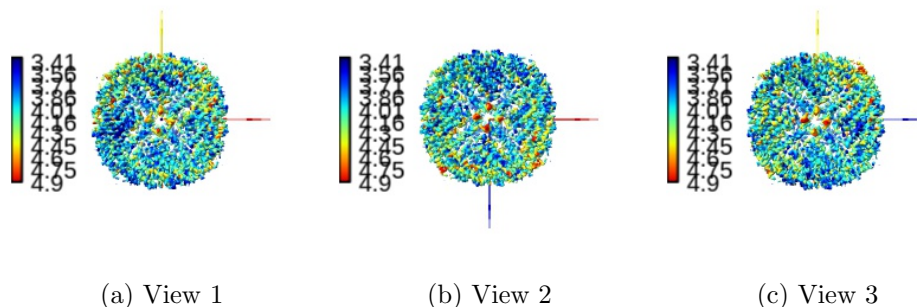


Figure 12: Local resolution according to DeepRes. Views generated by ChimeraX at a the following X, Y, Z angles: View 1 (0,0,0), View 2 (90, 0, 0), View 3 (0, 90, 0).

Automatic criteria: The validation is OK if the percentile of the user provided resolution is larger than 0.1% of the percentile of the local resolution as estimated by DeepRes.

WARNINGS: 1 warnings

1. **The reported resolution, 2.60 Å, is particularly with respect to the local resolution distribution. It occupies the 0.00 percentile**

2.6 Level 0.f Local B-factor

Explanation:

LocBfactor [Kaur et al., 2021] estimates a local resolution B-factor by decomposing the input map into a local magnitude and phase term using the spiral transform.

Results:

Fig. 13 shows the histogram of the local B-factor according to LocBfactor. Some representative percentiles are:

Percentile	Local B-factor (\AA^{-2})
2.5%	-184.43
25%	-159.09
50%	-146.41
75%	-133.15
97.5%	-106.90

Fig. 14 shows some representative views of the local B-factor.

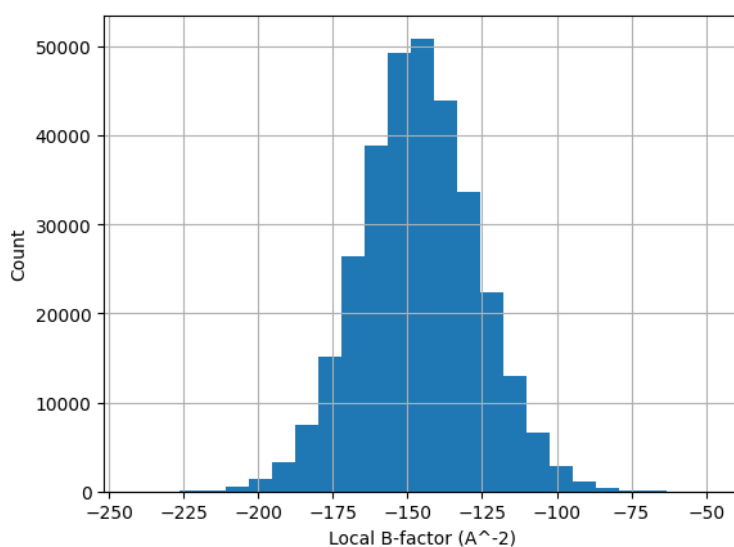


Figure 13: Histogram of the local B-factor according to LocBfactor.

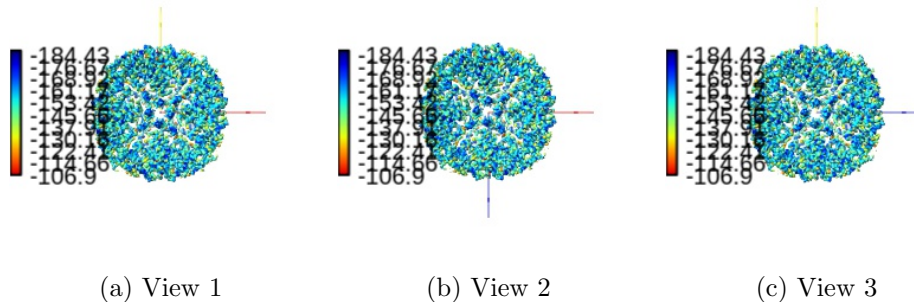


Figure 14: Local B-factor according to LocBfactor. Views generated by ChimeraX at a the following X, Y, Z angles: View 1 (0,0,0), View 2 (90, 0, 0), View 3 (0, 90, 0).

Automatic criteria: The validation is OK if the median B-factor is in the range [-300,0].

STATUS: OK

2.7 Level 0.g Local Occupancy

Explanation:

LocOccupancy [Kaur et al., 2021] estimates the occupancy of a voxel by the macromolecule.

Results:

Fig. 15 shows the histogram of the local occupancy according to LocOccupancy. Some representative percentiles are:

Percentile	Local Occupancy [0-1]
2.5%	0.08
25%	0.58
50%	0.83
75%	1.00
97.5%	1.00

Fig. 16 shows some representative views of the local occupancy.

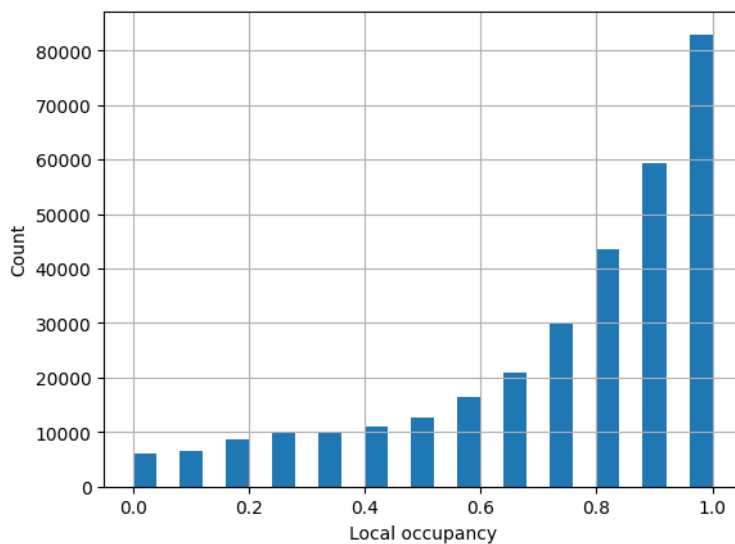


Figure 15: Histogram of the local occupancy according to LocOccupancy.

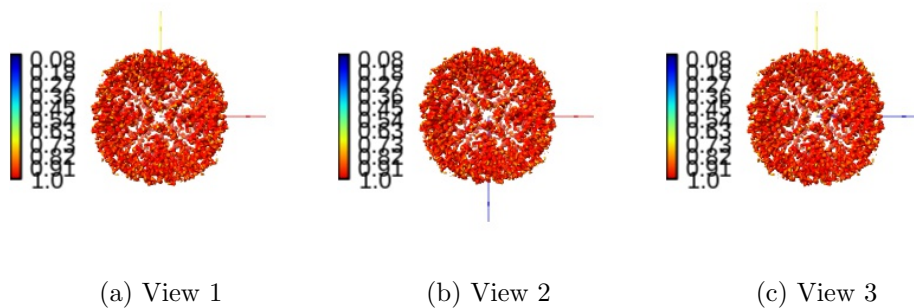


Figure 16: Local occupancy according to LocOccupancy. Views generated by ChimeraX at the following X, Y, Z angles: View 1 (0,0,0), View 2 (90, 0, 0), View 3 (0, 90, 0).

Automatic criteria: The validation is OK if the median occupancy is larger than 50%.

STATUS: OK

2.8 Level 0.h Hand correction

Explanation:

Deep Hand determines the correction of the hand for those maps with a resolution smaller than 5Å. The method calculates a value between 0 (correct hand) and 1 (incorrect hand) using a neural network to assign its hand.

Results:

Deep hand assigns a score of 0.085 to the input volume.

Automatic criteria: The validation is OK if the deep hand score is smaller than 0.5.

STATUS: OK

3 Half maps

Half map 1: /home/coss/ScipionUserData/projects/Example_10248_Scipion3/-
Runs/010450_XmippProtReconstructHighRes/extra/Iter001/volume01.vol
SHA256 hash: a8d09c9ee945f8eeae5704ed042fceb0de6d128d80dab51ea23f2c046a91993

Half map 2: /home/coss/ScipionUserData/projects/Example_10248_Scipion3/-
Runs/010450_XmippProtReconstructHighRes/extra/Iter001/volume02.vol
SHA256 hash: a93a1717f03b3c901f4800f1e0fe7fe3824aa71b0abc131dcf8897aa863eb6e7

Slices of the first half map can be seen in Fig. 17.

Slices of the second half map can be seen in Fig. 18.

Slices of the difference between both maps can be seen in Fig. 19. There should not be any structure in this difference. Sometimes some patterns are seen if the map is symmetric.

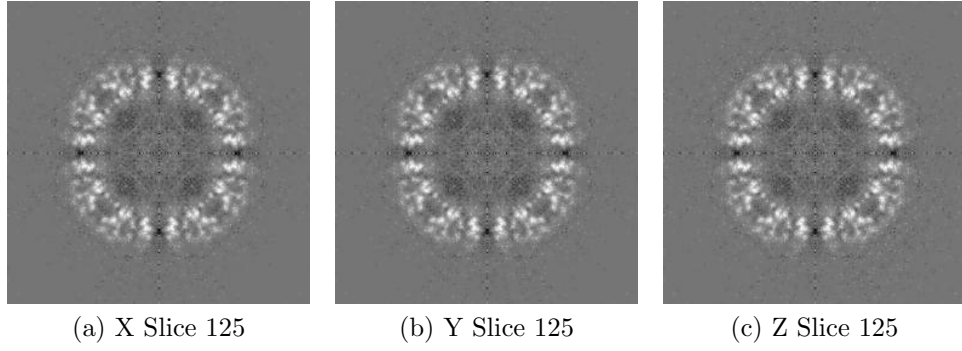


Figure 17: Slices of maximum variation in the three dimensions of Half 1

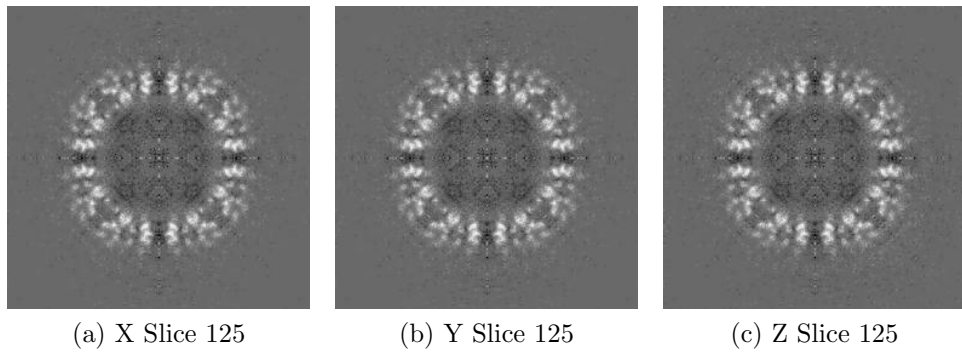


Figure 18: Slices of maximum variation in the three dimensions of Half 2

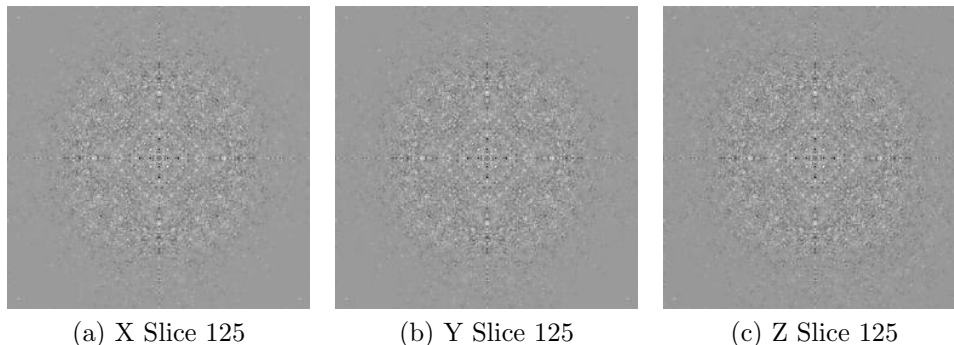


Figure 19: Slices of maximum variation in the three dimensions of the difference Half1-Half2.

4 Level 1 analysis

4.1 Level 1.a Global resolution

Explanation: The Fourier Shell Correlation (FSC) between the two half maps is the most standard method to determine the global resolution of a map. However, other measures exist such as the Spectral Signal-to-Noise Ratio and the Differential Phase Residual. There is a long debate about the right thresholds for these measures. Probably, the most clear threshold is the one of the SSNR (SSNR=1). For the DPR we have chosen 103.9° and for the FSC, the standard 0.143. For a deep discussion of all these thresholds, see [Sorzano et al., 2017]. Note that these thresholds typically result in resolution values that are at the lower extreme of the local resolution range, meaning that this resolution is normally in the first quarter. It should not be understood as the average resolution of the map.

Except for the noise, the FSC and DPR should be approximately monotonic. They should not have any “coming back” behavior. If they have, this is typically due to the presence of a mask in real space or non-linear processing.

Results:

Fig. 20 shows the FSC and the 0.143 threshold. The resolution according to the FSC is 3.09\AA . The map information is well preserved (FSC>0.9) up to

4.75Å.

Fig. 21 shows the DPR and the 103.9° threshold. The resolution according to the DPR is 2.69Å.

Fig. 22 shows the SSNR and the SSNR=1 threshold. The resolution according to the SSNR is 2.92Å.

The mean resolution between the three methods is 2.90Å and its range is within the interval [2.69, 3.09]Å.

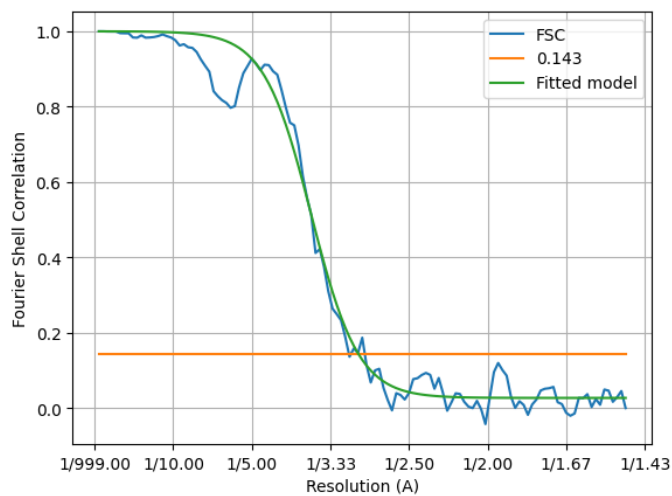


Figure 20: Fourier Shell correlation between the two halves.

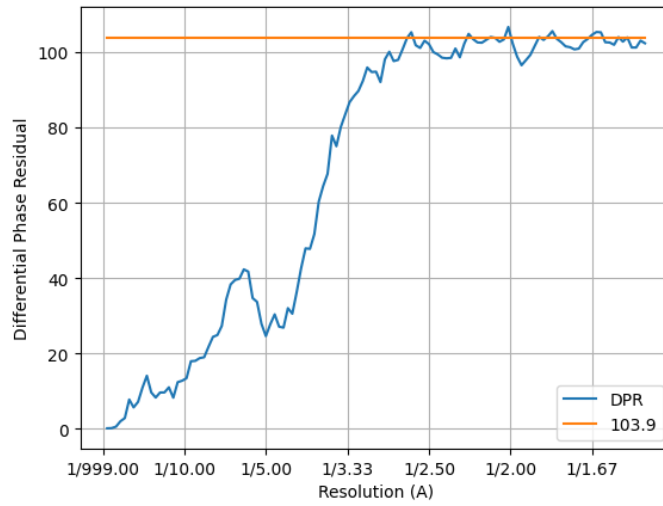


Figure 21: Differential Phase Residual between the two halves.

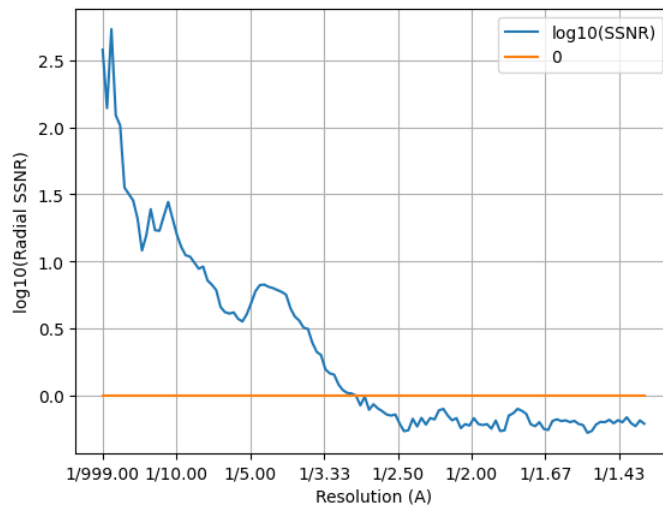


Figure 22: Spectral Signal-to-Noise Ratio estimated from the two halves.

Automatic criteria: The validation is OK if the user provided resolution is larger than 0.8 times the resolution estimated by 1) FSC, 2) DPR, and 3) SSNR.

STATUS: OK

4.2 Level 1.b FSC permutation

Explanation:

This method [Beckers and Sachse, 2020] calculates a global resolution by formulating a hypothesis test in which the distribution of the FSC of noise is calculated from the two maps.

Results:

The resolution at 1% of FDR was 2.7. The estimated B-factor was -85.7. Fig. 23 shows the estimated FSC and resolution.

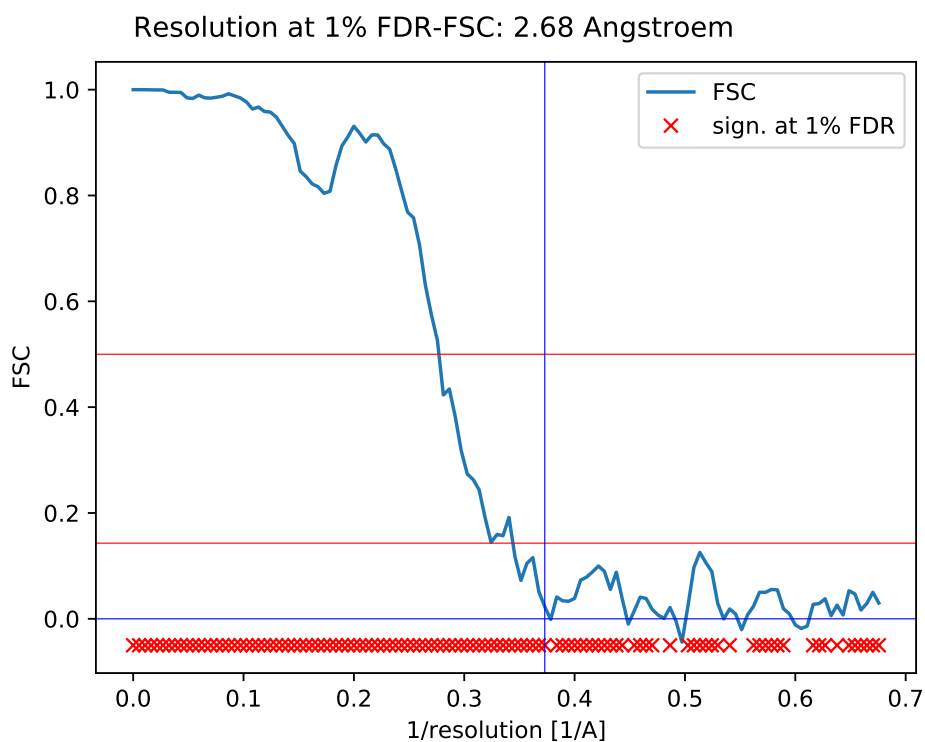


Figure 23: FSC and resolution estimated by a permutation test.

Automatic criteria: The validation is OK if the user provided resolution is larger than 0.8 times the resolution estimated by FSC permutation.

STATUS: OK

4.3 Level 1.c Local resolution with Blocres

Explanation:

This method [Cardone et al., 2013] computes a local Fourier Shell Correlation (FSC) between the two half maps.

Results:

Fig. 24 shows the histogram of the local resolution according to Blocres. Some representative percentiles are:

Percentile	Resolution(Å)
2.5%	2.75
25%	2.91
50%	3.04
75%	3.21
97.5%	4.31

The reported resolution, 2.60 Å, is at the percentile 0.2. Fig. 25 shows some representative views of the local resolution.

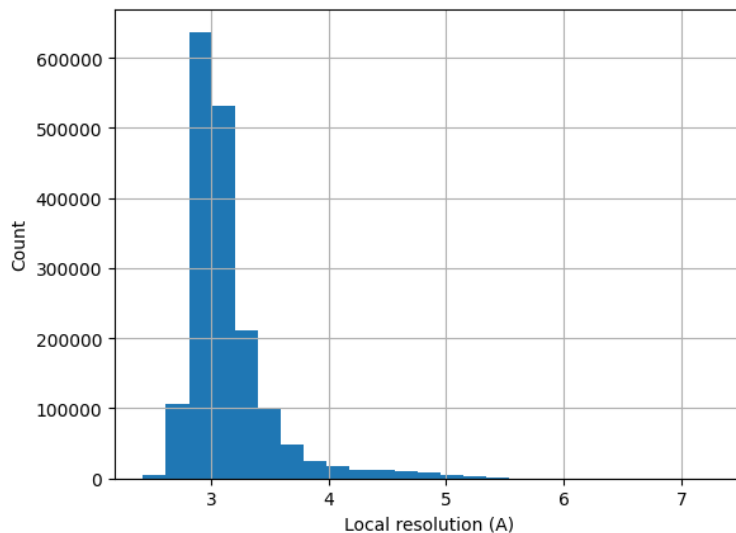


Figure 24: Histogram of the local resolution according to blocres.

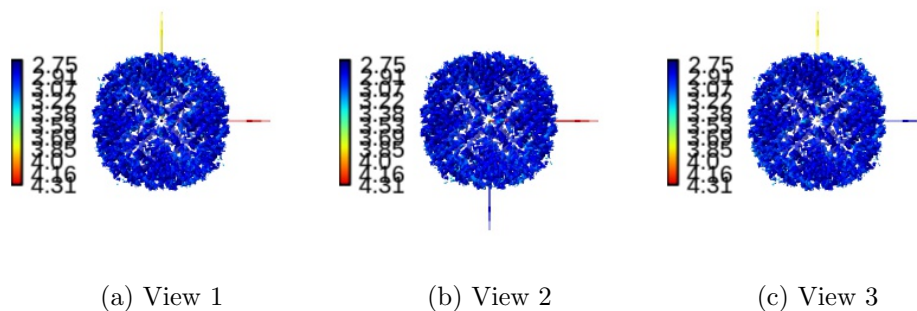


Figure 25: Local resolution according to Blocres. Views generated by ChimeraX at a the following X, Y, Z angles: View 1 (0,0,0), View 2 (90, 0, 0), View 3 (0, 90, 0).

Automatic criteria: The validation is OK if the percentile of the user provided resolution is larger than 0.1% of the percentile of the local resolution as estimated by BlocRes.

STATUS: OK

4.4 Level 1.d Local resolution with Resmap

Explanation:

This method [Kucukelbir et al., 2014] is based on a test hypothesis testing of the superiority of signal over noise at different frequencies.

Results:

Fig. 26 shows the histogram of the local resolution according to Resmap. Some representative percentiles are:

Percentile	Resolution(\AA)
2.5%	3.13
25%	3.45
50%	3.52
75%	3.55
97.5%	3.58

The reported resolution, 2.60 \AA , is at the percentile 0. Fig. 27 shows some representative views of the local resolution.

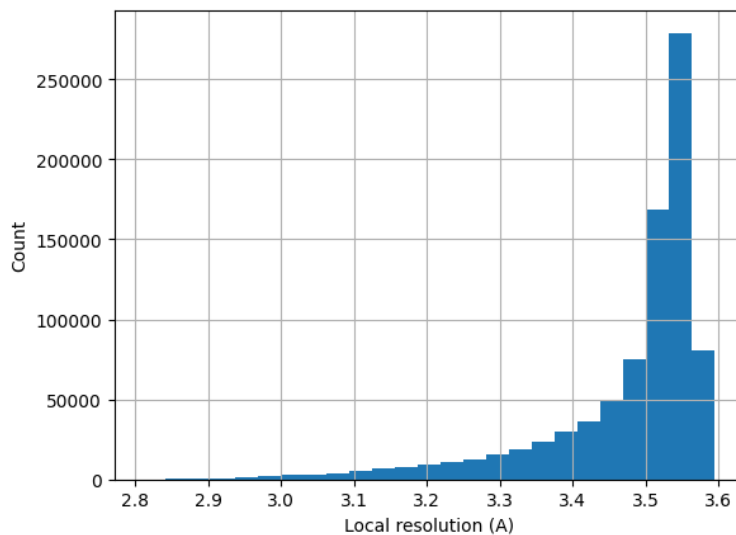


Figure 26: Histogram of the local resolution according to Resmap.

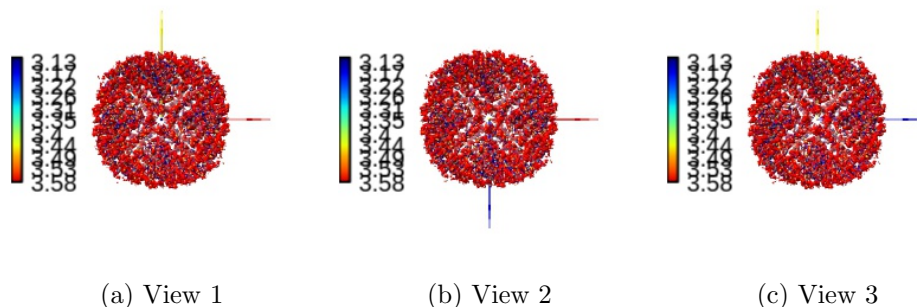


Figure 27: Local resolution according to Resmap. Views generated by ChimeraX at a the following X, Y, Z angles: View 1 (0,0,0), View 2 (90, 0, 0), View 3 (0, 90, 0).

Automatic criteria: The validation is OK if the percentile of the user provided resolution is larger than 0.1% of the percentile of the local resolution as estimated by Resmap.

WARNINGS: 1 warnings

1. **The reported resolution, 2.60 Å, is particularly with respect to the local resolution distribution. It occupies the 0.00 percentile**

4.5 Level 1.e Local resolution with MonoRes

Explanation:

MonoRes [Vilas et al., 2018] evaluates the local energy of a point with respect to the distribution of energy in the noise. This comparison is performed at multiple frequencies and for each one, the monogenic transformation separates the amplitude and phase of the input map. Then the energy of the amplitude within the map is compared to the amplitude distribution observed in the noise, and a hypothesis test is run for every voxel to check if its energy is significantly above the level of noise.

Results:

Fig. 28 shows the histogram of the local resolution according to MonoRes. Some representative percentiles are:

Percentile	Resolution(\AA)
2.5%	1.74
25%	3.97
50%	4.58
75%	6.39
97.5%	9.08

The reported resolution, 2.60 \AA , is at the percentile 5.6. Fig. 29 shows some representative views of the local resolution

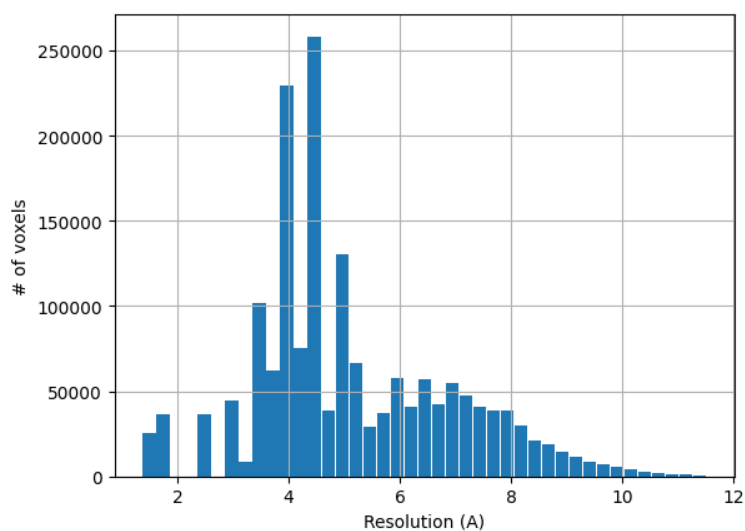


Figure 28: Histogram of the local resolution according to MonoRes.

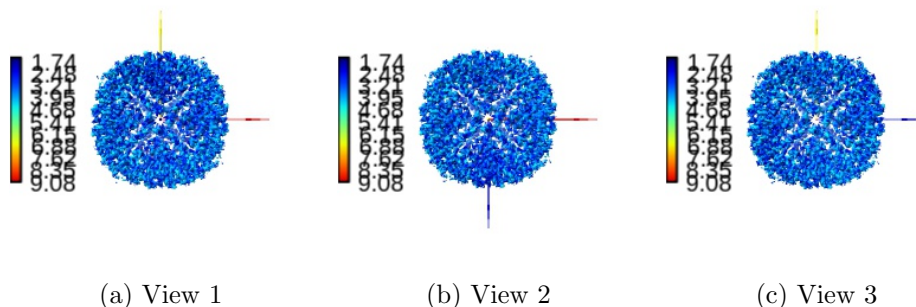


Figure 29: Local resolution according to MonoRes. Views generated by ChimeraX at a the following X, Y, Z angles: View 1 (0,0,0), View 2 (90, 0, 0), View 3 (0, 90, 0).

Automatic criteria: The validation is OK if the percentile of the user provided resolution is larger than 0.1% of the percentile of the local resolution as estimated by MonoRes.

STATUS: [OK](#)

4.6 Level 1.f Local and directional resolution with MonoDir

Explanation:

MonoDir [Vilas et al., 2020] extends the concept of local resolution to local and directional resolution by changing the shape of the filter applied to the input map. The directional analysis can reveal image alignment problems.

The histogram of best resolution voxels per direction (Directional Histogram 1D) shows how many voxels in the volume have their maximum resolution in that direction. Directions are arbitrarily numbered from 1 to N. This histogram should be relatively flat. We perform a Kolmogorov-Smirnov test to check its uniformity. If the null hypothesis is rejected, then the directional resolution is not uniform. It does not mean that it is wrong, and it could be caused by several reasons: 1) the angular distribution is not uniform, 2) there are missing directions, 3) there is some anisotropy in the data (including some preferential directional movement).

Ideally, the radial average of the minimum, maximum, and average res-

olution at each voxel (note that these are spatial radial averages) should be flat and as low as possible. If they show some slope, this is associated with inaccuracies in the angular assignment. These averages make sense when the shells are fully contained within the protein. As the shells approach the outside of the protein, these radial averages make less sense.

Results:

Fig. 30 shows the 1D directional histogram and Fig. 31 the 2D directional histogram. We compared the 1D directional histogram to a uniform distribution using a Kolmogorov-Smirnov test. The D statistic was 0.064887, and the p-value of the null hypothesis 0.000000.

The radial average of the minimum, maximum and average resolution at each voxel is shown in Fig. 32. The overall mean of the directional resolution is 2.03

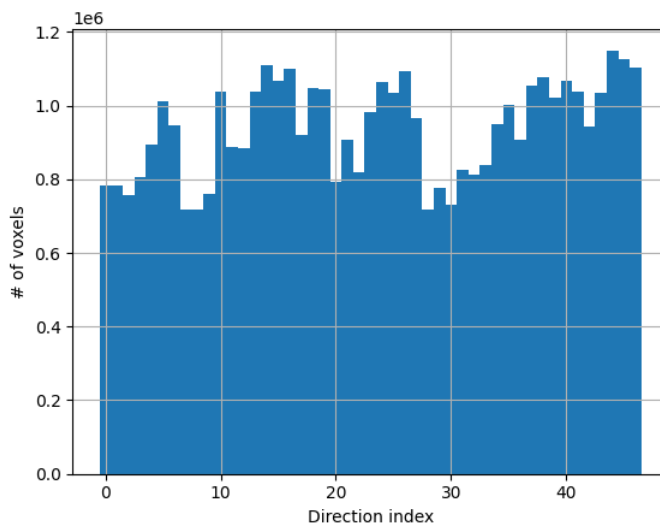


Figure 30: Histogram 1D of the best direction at each voxel.

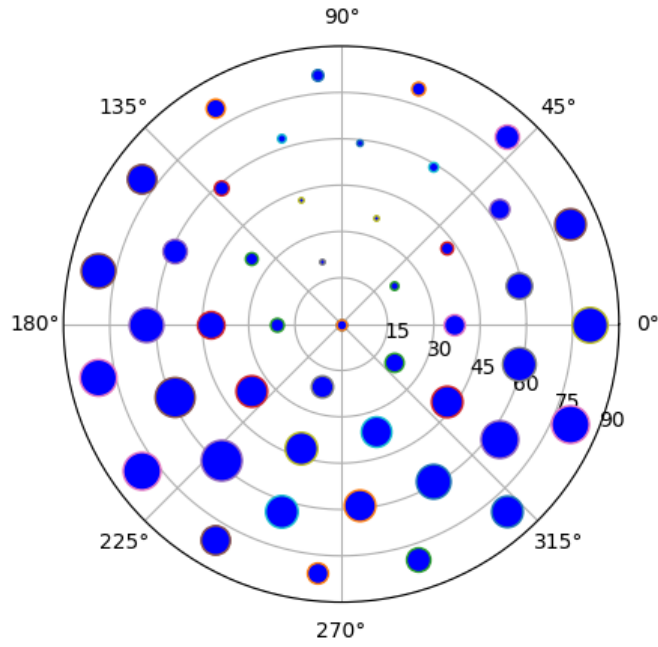


Figure 31: Histogram 2D of the best direction at each voxel. The azimuthal rotation is circular, while the tilt angle is the radius. The size of the point is proportional to the number of voxels whose maximum resolution is in that direction (this count can be seen in Fig. 30).

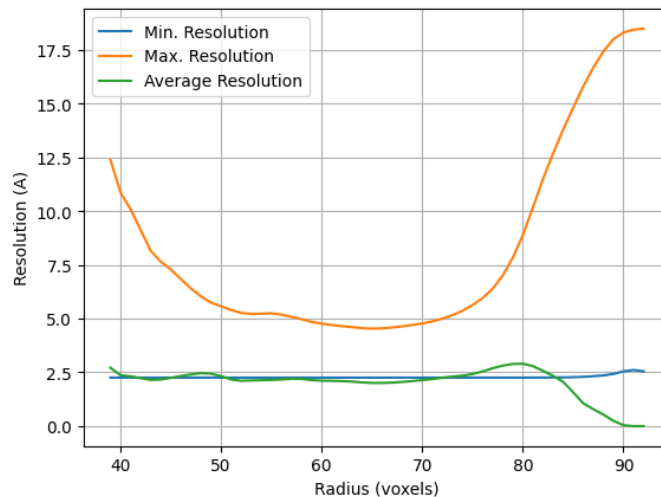


Figure 32: Radial averages (in space) of the minimum, maximum and average resolution at each voxel.

Automatic criteria: The validation is OK if 1) the null hypothesis that the directional resolution is not uniform is not rejected with a threshold of 0.001 for the p-value, and 2) the resolution provided by the user is not smaller than 0.8 times the average directional resolution.

WARNINGS: 1 warnings

1. **The distribution of best resolution is not uniform in all directions. The associated p-value is 0.000000.**

4.7 Level 1.g Fourier Shell Occupancy

Explanation:

This method calculates the anisotropy of the energy distribution in Fourier shells. This is an indirect measure of anisotropy of the angular distribution or the presence of heterogeneity. A natural threshold for this measure is 0.5. However, 0.9 and 0.1 are also interesting values that define the frequency at which the occupancy is 90% and 10%, respectively. This region is shaded in the plot.

Results:

Fig. 33 shows the Fourier Shell Occupancy and its anisotropy. The directional resolution is shown in Fig. 34. The resolution according to the FSO is 2.85\AA . Fourier shells are occupied at between 90 and than 10% in the range $[2.91, 2.27]\text{\AA}$.

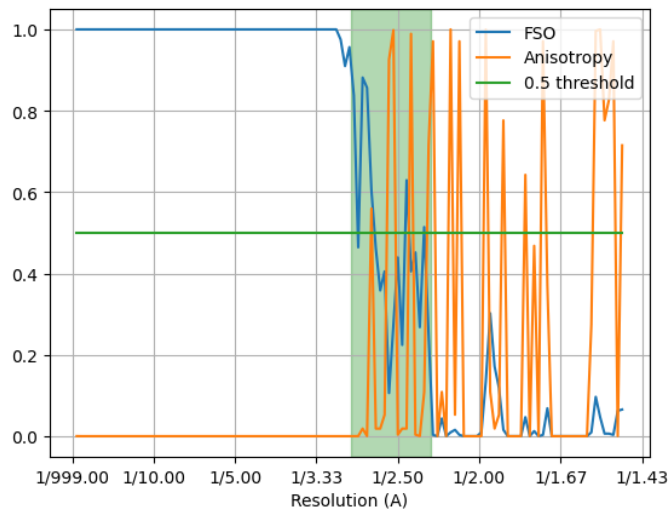


Figure 33: FSO and anisotropy.

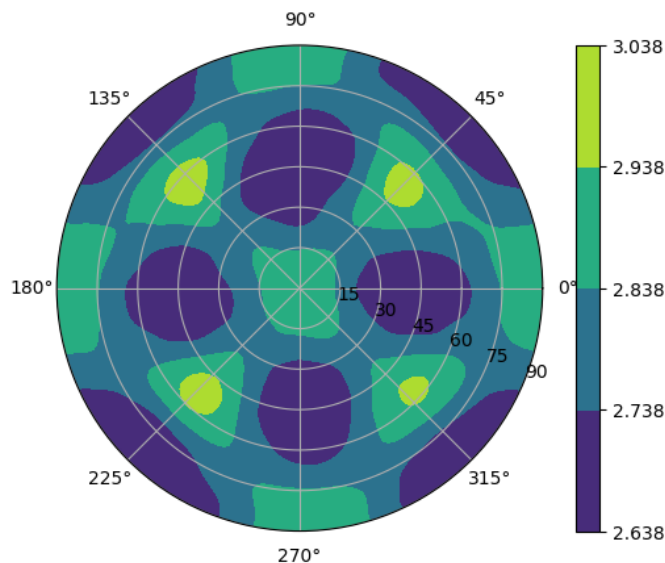


Figure 34: Directional resolution in the projection sphere.

Automatic criteria: The validation is OK if the resolution provided by the user is not smaller than 0.8 times the resolution estimated by the first cross of FSO below 0.5.

STATUS: OK

4.8 Level 1.h Fourier Shell Correlation 3D

Explanation:

This method analyzes the FSC in different directions and evaluates its homogeneity.

Results:

Fig. 35 shows the FSCs in X, Y, Z, and the global FSC. Fig. 36 shows the global FSC and the histogram of the directional FSC. Finally, Fig. 37 shows the rotational average of the map power in Fourier space. The FSC 3D resolutions at a 0.143 threshold in X, Y, and Z are 2.64, 2.66, and 2.66 Å, respectively. The global resolution at the same threshold is 2.60 Å. The resolution range is [2.60, 2.66]Å.

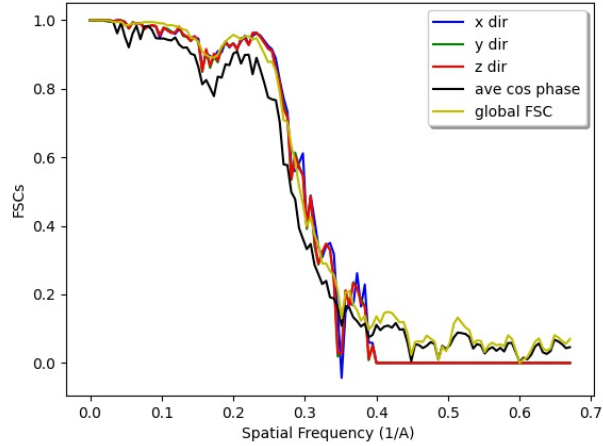


Figure 35: FSC in X, Y, Z, the global FSC, and the Average Cosine Phase.

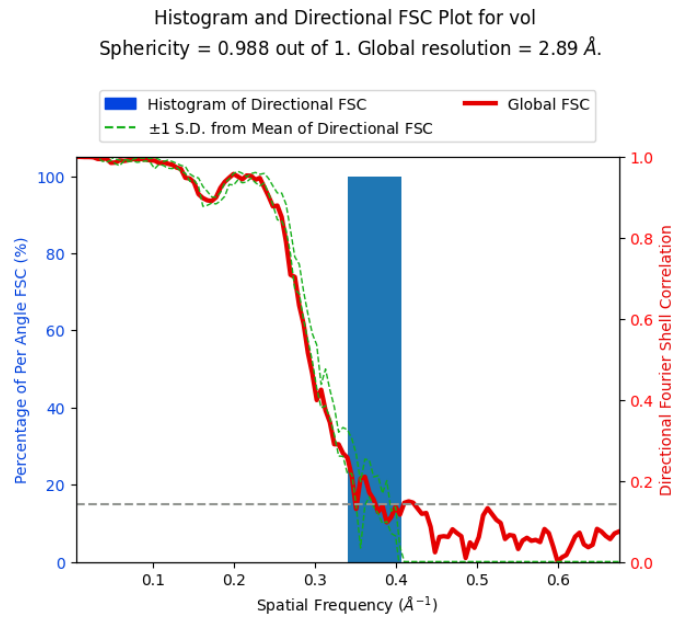


Figure 36: Global FSC and histogram of the directional FSC.

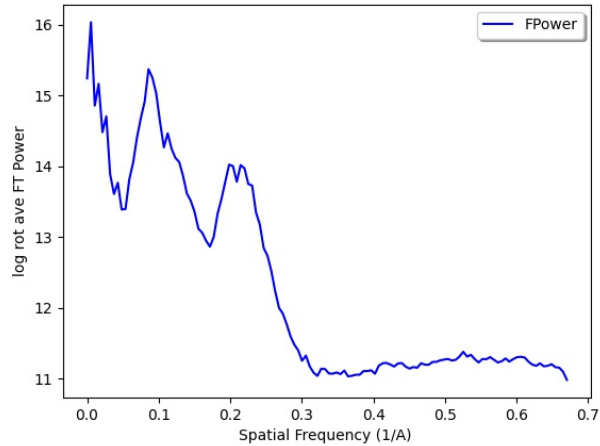


Figure 37: Logarithm of the radial average of the input map power in Fourier space.

Automatic criteria: The validation is OK if the resolution provided by the user is not smaller than 0.8 the resolution estimated by the first cross of the global directional FSC below 0.143.

STATUS: OK

5 2D Classes

Set of 2D classes: /home/coss/ScipionUserData/projects/Example_10248_Scipion3/-Runs/012458_XmippProtCropResizeParticles/extra/output_images.stk

The classes can be seen in Fig. 38.

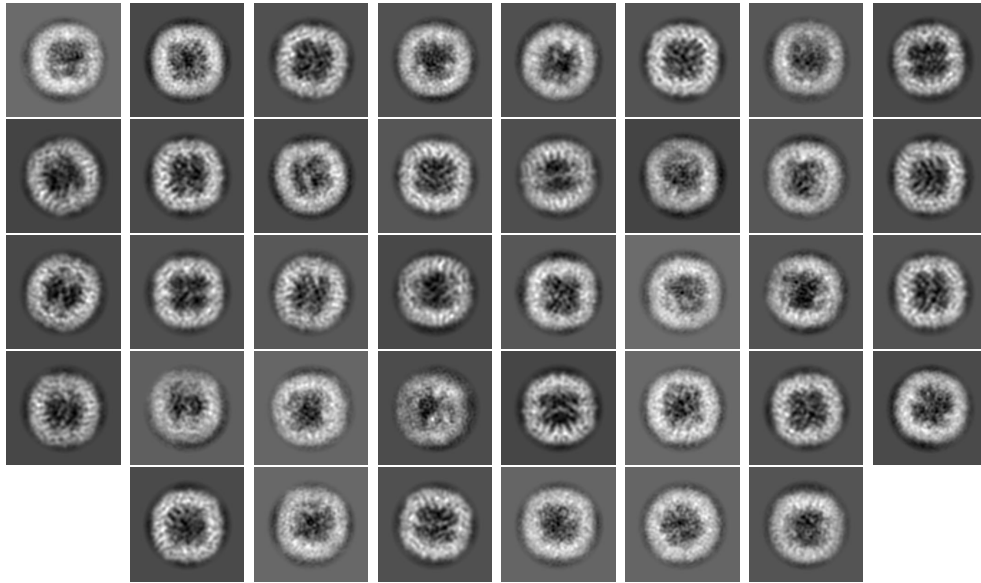


Figure 38: Set of 2D classes provided by the user

6 Level 2 analysis

6.1 Level 2.a Reprojection consistency

Explanation:

The 2D classes can be aligned against the reconstructed map, then the correlation between rejections of the map and the 2D classes can be analyzed. Also, analyzing the residuals (2D class minus the corresponding reprojction) can reveal systematic differences between them.

Results:

Fig. 39 shows the histogram of the cross-correlation between the 2D classes and the map rejections. The average correlation is 0.843624, and its range is [0.717260,0.906353]. Now we show the 2D classes, the corresponding reprojction, the difference between both (residual), the covariance matrix of the residual image, and the correlation between the 2D class and the reprojction. For a perfect match, the residual would be just noise, and its covariance matrix should be a diagonal. Rows have been sorted by correlation so that

the worse correlating images are displayed at the beginning.

Also, 2D classes of a high-resolution map should also be of high resolution. This cannot, for the moment, be automatically assessed. But a visual inspection should confirm that the resolution of the 2D classes match the reported resolution of the map.

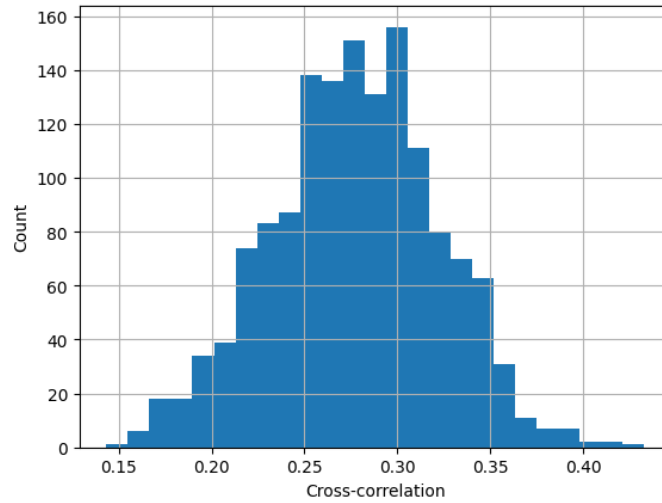
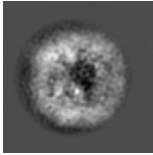
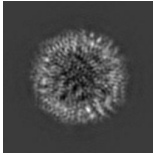
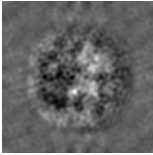
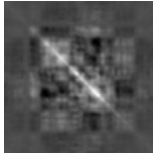
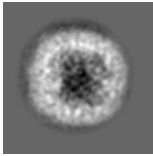
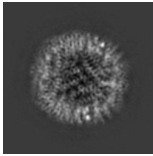
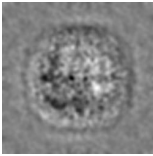
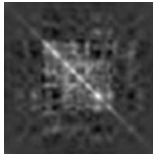
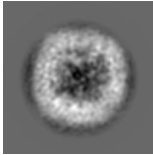
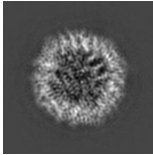
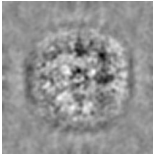
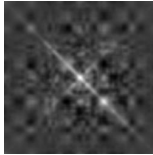
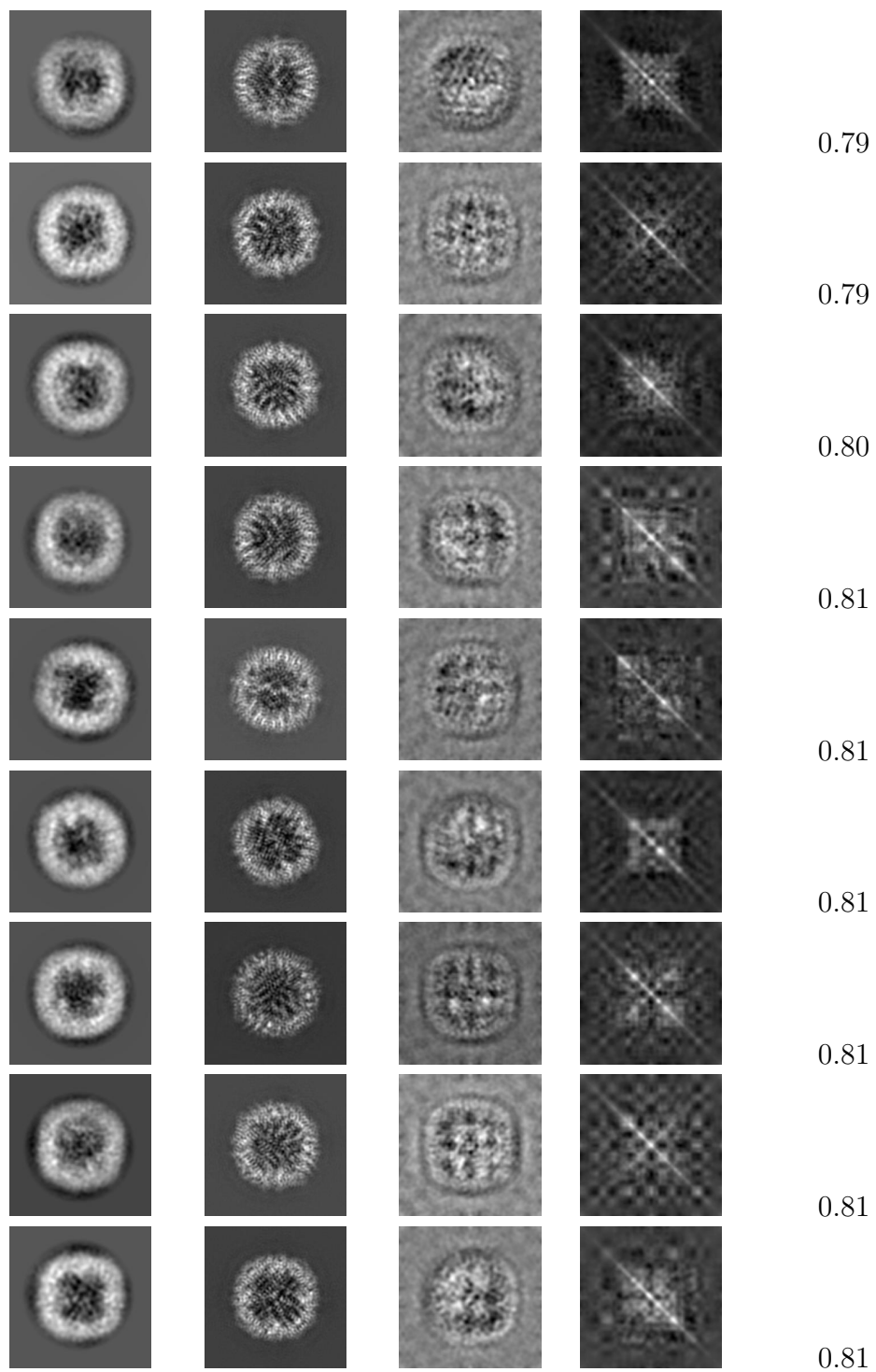
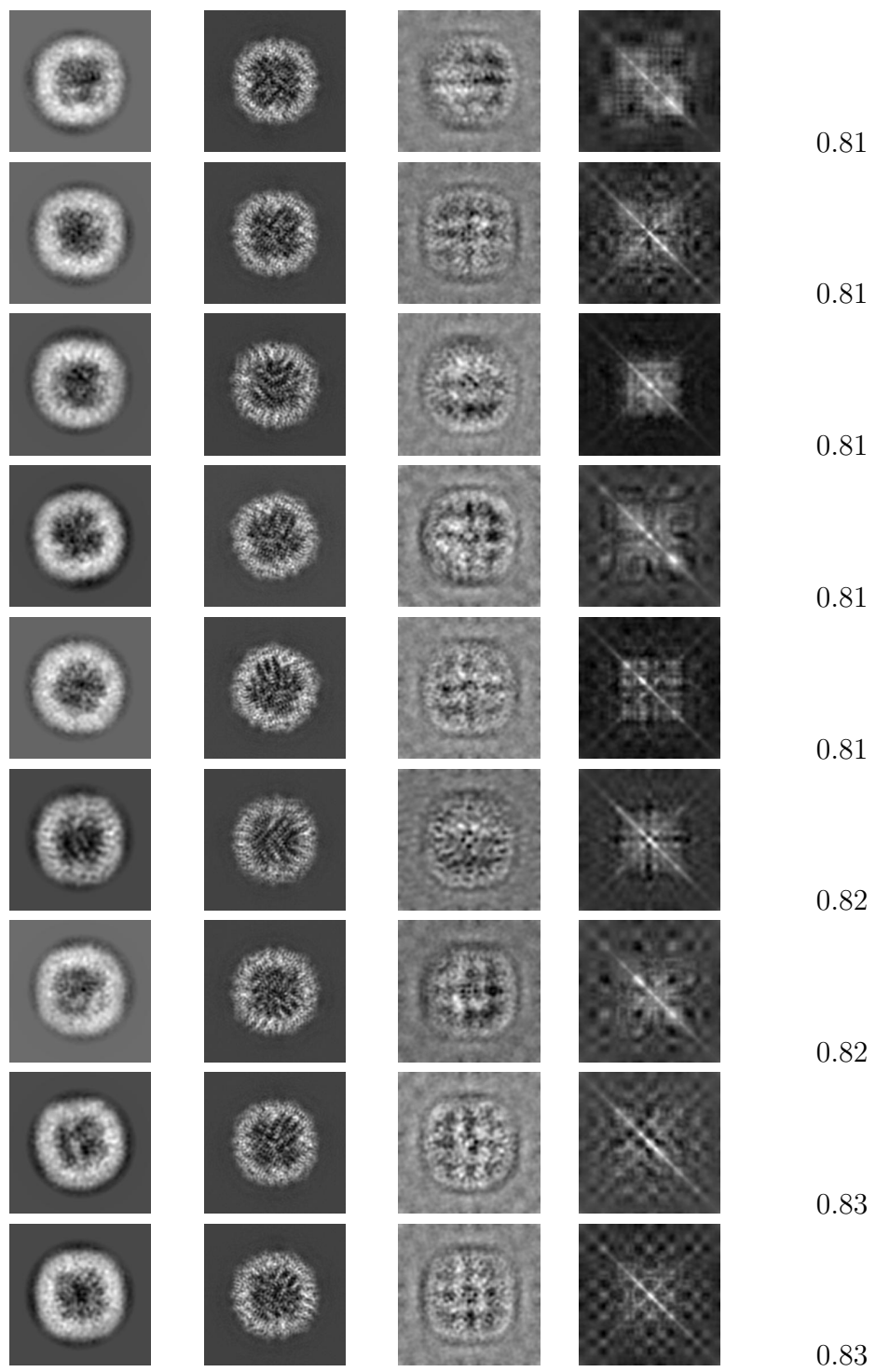
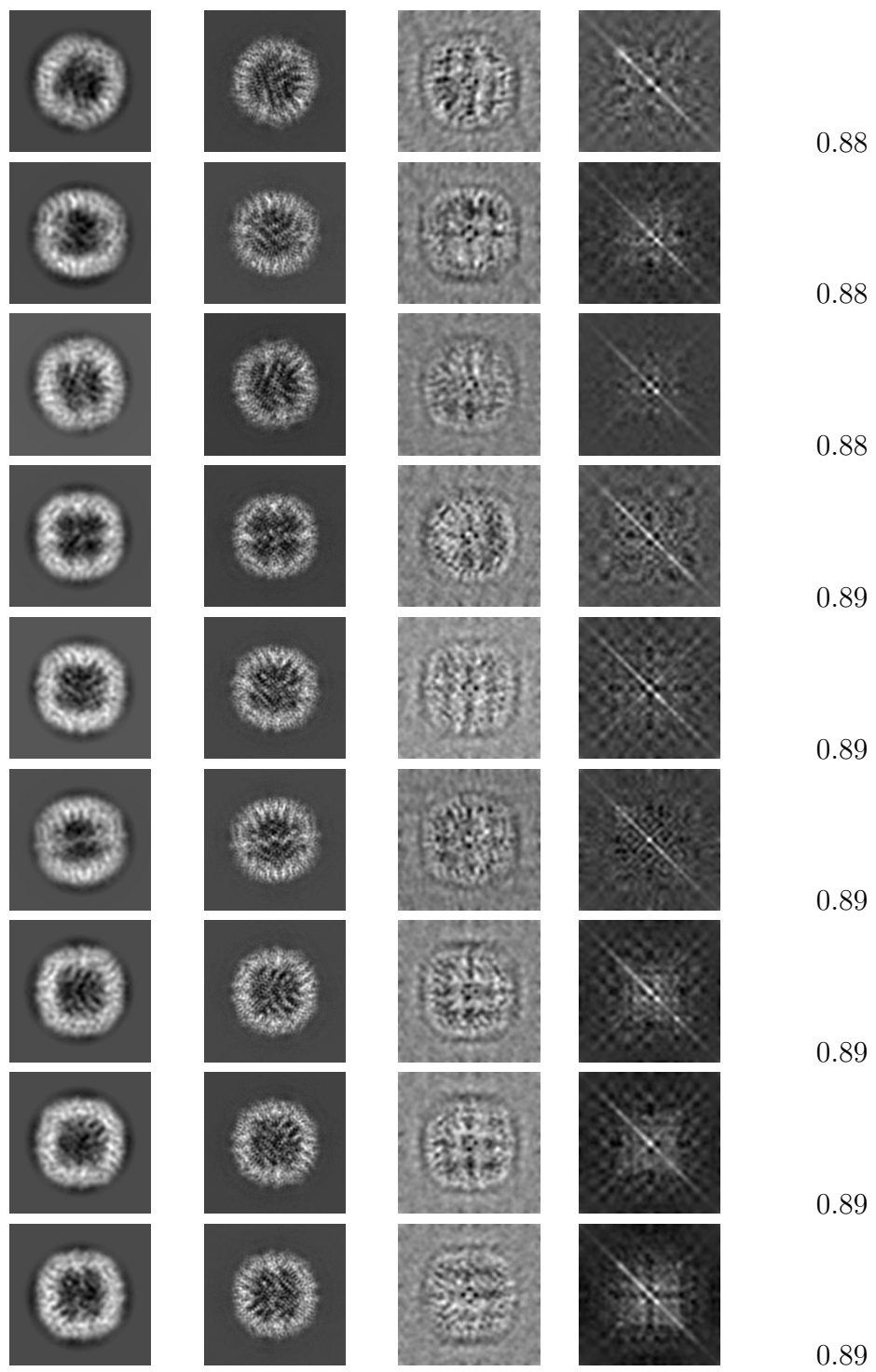


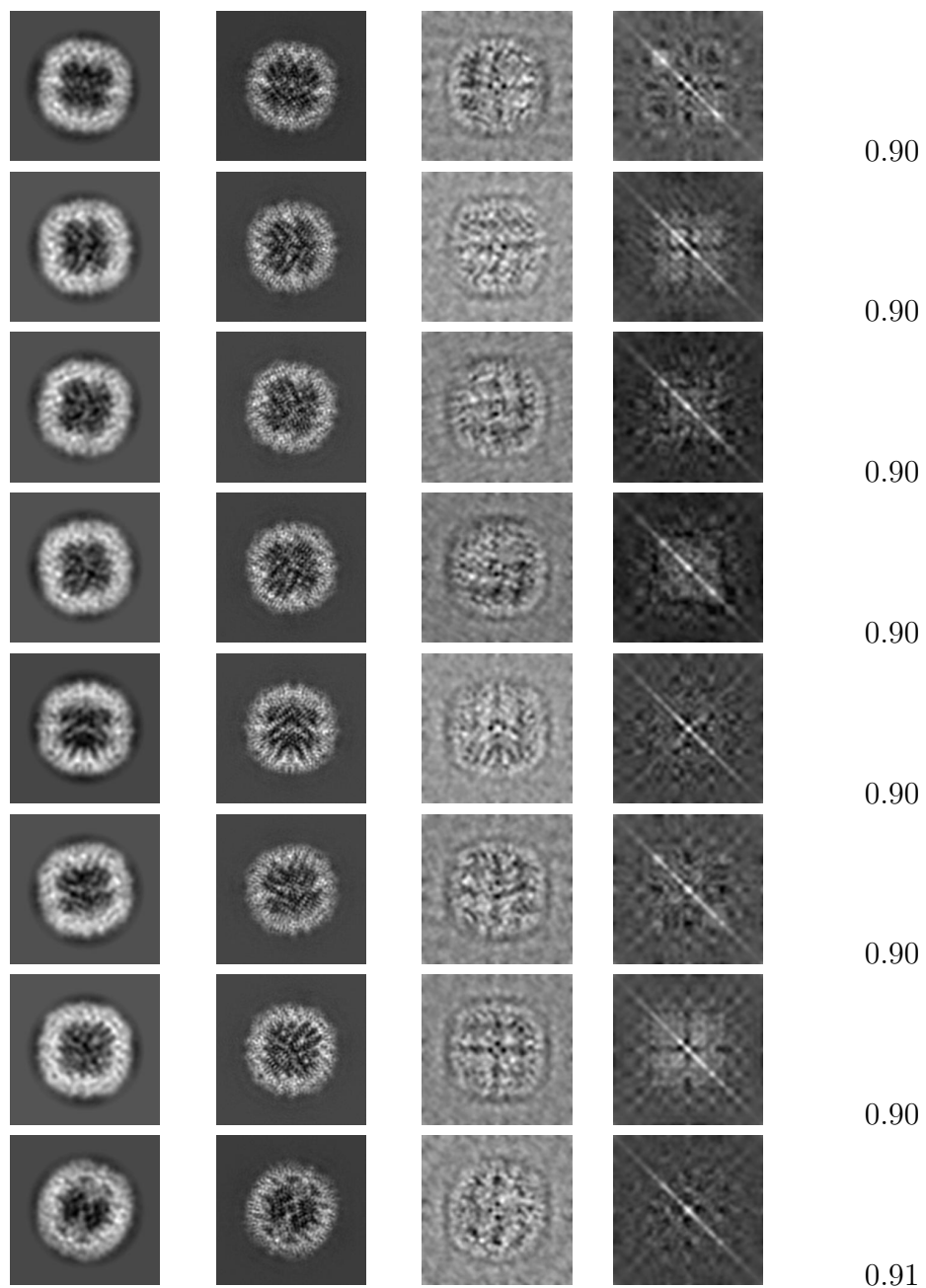
Figure 39: Histogram of the correlation coefficient between the 2D classes provided by the user and the corresponding reprojections.

2D Class	Reprojection	Residual	Covariance	Correlation
				0.72
				0.78
				0.79









Automatic criteria: The validation is OK if the proportion of classes for which the correlation is below 0.7 is smaller than 20%.

STATUS: OK

7 Particles

Set of Particles: /home/coss/ScipionUserData/projects/Example_10248_Scipion3/-Runs/010450_XmippProtReconstructHighRes/particles.sqlite

1457 images were provided by the user. The first 32 can be seen in Fig. 40.

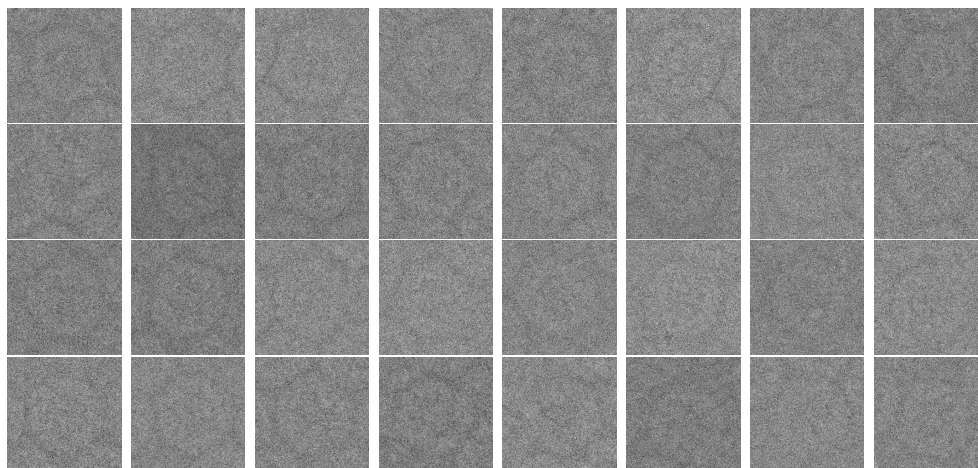


Figure 40: First particles of the set of particles provided by the user

8 Level 3 analysis

This analysis compares the experimental images provided to the 2D classes provided of Level 2.

8.1 Level 3.a Outlier detection

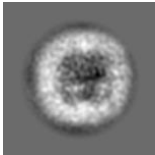
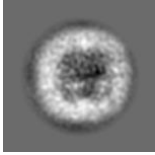
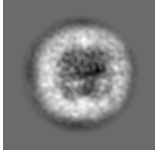
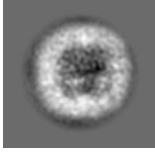
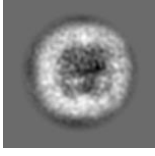
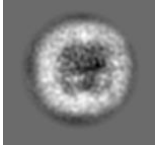
Explanation:

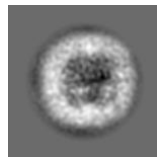
The set of particles is classified into the input set of 2D classes of Level 2. The number of particles that are considered to be outliers in those classes is

reported. A particle is an outlier if its Mahalanobis distance to the centroid of the class is larger than 3 [Sorzano et al., 2014]. This distance takes into account the covariance of the images assigned to that class.

Results:

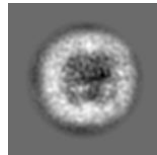
The following table shows the input classes, the number of particles assigned to them, and the fraction of these particles that are considered to be part of the core (the closer to 1, the better).

2D Class	No. Particles	Core fraction
	17	0.810
	10	0.833
	18	0.857
	35	0.875
	14	0.875
	22	0.880



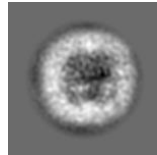
23

0.885



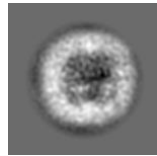
24

0.889



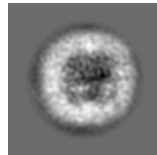
25

0.893



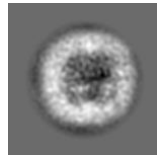
37

0.902



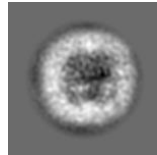
28

0.903



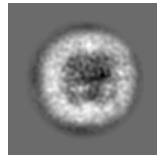
19

0.905



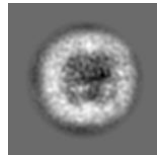
48

0.906



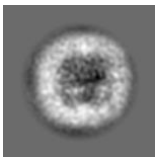
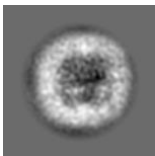
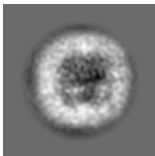
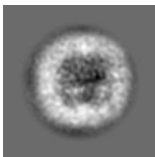
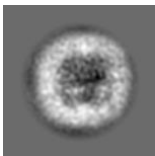
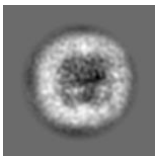
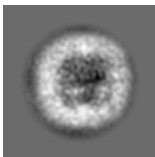
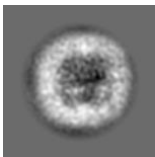
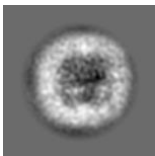
125

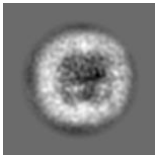
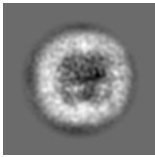
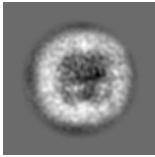
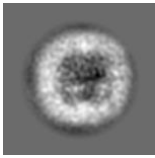
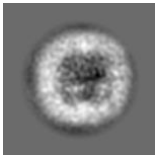
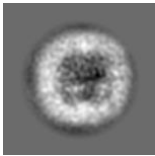
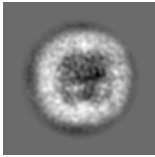
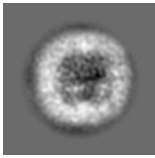
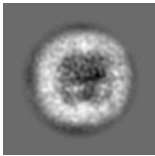
0.906



49

0.907

	20	0.909
	42	0.913
	32	0.914
	33	0.917
	46	0.920
	36	0.923
	40	0.930
	82	0.932
	102	0.936

	44	0.936
	64	0.941
	81	0.942
	88	0.946
	65	0.956
	25	0.962
	10	1.000
	5	1.000
	6	1.000

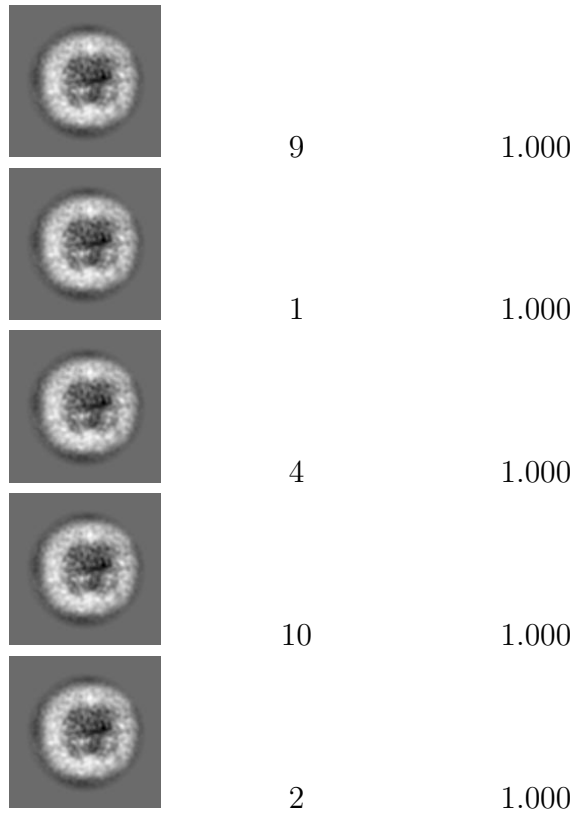


Fig. 41 shows the histogram of the core fraction of the classes. Fig. 42 shows the histogram of the size of the classes.

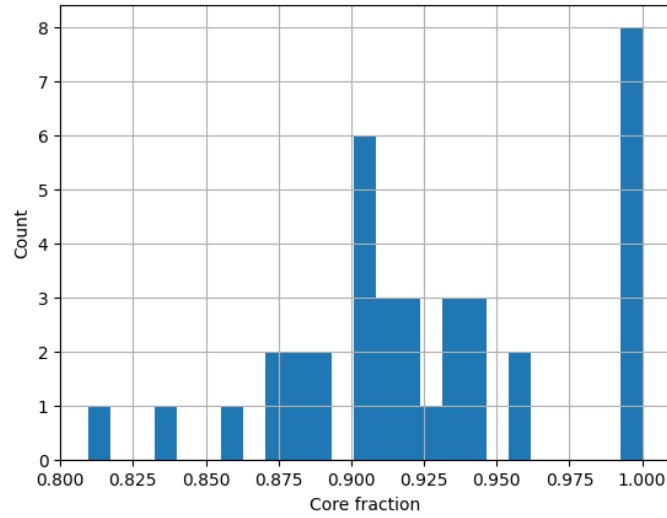


Figure 41: Histogram of the core fraction of the 2D classes.

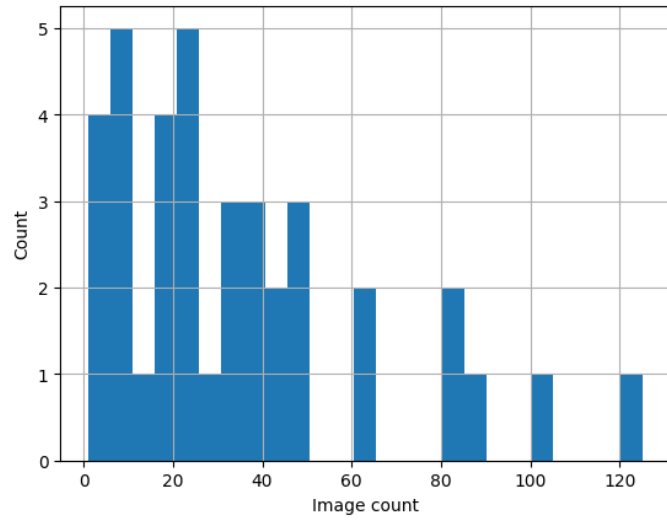


Figure 42: Histogram of the number of particles assigned to the 2D classes.

Automatic criteria: The validation is OK if the number of classes whose core is smaller than 70% of the size of the class is smaller than 20%.

STATUS: OK

8.2 Level 3.b Classification internal consistency

Explanation:

The input particles are classified in 2D clusters. The quality of the 2D clusters is assessed through Fourier Ring Correlation.

Results:

Fig. 43 shows the histogram of the resolution of each one of the classes. This resolution strongly depends on the number of particles assigned to the class, and this server only sees a small fraction of the particles. Fig. 44 shows a scatter plot of the resolution (in \AA^{-1}) in the classes versus the number of particles as measured by FRC=0.5.

The following table shows each class, the number of particles assigned to it, and its resolution as measured by FRC=0.5.

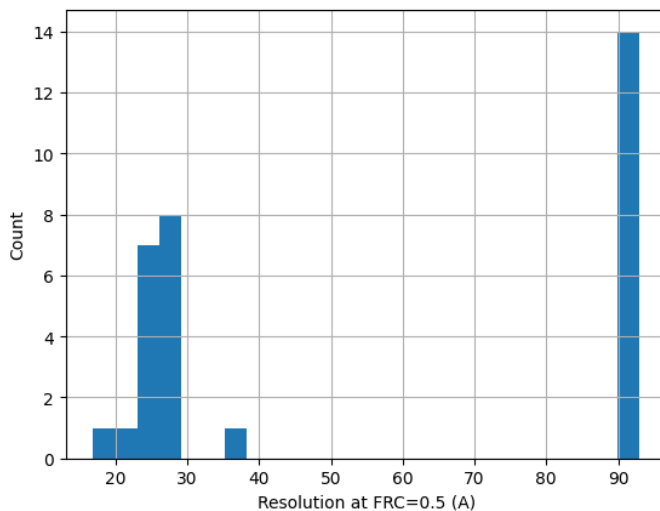


Figure 43: Histogram of the resolution at FRC=0.5 of the different classes.

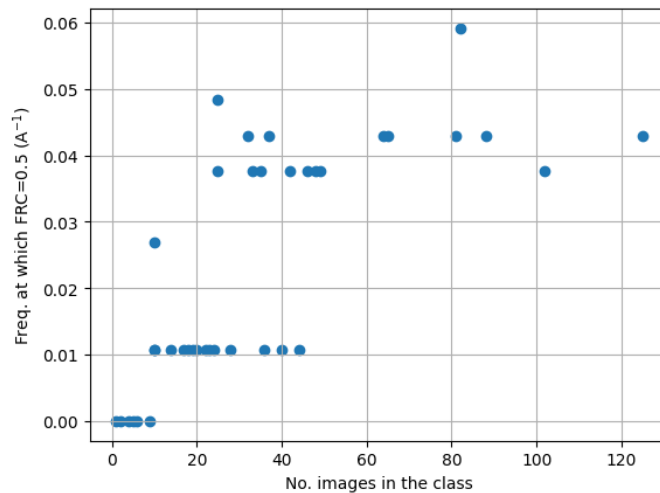


Figure 44: Scatter plot of the frequency at which FRC=0.5 (\AA^{-1}) vs the number of particles assigned to each class.

STATUS: Cannot be automatically evaluated

8.3 Level 3.c Classification external consistency

Explanation:

The input particles were classified with CryoSparc [Punjani et al., 2017] using the same number of classes as the ones provided by the user. Except for the difference in number of particles between the original classification and the number of particles available to the server, the new classes should resemble the old ones.

Results:

Fig. 45 shows the new classification. The classification provided by the user is in Fig. 38.

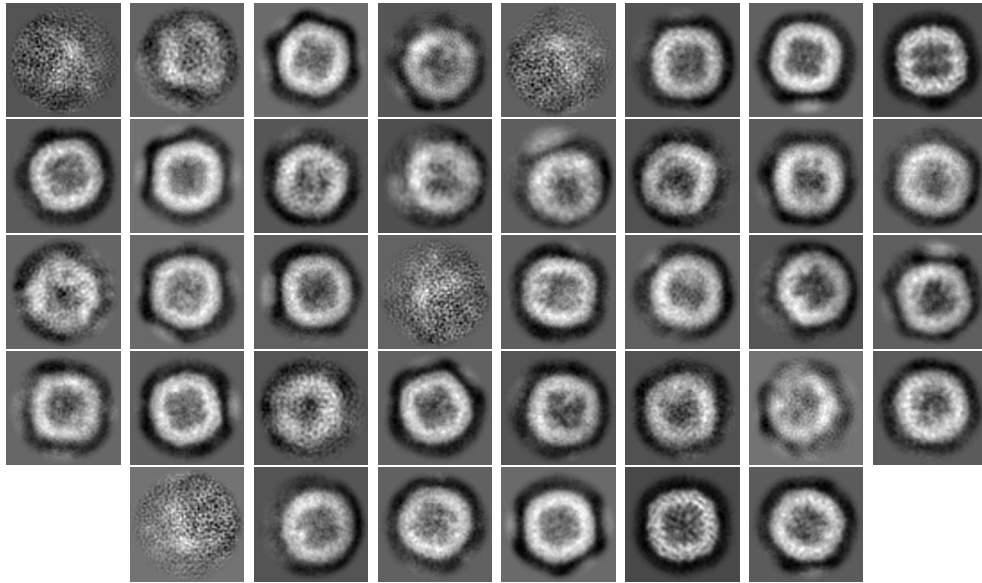


Figure 45: Set of 2D classes calculated by CryoSparc. These should be compared to those in Fig. 38.

Fig. 46 shows the probability density function of the correlation of the user classes compared to the newly computed and vice versa. Ideally, these two distributions should be similar. We compared these two distributions with a Kolmogorov-Smirnov (KS) two-sample test. The KS statistic was 0.236842 and the p-value 0.238941.

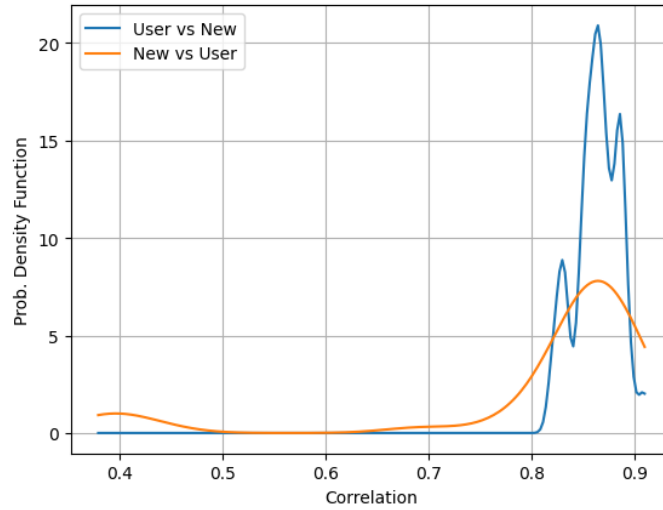
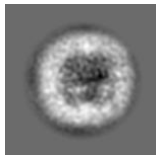
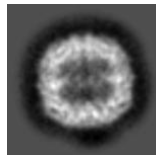
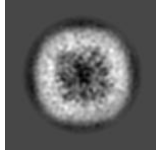
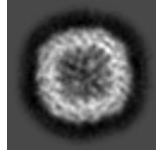
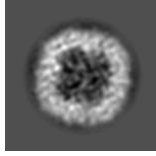
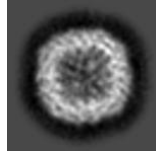
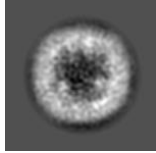
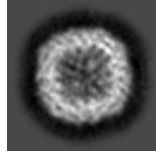
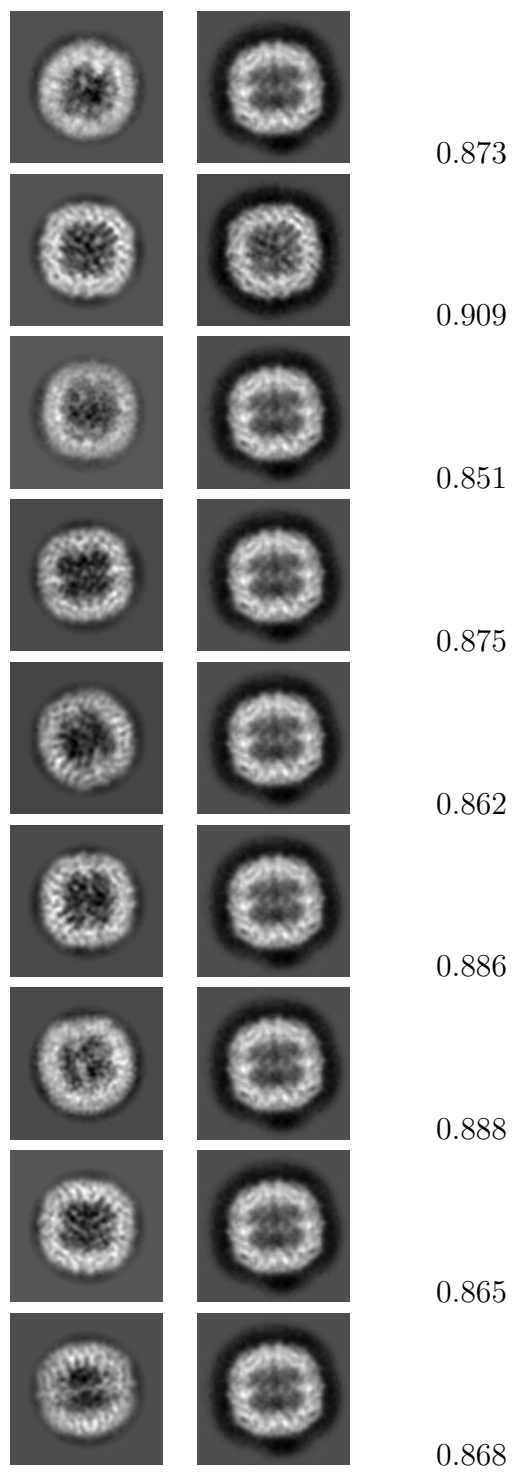
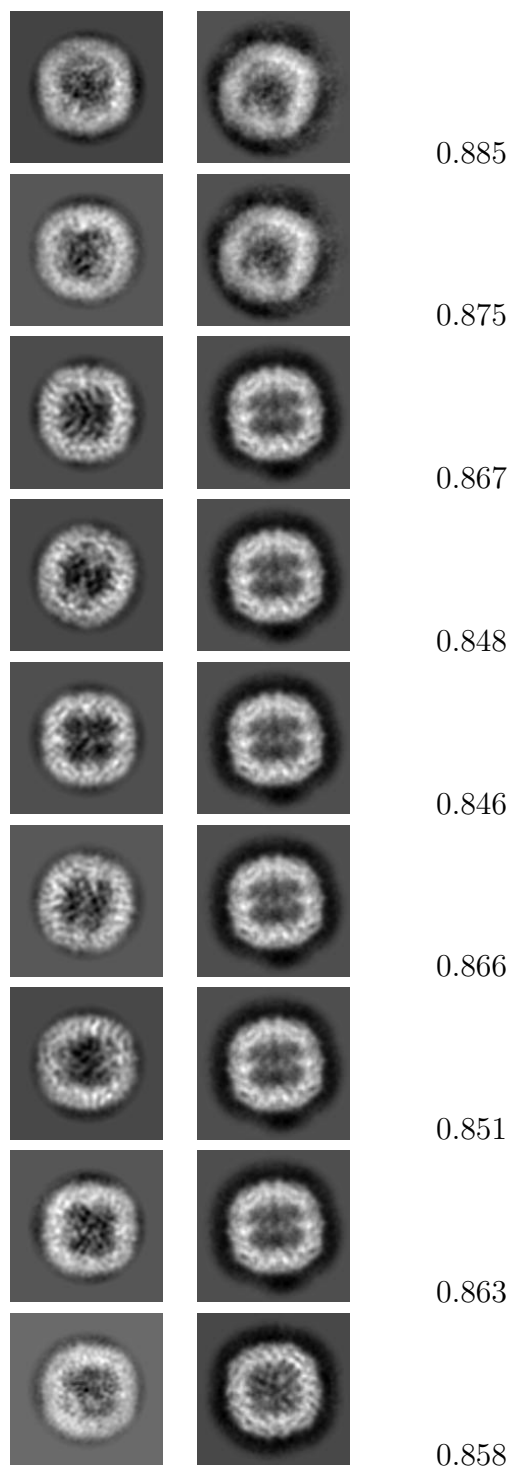


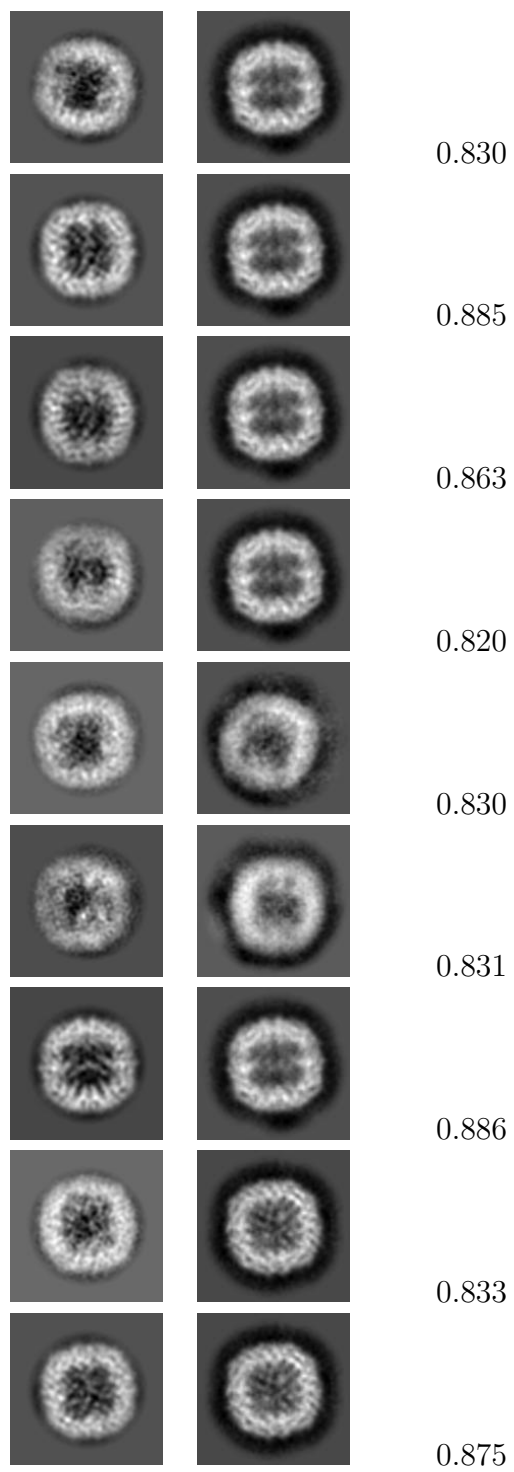
Figure 46: Probability density function of the correlation of the user classes compared to the newly computed classes and vice versa.

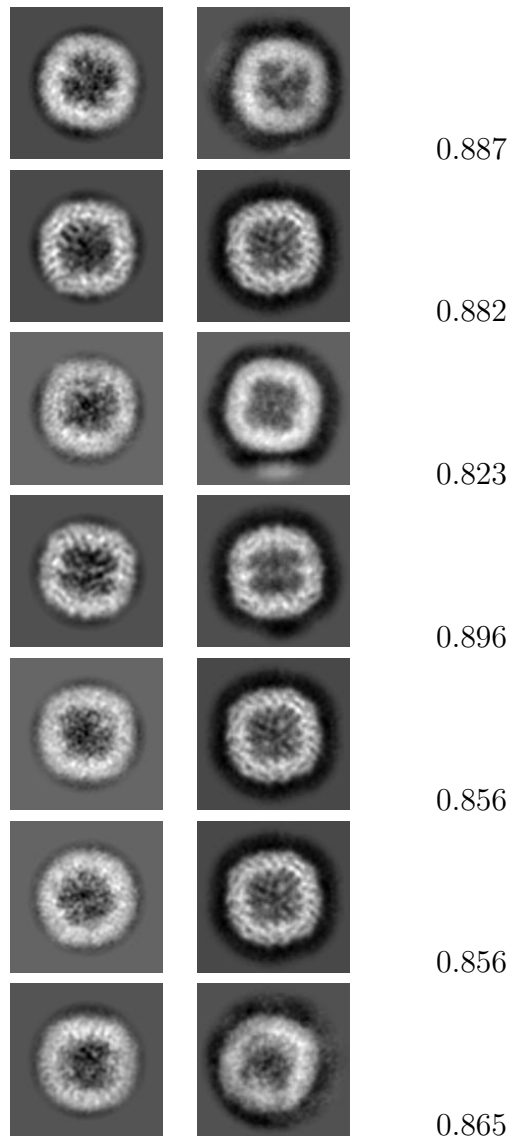
The following table shows for each class in the User set which is the best match in the New set and its correlation coefficient.

User class	New class	Correlation
		0.856
		0.887
		0.853
		0.866









Automatic criteria: The validation is OK if 1) no class from the user correlates less than 0.8 with the newly computed classes, and 2) the equality of the two correlation distributions (user vs new, new vs user) cannot be rejected with a threshold for the p-value of 0.001.

STATUS: [OK](#)

9 Level 4 analysis

This analysis compares the experimental images provided along with their angular assignment to the reconstructed map.

9.1 Level 4.a Similarity criteria

Explanation:

We measured the similarity between the experimental images, with the angles and shifts provided by the user, and reprojections of the input map along the same direction. We measured the correlation and IMED (IMage Euclidean Distance, which is a generalized measure of the standard Euclidean Distance in which nearby pixels also contribute to the calculation of the final distance between the image at a given point) [Sorzano et al., 2015] between both sets of images. If the set of particles is properly assigned there should be a single peak in the 1D histograms of these two similarity measures, and a single cloud in their joint scatter plot. The presence of multiple peaks could reveal a mixture of different conformations, the presence of misaligned particles or contaminations, or the difference between isolated particles and particles with other objects around.

It must be noted that there is a dependence between similarity metrics and defocus. Typically this dependence is such that lower defoci imply lower similarity due to the smallest contrast. You have to be sure that the groups seen in the similarity measures are not caused by defocus groups.

Results:

Fig. 47 shows the histograms of the cross-correlation and IMED, a joint scatter plot and the dependence of the cross-correlation with the defocus.

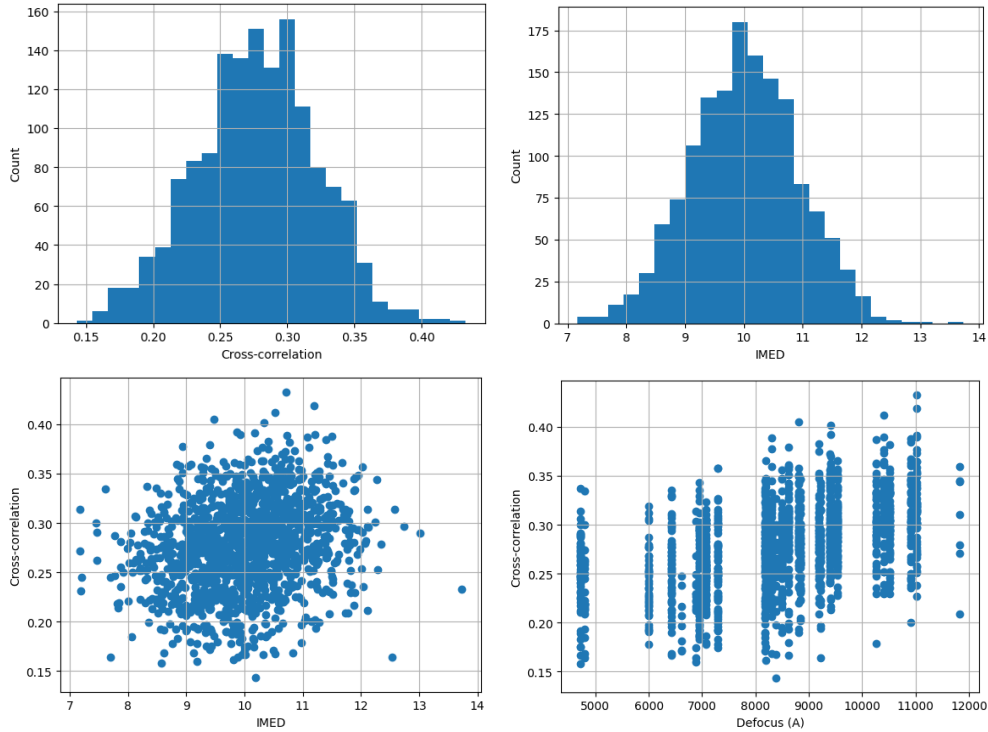


Figure 47: Top: Histogram of the cross-correlation (CC) and IMED between the experimental images and their corresponding reprojections. Bottom: Scatter plots of CC vs IMED, and CC vs defocus.

STATUS: Cannot be automatically evaluated

9.2 Level 4.b Alignability smoothness

Explanation:

This algorithm [Méndez et al., 2021] analyzes the smoothness of the correlation function over the projection sphere and the stability of its maximum. Ideally, the angular assignment given by the user should coincide with the maximum of the smoothed cross-correlation landscape.

Results:

Fig. 48 shows the histogram of the angular distance between the angular

assignment given by the user and the maximum of the smoothed landscape of cross-correlations. plot. The average angular distance 11.946. The percentage of images whose distance is larger than 10 is 50.2%.

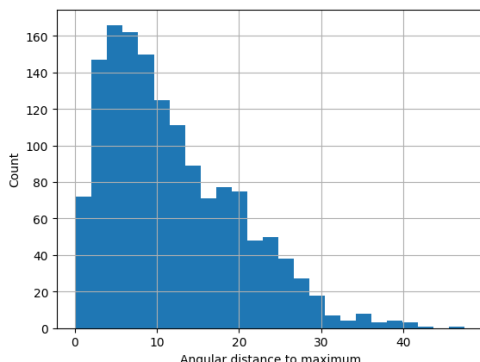


Figure 48: Histogram of the angular distance between the angular assignment given by the user and the maximum of the smoothed landscape of cross-correlation.

Automatic criteria: The validation is OK if less than 30% of the images have their angular assignment is further than 10 degrees from the smoothed cross-correlation maximum.

WARNINGS: 1 warnings

1. **The percentage of images whose angular assignment is significantly away from the smoothed maximum is too high, 50.2%**

9.3 Level 4.c Alignability precision and accuracy

Explanation:

The precision [Vargas et al., 2016] analyzes the orientation distribution of the best matching reprojections from the reference volume. If the high values are clustered around the same orientation, then the precision is close to 1. Otherwise, it is closer to -1. Below 0.5 the best directions tend to be scattered. The alignability accuracy [Vargas et al., 2017] compares the final angular assignment with the result of a new angular assignment. The similarity between both is again encoded between -1 and 1.

Results:

Fig. 49 shows the histograms of the accuracy and precision, and a joint scatter plot. The average accuracy was 0.701 and the average precision 0.789. The percentage of images whose accuracy is below 0.5 is 18.3%, and the percentage of images whose precision is below 0.5 is 8.1%.

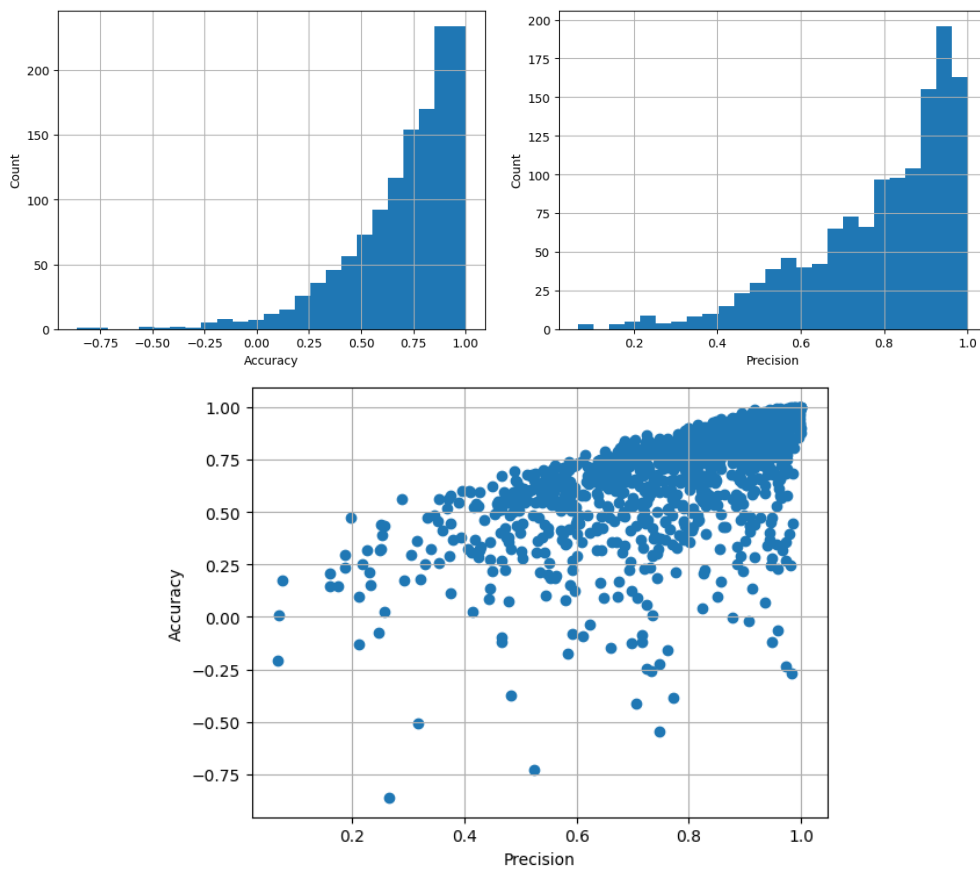


Figure 49: Top: Histogram of the accuracy and precision. Bottom: Scatter plot of both measures.

Automatic criteria: The validation is OK if less than 30% of the images have an 1) accuracy and 2) precision smaller than 0.5.

STATUS: OK

9.4 Level 4.d1 Relion alignment

Explanation:

We have performed an independent angular assignment using Relion autorefine [Scheres, 2012]. Images were downsampled to a pixel size of 3\AA . Then, we measured the difference between the angular assignment of the particles given by the user and the one done by Relion.

Results:

Fig. 50 shows some representative slices of the reconstruction performed by Relion for checking its correctness.

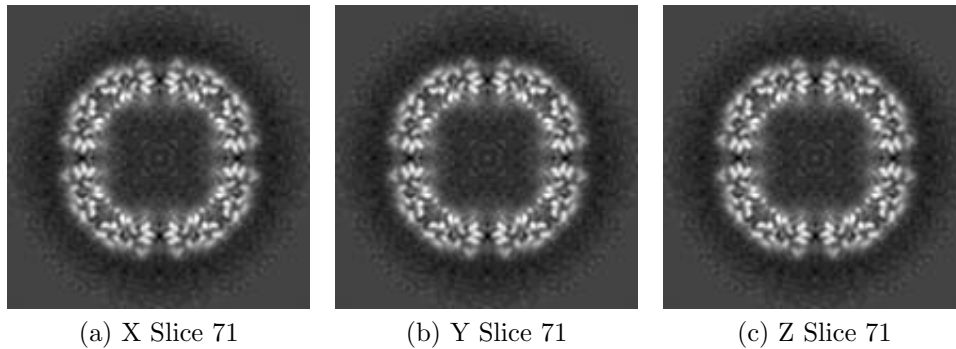


Figure 50: Slices of maximum variation in the three dimensions of the map reconstructed by Relion

Fig. 51 shows the shift and angular difference between the alignment given by the user and the one calculated by Relion. The median shift difference was 0.3\AA , and the median angular difference 0.5 degrees. Their corresponding median absolute deviations were 0.2 and 0.3 , respectively. Particles with a shift difference larger than 5\AA or an angular difference larger than 5 degrees would be considered as incorrectly assigned in one of the two assignments (the user's or the new one). 0.1% of particles were considered to have an uncertain shift, and 0.5% of particles were considered to have an uncertain

alignment.

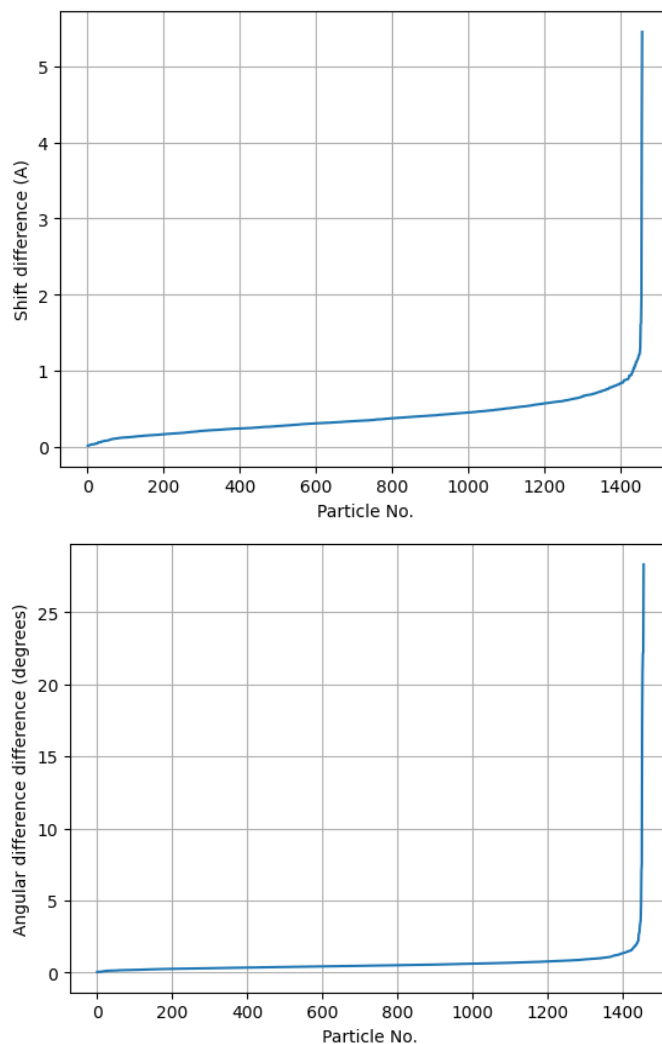


Figure 51: Top: Shift difference between the alignment given by the user and the one calculated by Relion. Bottom: Angular difference. The X-axis represents all particles sorted by their difference.

Automatic criteria: The validation is OK if less than 20% of the images have 1) a shift difference larger than 5\AA , and 2) an angular difference larger than 5 degrees.

STATUS: OK

9.5 Level 4.d2 CryoSparc alignment

Explanation:

We have performed an independent angular assignment using CryoSparc non-homogeneous refinement [Punjani et al., 2020]. Images were downsampled to a pixel size of 3\AA . Then, we measured the difference between the angular assignment of the particles given by the user and the one done by CryoSparc.

Results:

Fig. 52 shows some representative slices of the reconstruction performed by Cryosparc for checking its correctness.

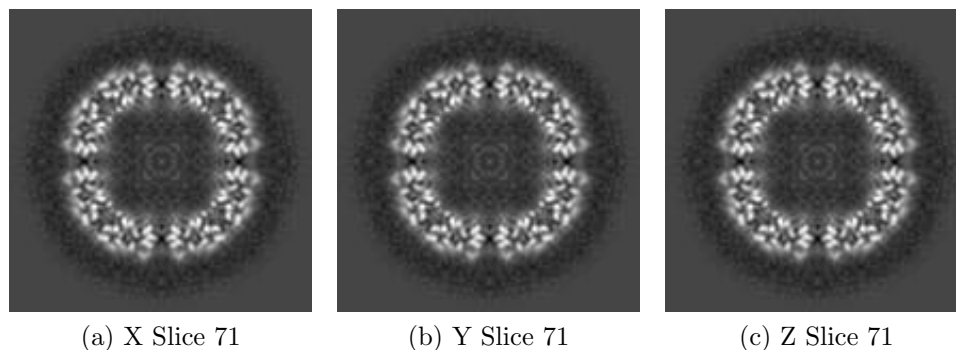


Figure 52: Slices of maximum variation in the three dimensions of the map reconstructed by Cryosparc

Fig. 53 shows the shift and angular difference between the alignment given by the user and the one calculated by CryoSparc. The median shift difference was 3.2\AA , and the median angular difference 0.5 degrees. Their corresponding median absolute deviations were 1.9 and 0.2 , respectively. Particles with a shift difference larger than 5\AA or an angular difference larger than 5 degrees would be considered as incorrectly assigned in one of the two assignments (the user's or the new one). 23.1% of particles were considered

to have an uncertain shift, and 0.1% of particles were considered to have an uncertain alignment.

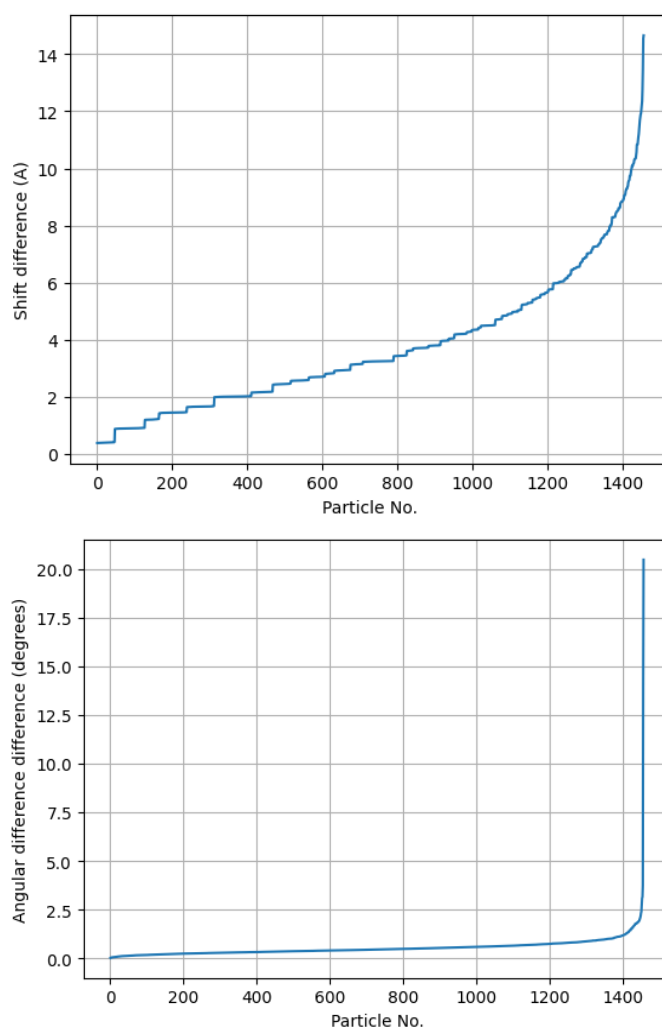


Figure 53: Top: Shift difference between the alignment given by the user and the one calculated by CryoSparc. Bottom: Angular difference. The X-axis represents all particles sorted by their difference.

Automatic criteria: The validation is OK if less than 20% of the images have 1) a shift difference larger than 5\AA , and 2) an angular difference

larger than 5 degrees.

WARNINGS: 1 warnings

1. **The percentage of images with uncertain shift is larger than 20%**

9.6 Level 4.d3 Relion/CryoSparc alignments

Explanation:

In Secs. 9.4 and 9.5 we compared the angular assignment given by the user to the angular assignment of Relion and CryoSparc, respectively. We now compare these two alignments as a way to measure the “intrinsic” uncertainty in the angular assignment. This comparison gives an estimate of the alignability of the input images.

Results:

Fig. 54 shows the shift and angular difference between the alignment given by Relion and the one calculated by CryoSparc. The median shift difference was 3.2\AA , and the median angular difference 0.3 degrees. Their corresponding median absolute deviations were 2.0 and 0.2 , respectively. Particles with a shift difference larger than 5\AA or an angular difference larger than 5 degrees would be considered as incorrectly assigned in one of the two assignments (the user’s or the new one). 23.7% of particles were considered to have an uncertain shift, and 0.6% of particles were considered to have an uncertain alignment.

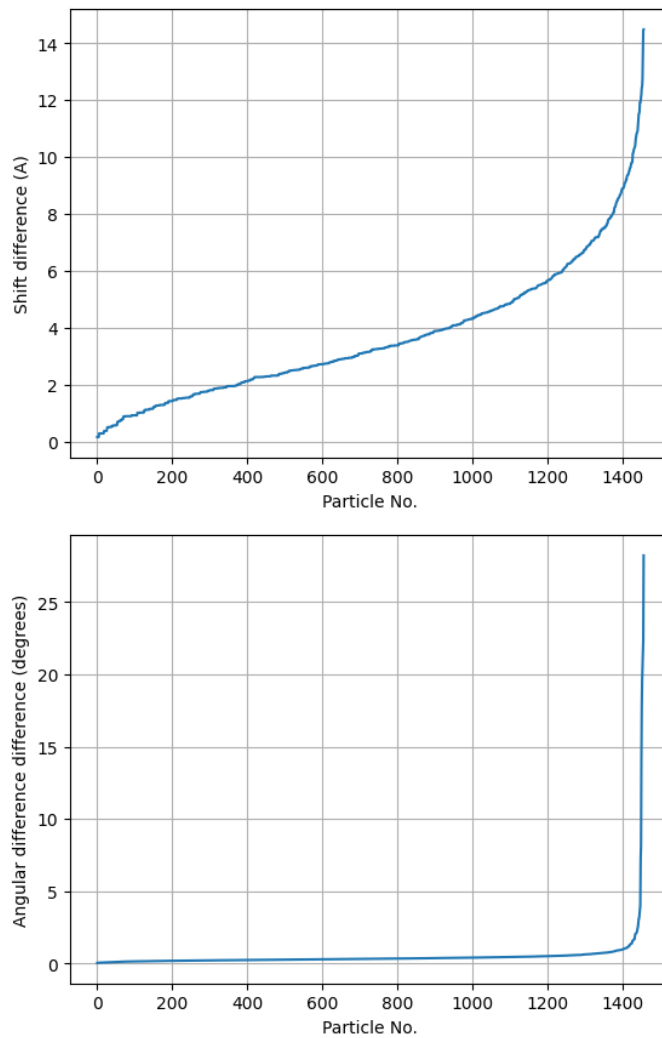


Figure 54: Top: Shift difference between the alignment given by Relion and the one calculated by CryoSparc. Bottom: Angular difference. The X-axis represents all particles sorted by their difference.

Automatic criteria: The validation is OK if less than 20% of the images have 1) a shift difference larger than 5\AA , and 2) an angular difference larger than 5 degrees.

WARNINGS: 1 warnings

1. **The percentage of images with uncertain shift is larger than 20%**

9.7 Level 4.e Classification without alignment

Explanation:

We have performed a 3D classification of the input particles in two classes without aligning them using Relion [Scheres, 2012] to confirm they belong to a single state. Images were downsampled to a pixel size of 3Å. A valid result would be: 1) a class attracting most particles and an almost empty class, 2) two classes with an arbitrary number of images in each one, but without any significant structural difference between the two.

Results:

The classification converged to a single class with 1457 out of 1457 images in it.

Automatic criteria: The validation is OK if the classification converged to a single class.

STATUS: OK

9.8 Level 4.f Overfitting detection

Explanation:

The detection of overfitting can be performed through a series of 5 reconstructions with an increasing number of experimental particles and the same number of pure noise particles [Heymann, 2015]. The resolution of the reconstructions with experimental particles should always be better than those from noise.

Results:

We tested with subsets of 21, 72, 218, 546 and 728 particles. Fig. 55 shows the inverse of the resolution as a function of the number of particles.

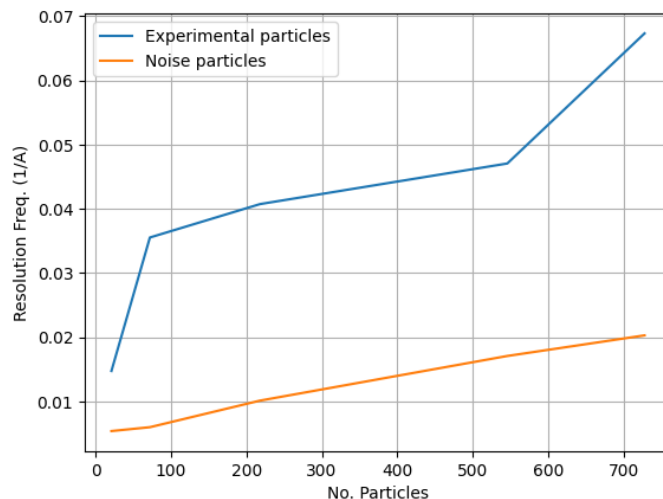


Figure 55: Inverse of the resolution as a function of the number of particles.

Automatic criteria: The validation is OK if the resolution of noise particles is never better than the resolution of true particles.

STATUS: OK

9.9 Level 4.g Angular distribution efficiency

Explanation:

This method [Naydenova and Russo, 2017] evaluates the ability of the angular distribution to fill the Fourier space. It determines a resolution per direction based on the number of particles in each direction and reports the distribution efficiency, a number between 0 (inefficient) and 1 (total efficiency).

Results:

Fig. 56 shows the histogram of the measured resolutions per direction. The average resolution was 2.6 Å, and its range [1.5, 3.4].

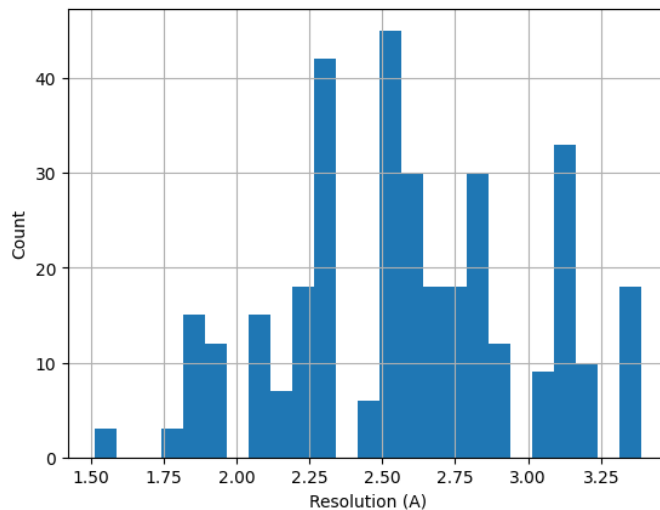


Figure 56: Histogram of the directional resolution according to the angular distribution efficiency.

Automatic criteria: The validation is OK if the resolution reported by the user is larger than 0.8 times the average directional resolution.

STATUS: OK

9.10 Level 4.h Sampling compensation factor

Explanation:

SCF [Baldwin and Lyumkis, 2020] measures the ability of the angular distribution to fill the Fourier space.

Results:

The results of the SCF analysis was:

Tilt= 0.0000

Number of zeros= 0.0000

Fraction of zeros= 0.0000

QkoverPk= 0.0000

SCF= 0.9498

SCFStar= 0.9498

Fig. 57 shows the SCF plot for this angular distribution.

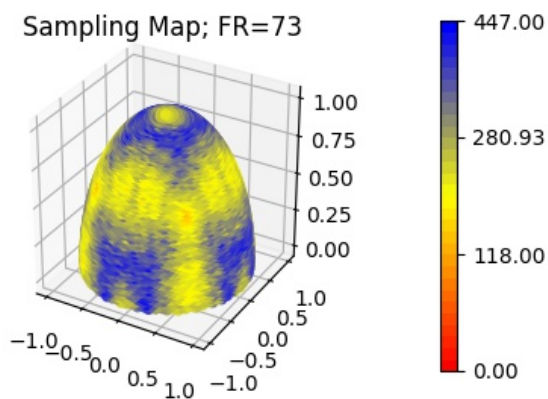


Figure 57: SCF plot.

Automatic criteria: The validation is OK if the $SCF^* > 0.5$.

STATUS: OK

9.11 Level 4.i CTF stability

Explanation:

We estimated the per-particle defocus, B-factor, astigmatism, and phase shift using Relion's ctf refine. Ideally, the differences in defoci cannot be larger than the ice thickness. We also estimated the local magnification offsets (which should be around 0) and the B-factor.

Results:

The following list shows the median, confidence intervals and links to the histograms for the refined parameters. Ideally these should all concentrate around 0, except for the defocus and the phase shift that must be centered around their true values.

Parameter	Median	95% Confidence interval	Histogram
Defocus (\AA)	8596.51	[4707.2,11021.6]	Fig. 58
Astigmatism (\AA)	336.38	[63.0,587.7]	Fig. 59
Defocus difference (\AA)	73.58	[-4515.4,3342.9]	Fig. 60
Astigmatism difference (\AA)	-17.92	[-430.6,327.5]	Fig. 61
Phase shift (degrees)	-5.06	[-20.7, 9.0]	Fig. 62
B-factor (\AA^2)	0.19	[-1.3, 3.4]	Fig. 63
Scale factor	0.052	[0.037,0.065]	Fig. 64

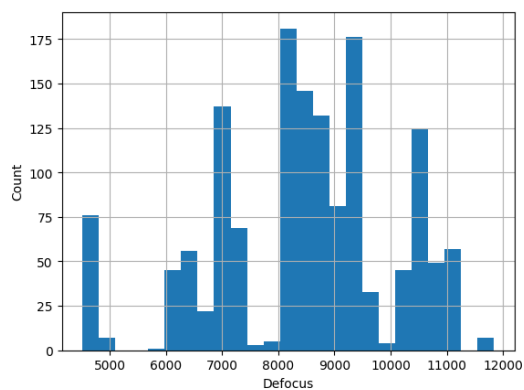


Figure 58: Histogram of the defocus after local refinement (\AA).

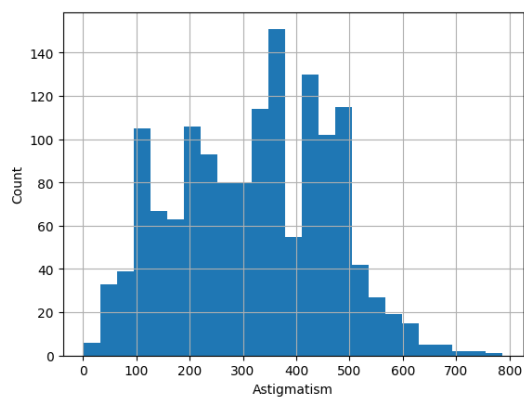


Figure 59: Histogram of the astigmatism after local refinement (\AA).

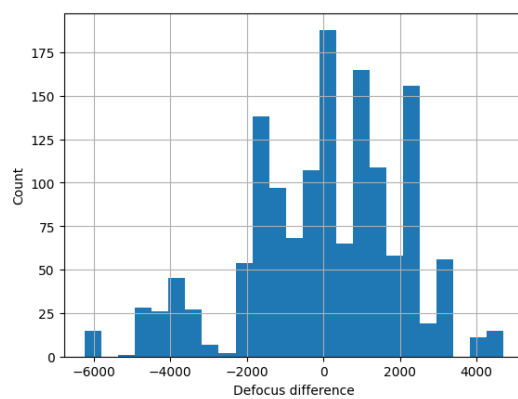


Figure 60: Histogram of the difference in defocus after local refinement (\AA).

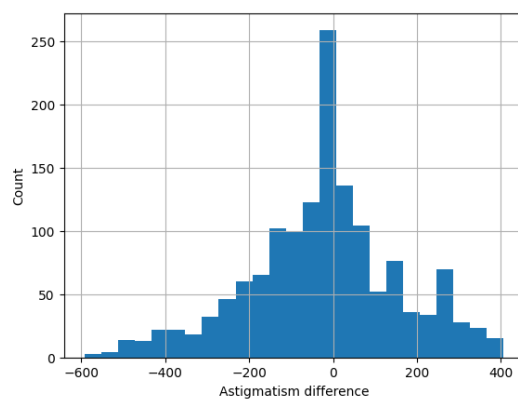


Figure 61: Histogram of the difference in astigmatism after local refinement (\AA).

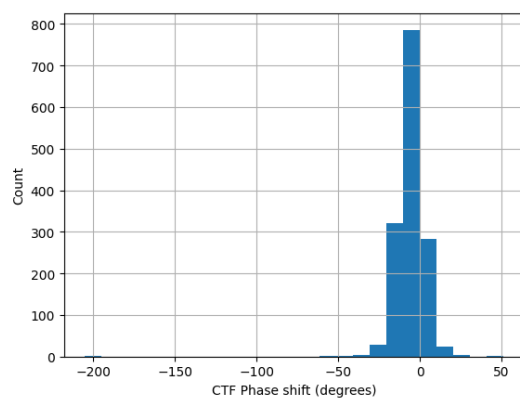


Figure 62: Histogram of the CTF phase shift (degrees).

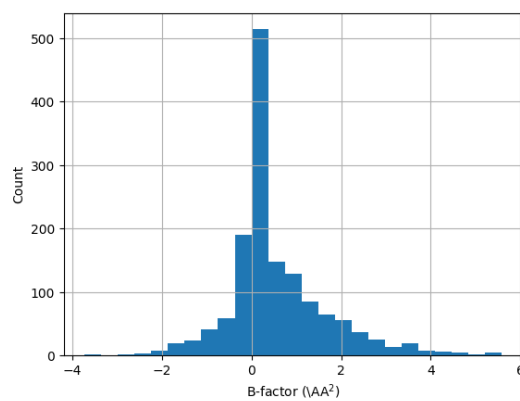


Figure 63: Histogram of the B-factor (\AA^2).

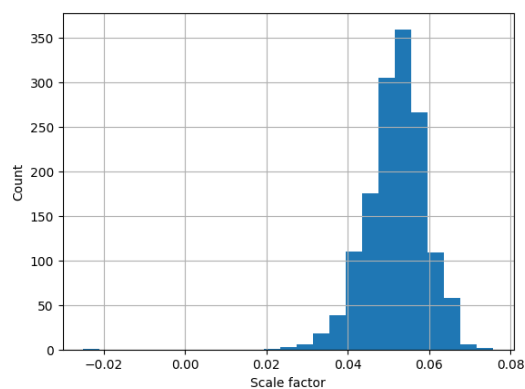


Figure 64: Histogram of the Scale factor.

Automatic criteria: The validation is OK if 1) astigmatism is between -5000 and 5000; 2) the defocus difference is between -5000 and 5000; 3) the astigmatism difference is between -5000 and 5000; 4) the B-factor is between -5 and 5; and 5) the scale factor is between -0.1 and 0.1.

WARNINGS: 1 warnings

1. **The 95% confidence interval of scale factor is not centered.**

10 Micrographs

Set of Micrographs: /home/coss/ScipionUserData/projects/Example_10248_Scipion3/-Runs/006458_XmippProtMovieCorr/extra/*mic.mrc

30 micrographs were provided by the user. The first 2 can be seen in Fig. 65.

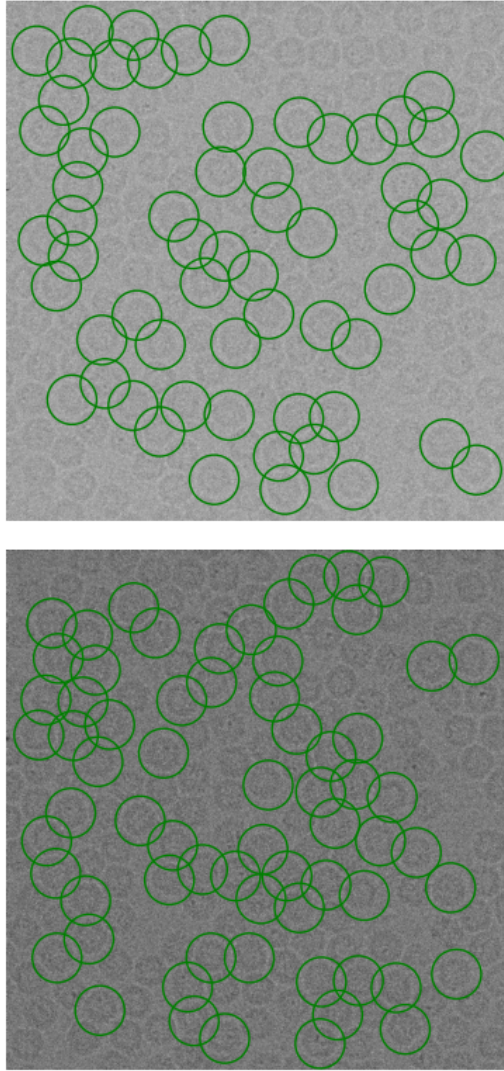


Figure 65: Two example micrographs with their coordinates.

11 Level 5 analysis

11.1 Level 5.a Micrograph cleaner

Explanation:

This method assigns a score between 0 (bad coordinate) and 1 (good coordi-

nate) reflecting the probability that the coordinate is outside a region with aggregations, ice crystals, carbon edges, etc. [Sanchez-Garcia et al., 2020]

Results:

0 coordinates out of 1457 (0.0 %) were scored below 0.9 by Micrograph-Cleaner.

Automatic criteria: The validation is OK if less than 20% of the coordinates are suspected to lie in aggregations, contaminations, ice crystals, etc.

STATUS: OK

12 Atomic model

Atomic model: /home/coss/ScipionUserData/projects/Example_10248_Scipion3/-centered4V1W.pdb

See Fig. 66.

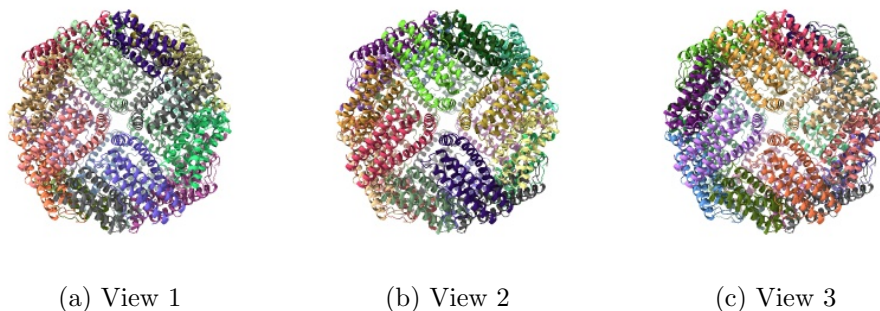


Figure 66: Input atomic model Views generated by ChimeraX at the following X, Y, Z angles: View 1 (0,0,0), View 2 (90, 0, 0), View 3 (0, 90, 0).

13 Level A analysis

13.1 Level A.a MapQ

Explanation:

MapQ [?] computes the local correlation between the map and each one of its atoms assumed to have a Gaussian shape.

Results:

Fig. 67 shows the histogram of the Q-score according calculated by MapQ. Some representative percentiles are:

Percentile	MapQ score [0-1]
2.5%	-0.38
25%	0.15
50%	0.40
75%	0.61
97.5%	0.81

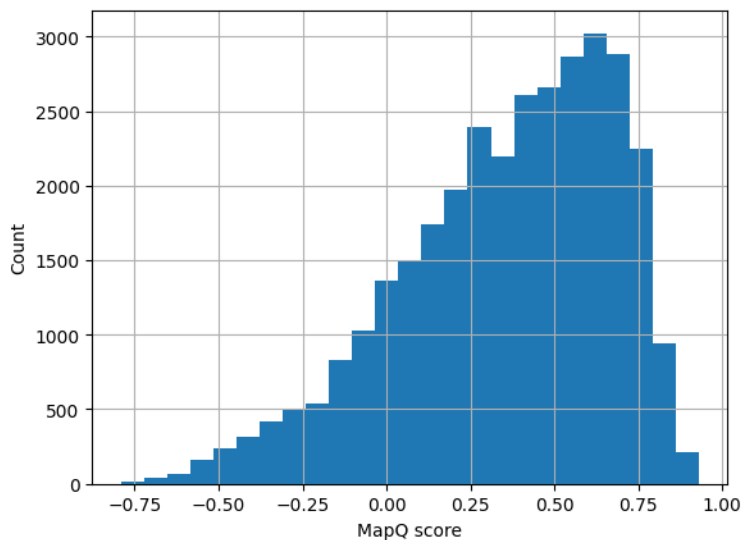


Figure 67: Histogram of the Q-score.

The following table shows the average Q score and estimated resolution for each chain.

Chain	Average Q score [0-1]	Estimated Resol. (Å)
A	0.36	4.3
B	0.36	4.3
C	0.37	4.2
D	0.36	4.3
E	0.36	4.3
F	0.36	4.3
G	0.35	4.3
H	0.36	4.3
I	0.35	4.3
J	0.36	4.3
K	0.36	4.3
L	0.36	4.3
M	0.35	4.3
N	0.35	4.3
O	0.36	4.3
P	0.35	4.3
Q	0.35	4.3
R	0.35	4.3
S	0.35	4.3
T	0.35	4.3
U	0.35	4.3
V	0.35	4.3
W	0.35	4.3
X	0.36	4.3

Automatic criteria: The validation is OK if the median Q-score is larger than 0.1.

STATUS: [OK](#)

13.2 Level A.b FSC-Q

Explanation:

FSC-Q [Ramírez-Aportela et al., 2021] compares the local FSC between the

map and the atomic model to the local FSC of the two half maps. FSC-Qr is the normalized version of FSC-Q to facilitate comparisons. Typically, FSC-Qr should take values between -1.5 and 1.5, being 0 an indicator of good matching between map and model.

Results:

Fig. 68 shows the histogram of FSC-Qr and Fig. 69 the colored isosurface of the atomic model converted to map. The average FSC-Qr is 0.53, its 95% confidence interval is [-1.00, 2.39]. The percentage of values whose FSC-Qr absolute value is beyond 1.5 is 7.2 %.

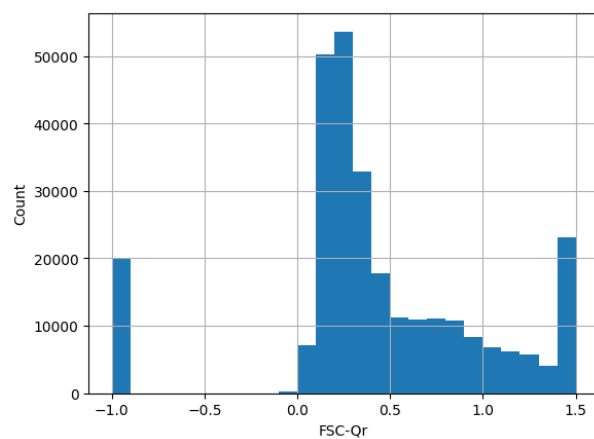


Figure 68: Histogram of the FSC-Qr limited to -1.5 and 1.5.

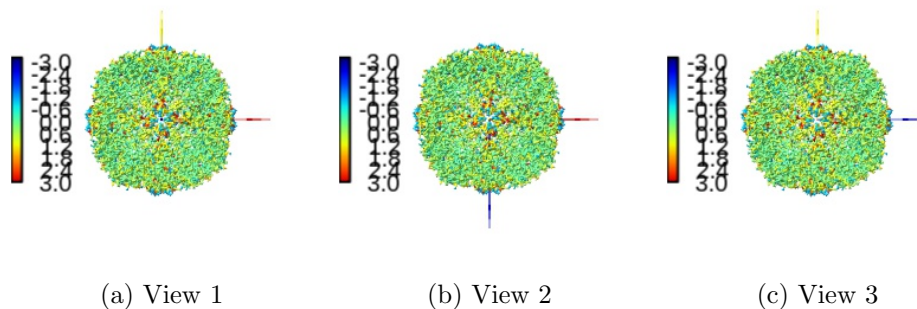


Figure 69: Isosurface of the atomic model colored by FSC-Qr between -1.5 and 1.5 Views generated by ChimeraX at a the following X, Y, Z angles: View 1 (0,0,0), View 2 (90, 0, 0), View 3 (0, 90, 0).

Automatic criteria: The validation is OK if the percentage of residues whose FSC-Q is larger than 1.5 in absolute value is smaller than 10%.

STATUS: OK

13.3 Level A.c Multimodel stability

Explanation:

The method of [Herzik et al., 2019] estimates the ambiguity of the atomic model in each region of the CryoEM map due to the different local resolutions or local heterogeneity.

Results:

Fig. 70 shows the histogram of the RMSD of the different models. The average RMSD between models is 0.45 Å. Fig. 71 shows the atomic model colored by RMSD.

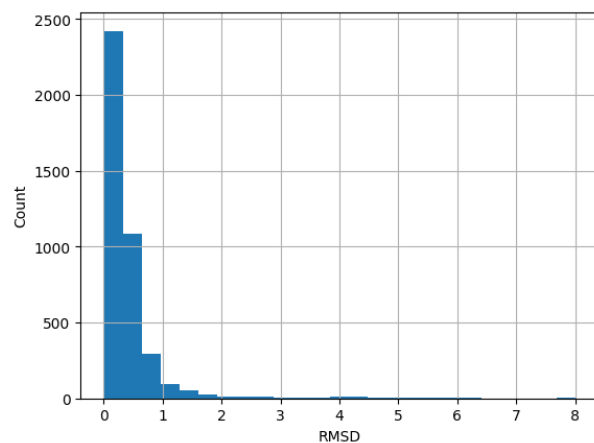


Figure 70: Histogram of RMSD of the different atoms of the multiple models.

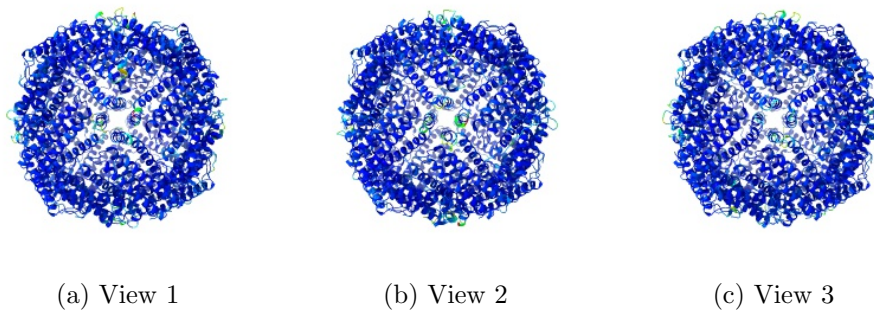


Figure 71: Atomic model colored by RMSD Views generated by ChimeraX at a the following X, Y, Z angles: View 1 (0,0,0), View 2 (90, 0, 0), View 3 (0, 90, 0).

Automatic criteria: The validation is OK if the average RMSD is smaller than 2Å.

STATUS: OK

13.4 Level A.d Map-Model Guinier analysis

Explanation:

We compared the Guinier plot [Rosenthal and Henderson, 2003] of the atomic model and the experimental map. We made the mean of both profiles to be equal (and equal to the mean of the atomic model) to make sure that they had comparable scales.

Results:

Fig. 72 shows the logarithm (in natural units) of the structure factor (the module squared of the Fourier transform) of the atom model and the experimental map. The correlation between the two profiles was 0.977.

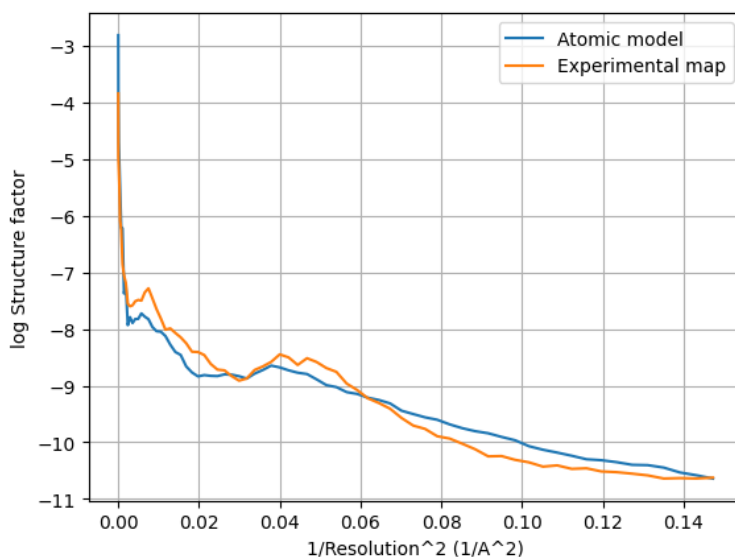


Figure 72: Guinier plot of the atom model and experimental map. The X-axis is the square of the inverse of the resolution in Å.

Automatic criteria: The validation is OK if the correlation between the two Guinier profiles is larger than 0.5.

STATUS: OK

13.5 Level A.e Phenix validation

Explanation:

Phenix provides a number of tools to assess the agreement between the experimental map and its atomic model [Afonine et al., 2018]. There are several cross-correlations to assess the quality of the fitting:

- CC (mask): Model map vs. experimental map correlation coefficient calculated considering map values inside a mask calculated around the macromolecule.
- CC (box): Model map vs. experimental map correlation coefficient calculated considering all grid points of the box.
- CC (volume) and CC (peaks) compare only map regions with the highest density values and regions below a certain contouring threshold level are ignored. CC (volume): The map region considered is defined by the N highest points inside the molecular mask. CC (peaks): In this case, calculations consider the union of regions defined by the N highest peaks in the model-calculated map and the N highest peaks in the experimental map.
- Local real-space correlation coefficients CC (main chain) and CC (side chain) involve the main skeleton chain and side chains, respectively.

There are also multiple ways of measuring the resolution:

- d99: Resolution cutoff beyond which Fourier map coefficients are negligibly small. Calculated from the full map.
- d_model: Resolution cutoff at which the model map is the most similar to the target (experimental) map. For d_model to be meaningful, the model is expected to fit the map as well as possible. d_model (B factors = 0) tries to avoid the blurring of the map.
- d_FSC_model; Resolution cutoff up to which the model and map Fourier coefficients are similar at FSC values of 0, 0.143, 0.5.

In addition to these resolution measurements the overall isotropic B factor is another indirect measure of the quality of the map.

Results:

To avoid ringing in Fourier space a smooth mask with a radius of 6.0 Å has been applied.

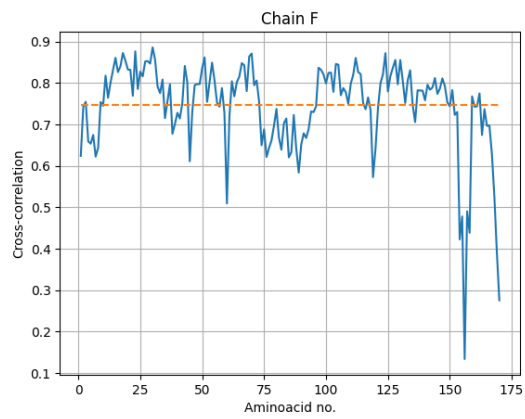
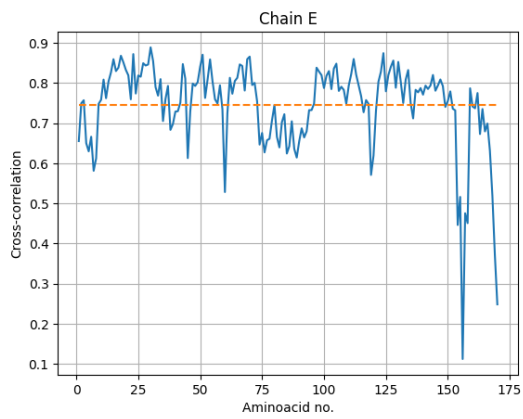
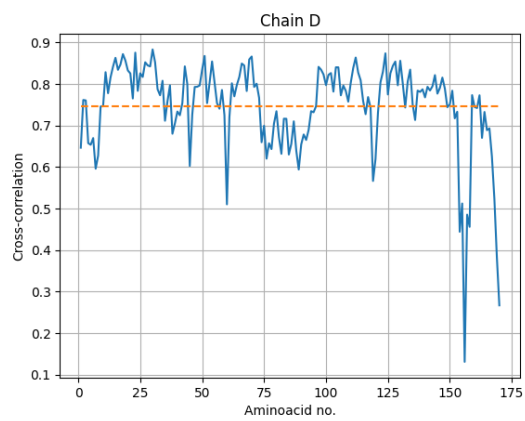
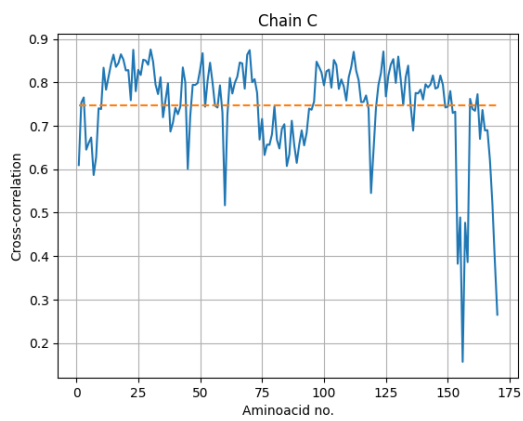
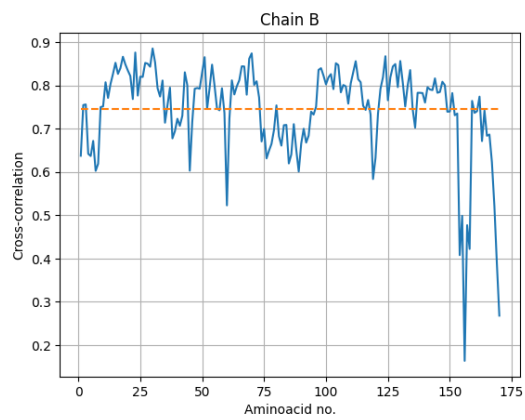
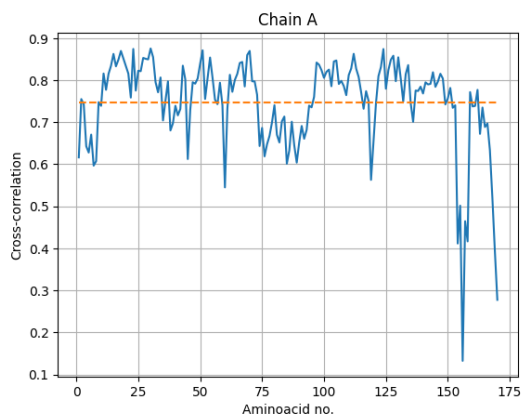
Overall correlation coefficients:

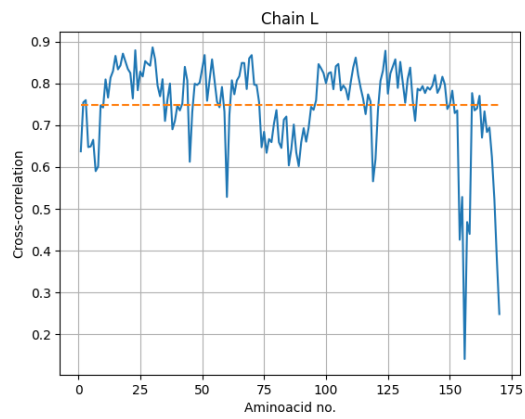
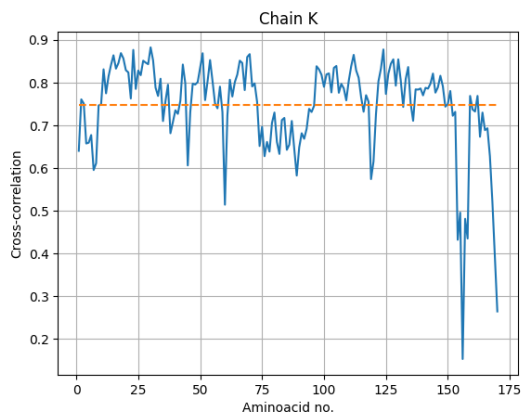
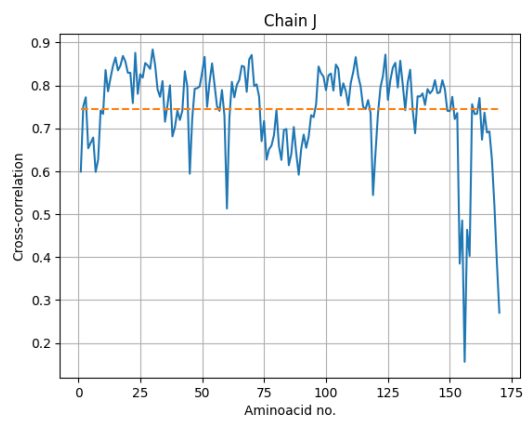
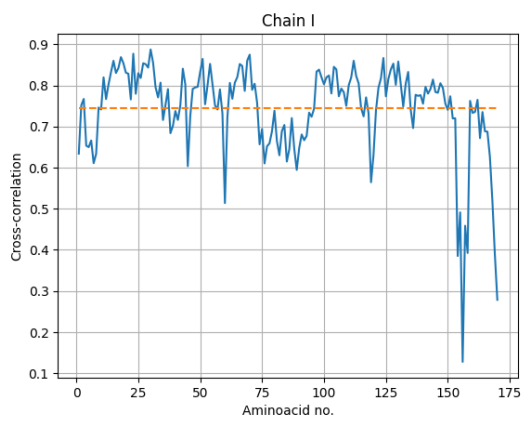
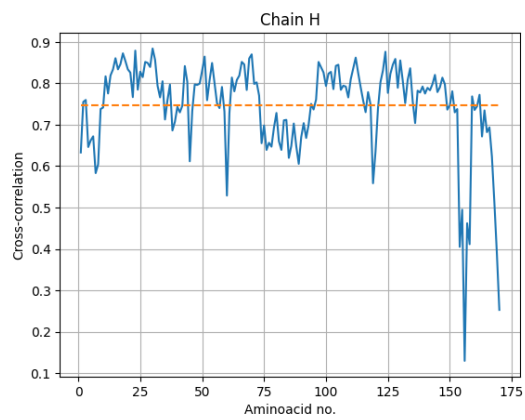
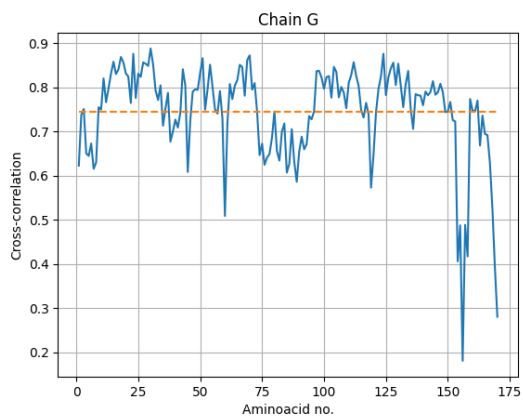
CC (mask) = 0.711
CC (box) = 0.665
CC (volume) = 0.714
CC (peaks) = 0.578
CC (main chain) = 0.684
CC (side chain) = 0.654

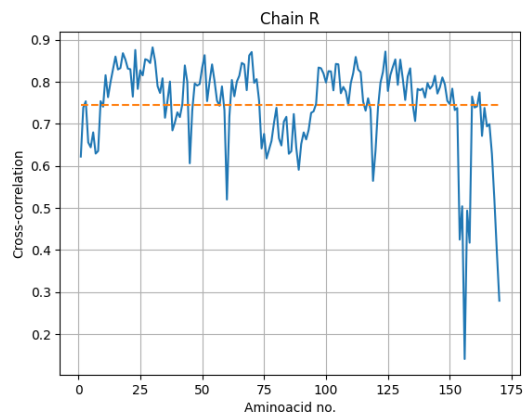
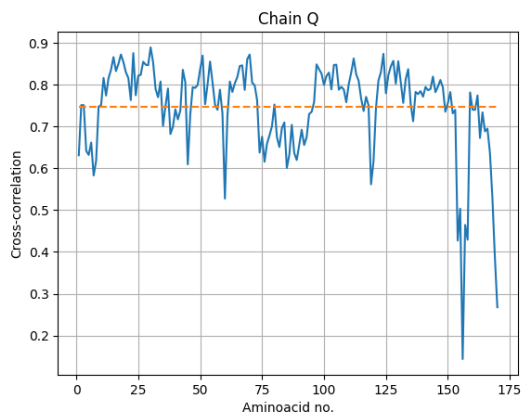
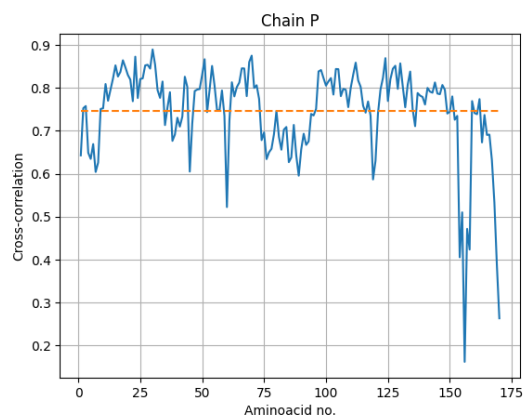
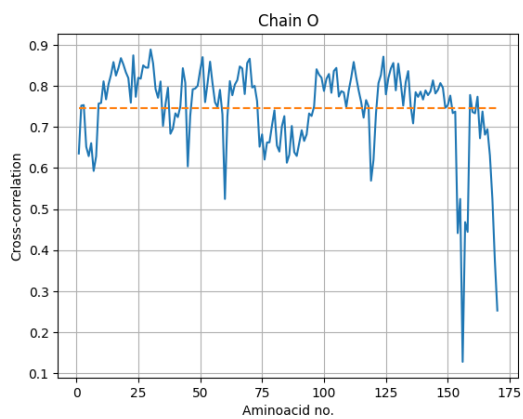
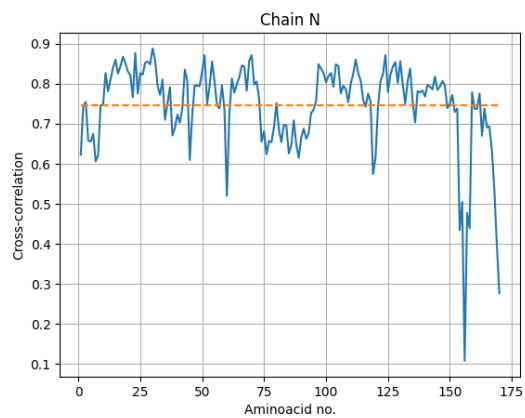
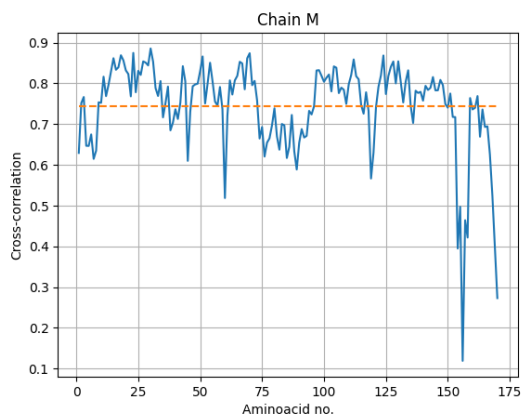
Correlation coefficients per chain:

Chain	Cross-correlation
A	0.685993
B	0.683896
C	0.687664
D	0.686794
E	0.683483
F	0.685114
G	0.685297
H	0.686324
I	0.684185
J	0.687296
K	0.686834
L	0.686390
M	0.684727
N	0.686484
O	0.683226
P	0.684781
Q	0.684891
R	0.683841
S	0.684050
T	0.687113
U	0.686038
V	0.686198
W	0.686749
X	0.684988

We now show the correlation profiles of the different chain per residue.







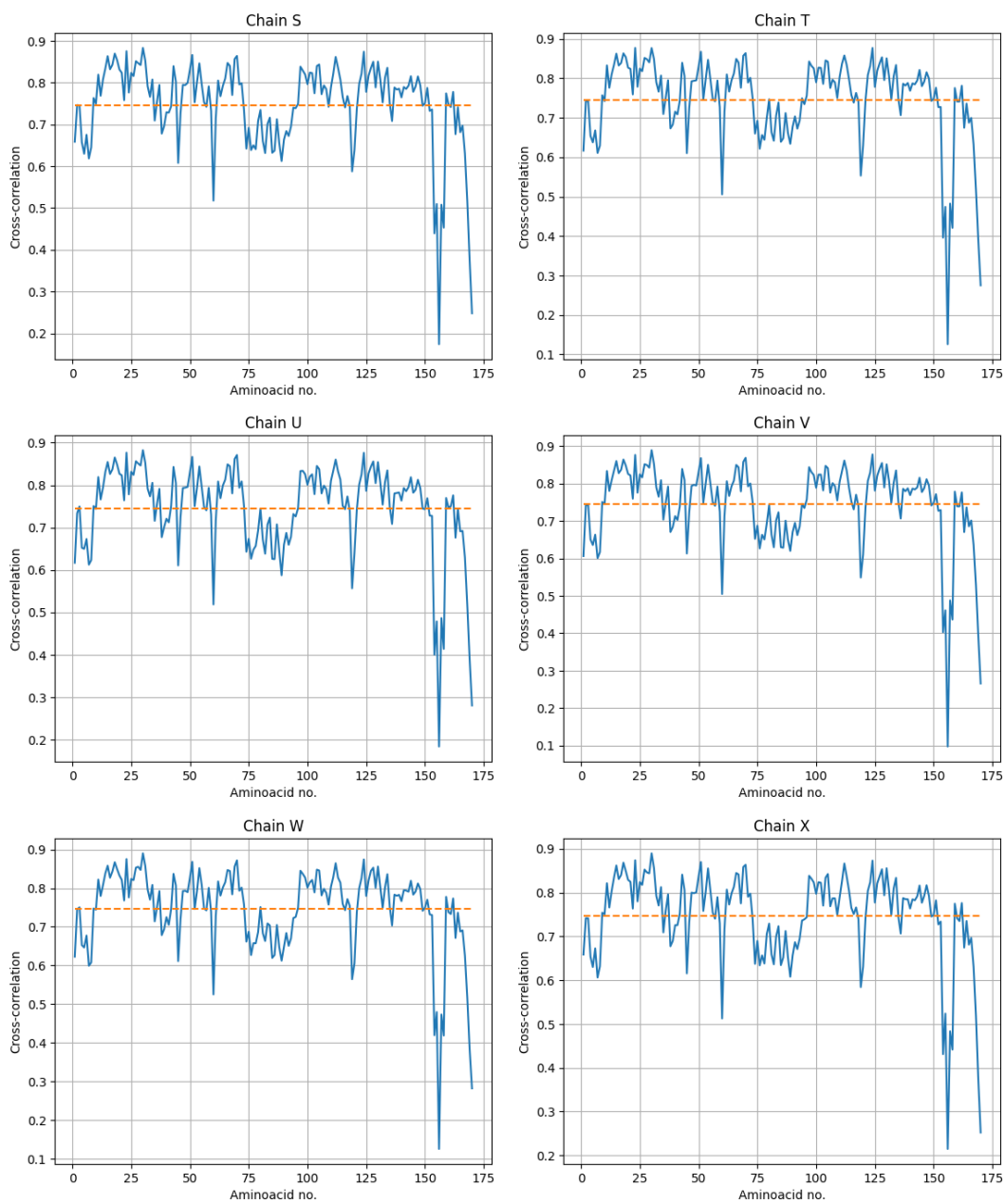


Fig. 73 shows the histogram of all cross-correlations evaluated at the residues. The percentage of residues whose correlation is below 0.5 is 3.8 %.

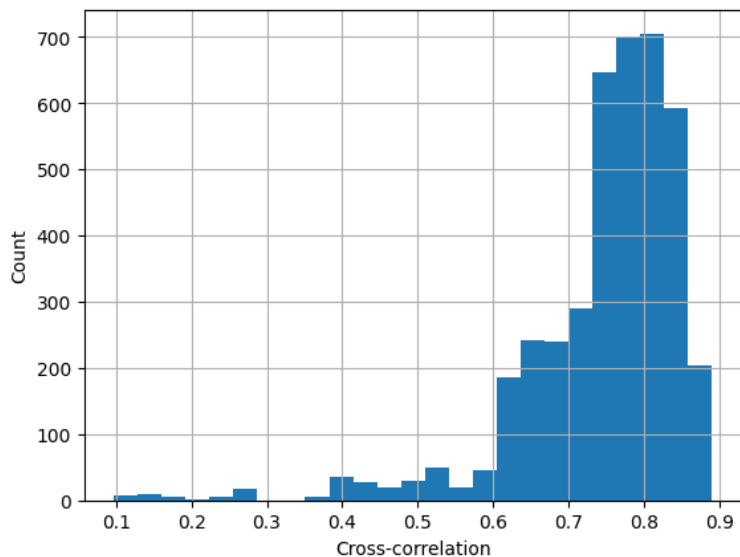


Figure 73: Histogram of the cross-correlation between the map and model evaluated for all residues.

Resolutions estimated from the model:

Resolution (\AA)	Masked	Unmasked
d99	1.7	1.6
d_model	3.8	3.8
d_model (B-factor=0)	4.3	4.3
FSC_model=0	3.0	2.9
FSC_model=0.143	3.4	3.4
FSC_model=0.5	4.4	4.5

Overall isotropic B factor:

B factor	Masked	Unmasked
Overall B-iso	85.0	85.0

Fig. 74 shows the FSC between the input map and the model.

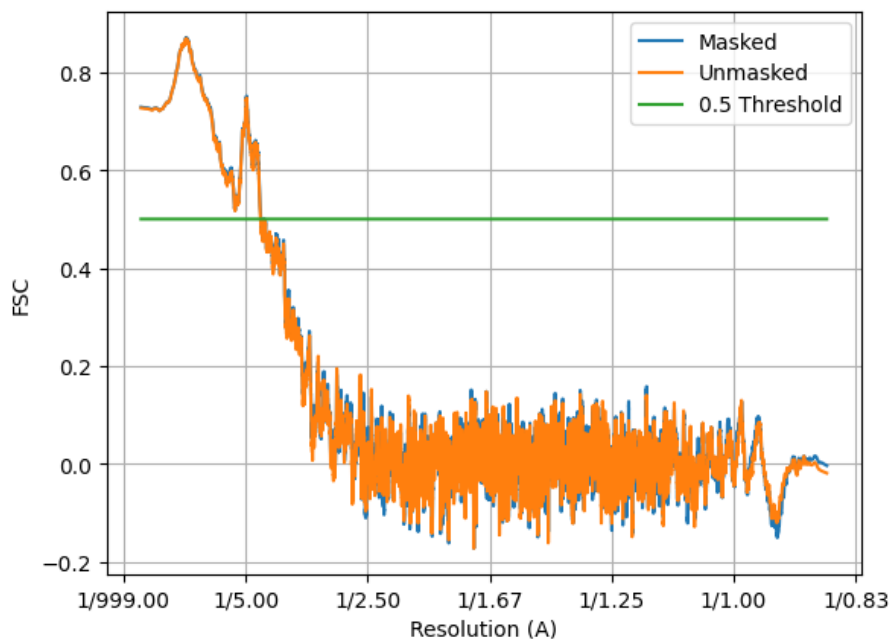


Figure 74: FSC between the input map and model with and without a mask constructed from the model. The X-axis is the square of the inverse of the resolution in Å.

Automatic criteria: The validation is OK if 1) the percentage of residues whose correlation is smaller than 0.5 is smaller than 10%, and 2) the resolution reported by the user is larger than 0.8 times the resolution estimated between the map and model at FSC=0.5.

WARNINGS: 1 warnings

1. **The resolution reported by the user, 2.6 Å, is significantly smaller than the resolution estimated between map and model (FSC=0.5), 4.4 Å**

13.6 Level A.f EMRinger validation

Explanation:

EMRinger [Barad et al., 2015] compares the side chains of the atomic model to the CryoEM map. The following features are reported:

- Optimal Threshold: Electron potential map cutoff value at which the maximum EMRinger score was obtained.
- Rotamer Ratio: Fraction of rotameric residues at the Optimal threshold value.
- Max Zscore: Z-score computed to determine the significance of the distribution at the Optimal threshold value.
- Model Length: Total of non-gamma-branched, non-proline aminoacids with a non-H gamma atom used in global EMRinger score computation.
- EMRinger Score: Maximum EMRinger score calculated at the Optimal Threshold.

A rotameric residue is one in which EMRinger peaks that fall within defined rotamers based on chi1, this often suggests a problem with the modelling of the backbone. In general, the user should look at the profiles and identify regions that may need improvement.

Results:

General results:

Optimal threshold	0.005050
Rotamer ratio	0.649
Max. Zscore	4.87
Model length	2976
EMRinger Score	0.892

Fig. 75 shows the EMRinger score and fraction of rotameric residues as a function of the map threshold. The optimal threshold was selected looking for the maximum EMRinger score in this plot.

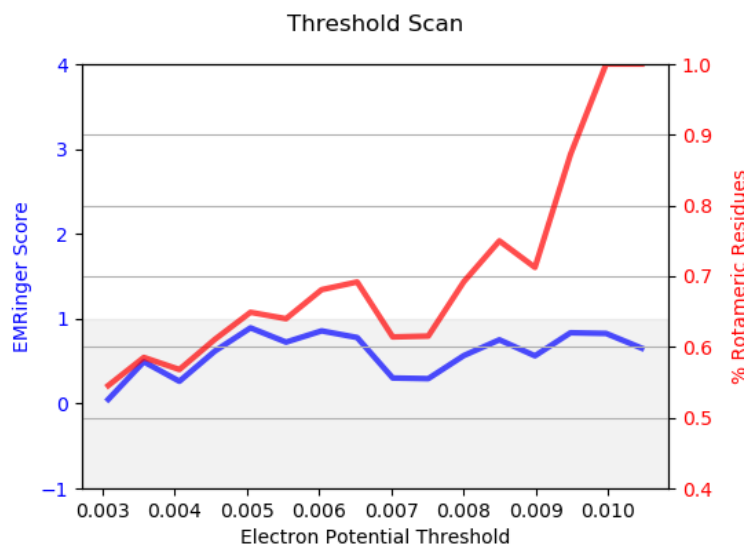


Figure 75: EMRinger score and fraction of rotameric residues as a function of the map threshold.

Fig. 76 shows the histogram for rotameric (blue) and non-rotameric (red) residues at the optimal threshold.

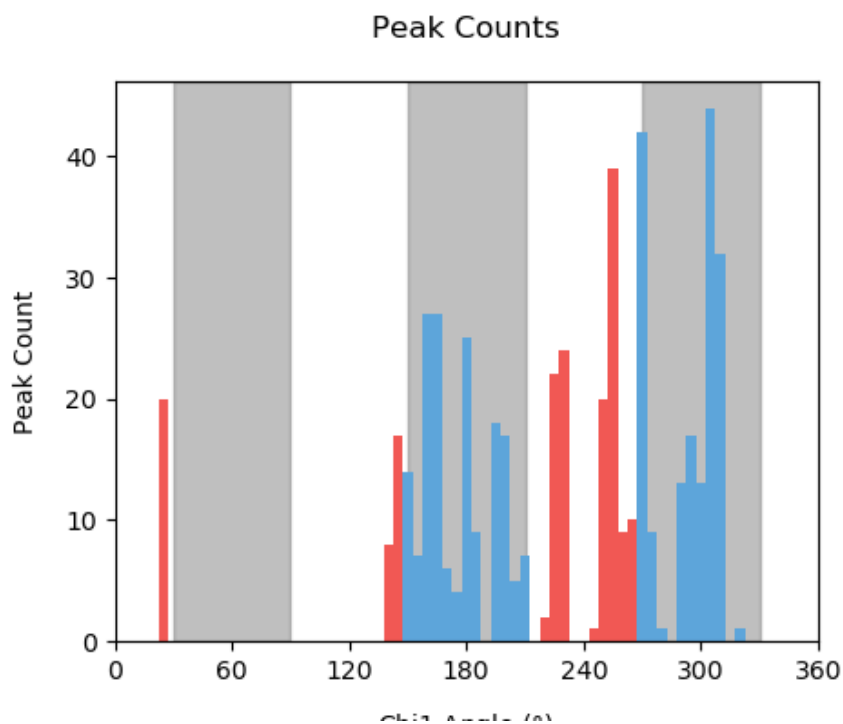
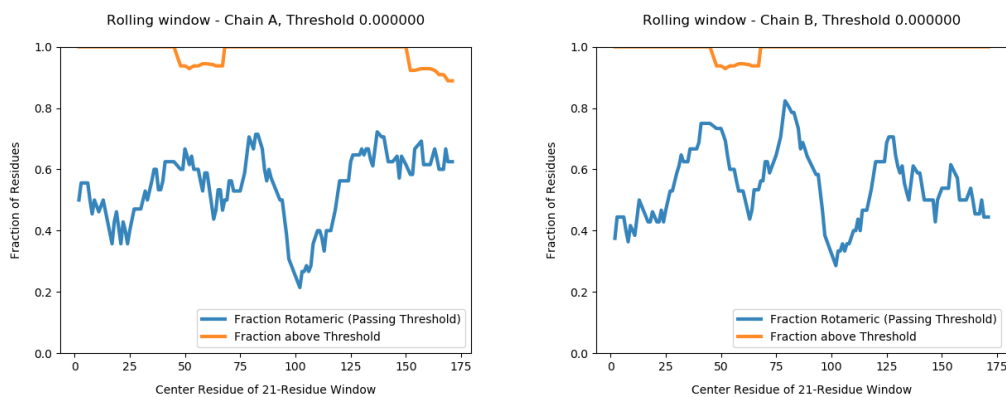
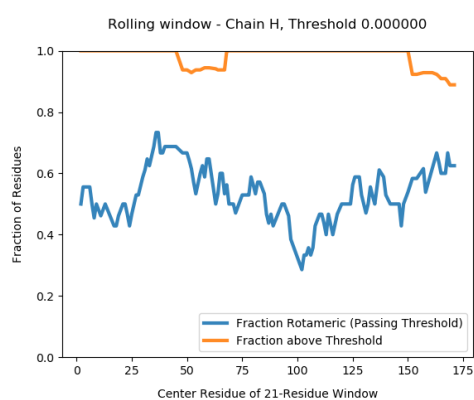
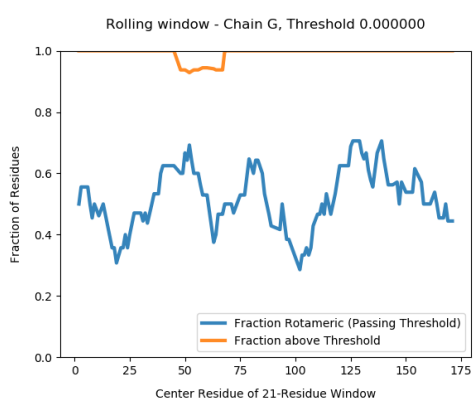
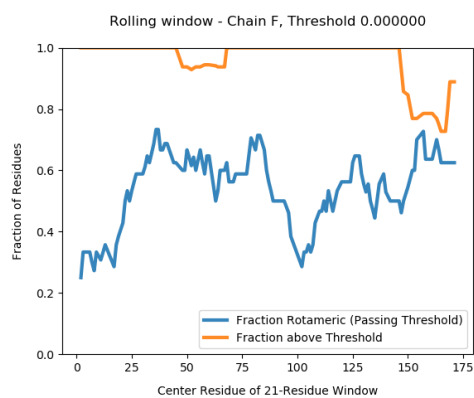
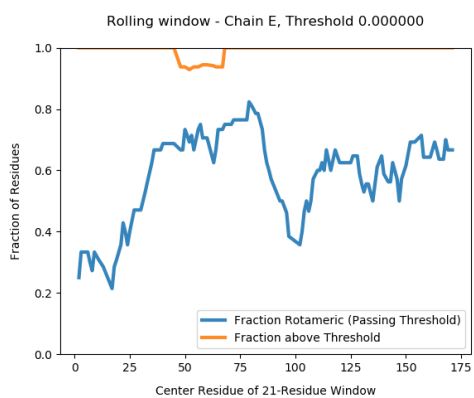
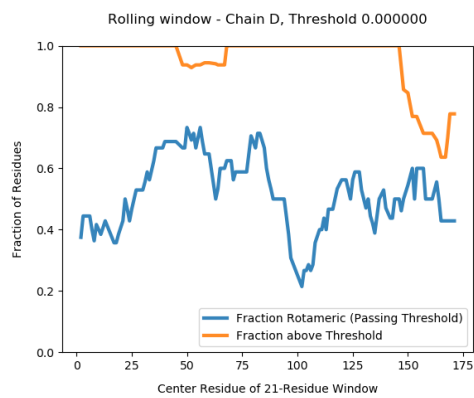
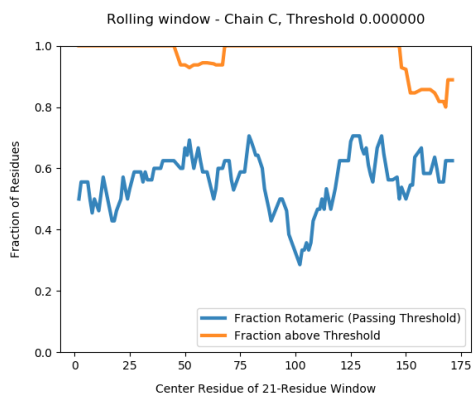
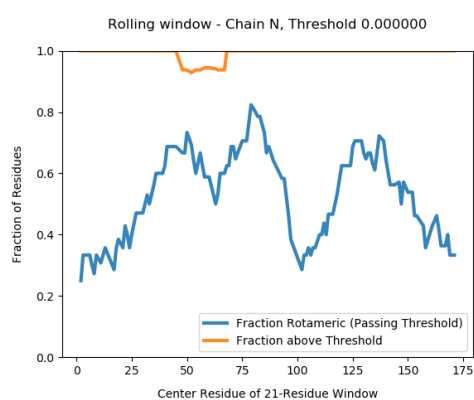
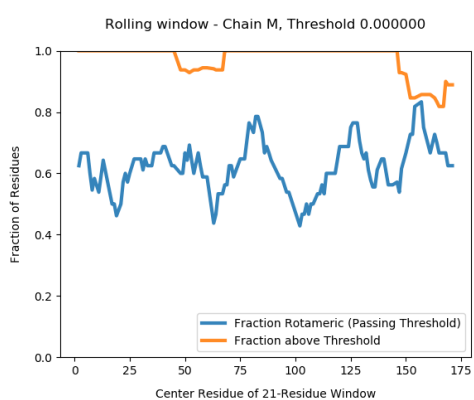
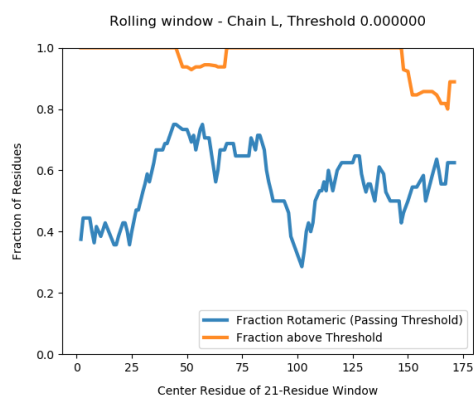
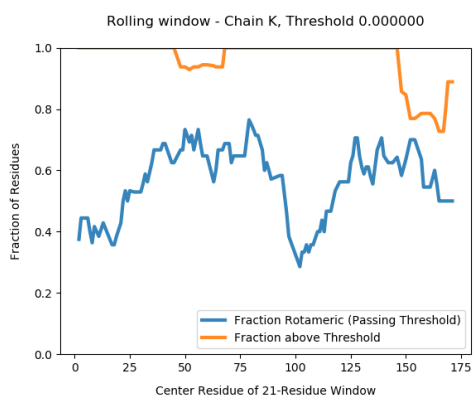
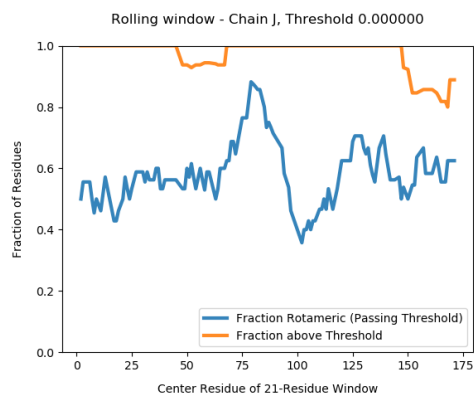
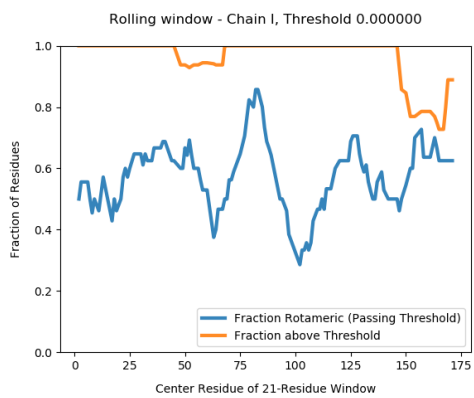


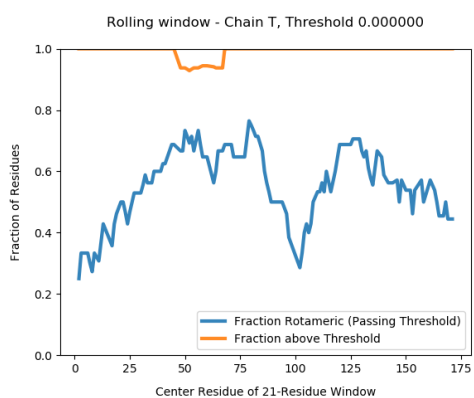
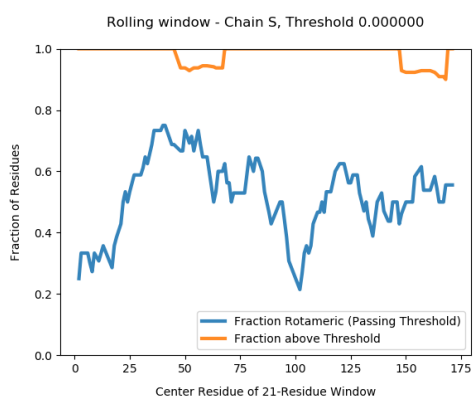
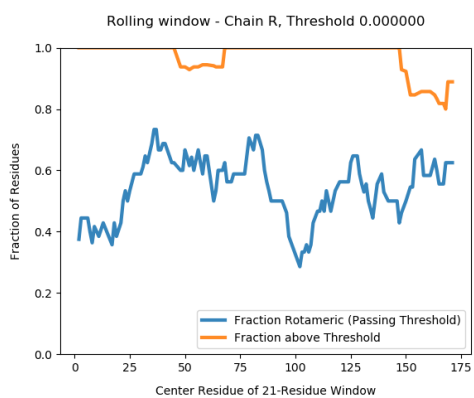
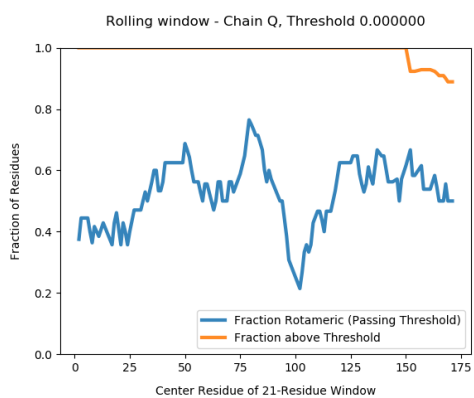
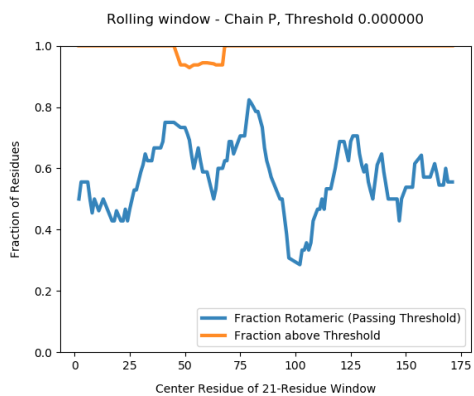
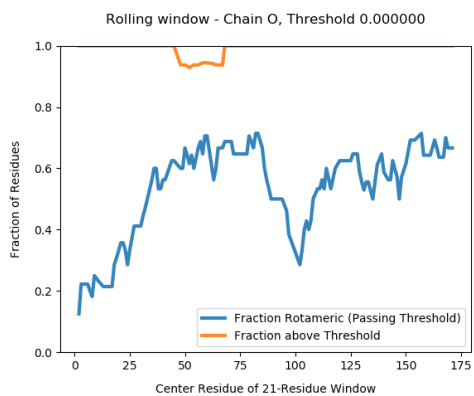
Figure 76: Histogram for rotameric (blue) and non-rotameric (red) residues at the optimal threshold as a function of the angle Chi1.

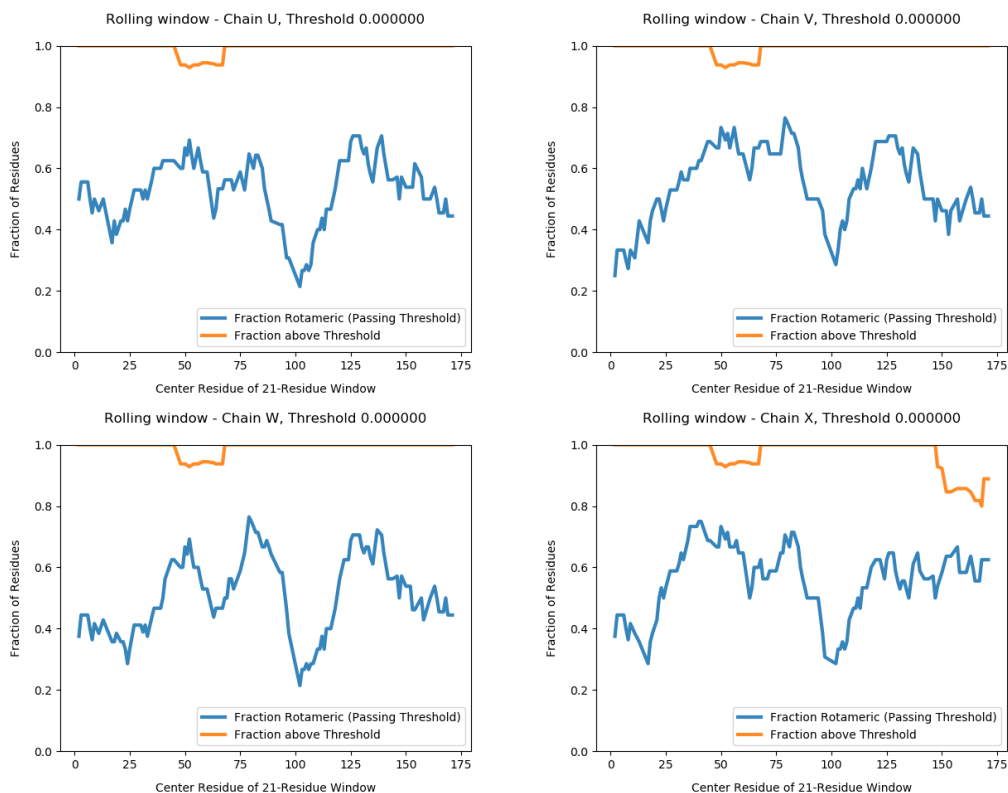
The following plots show the rolling window EMRinger analysis of the different chains to distinguish regions of improved model quality. This analysis was performed on rolling sliding 21-residue windows along the primary sequence of the protein chains.











Automatic criteria: The validation is OK if the EMRinger score and Max. Zscore are larger than 1.

WARNINGS: 1 warnings

1. **The EMRinger score is smaller than 1, it is 0.892.**

13.7 Level A.g DAQ validation

Explanation:

DAQ [Terashi et al., 2022] is a computational tool using deep learning that can estimate the residue-wise local quality for protein models from cryo-Electron Microscopy maps. The method calculates the likelihood that a given density feature corresponds to an aminoacid, atom, and secondary structure. These likelihoods are combined into a score that ranges from -1 (bad quality) to 1 (good quality).

Results:

Fig. 77 shows the histogram of the DAQ values. The mean and standard deviation were -0.0 and 0.3, respectively.

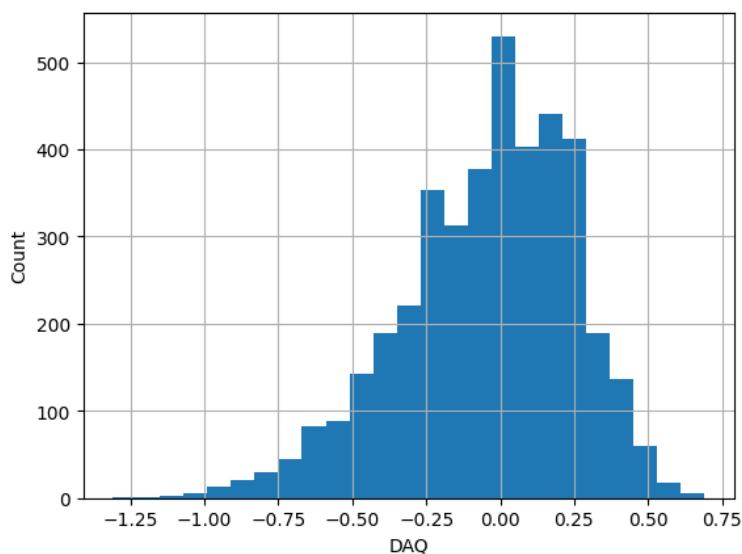


Figure 77: Histogram of the DAQ values.

The atomic model colored by DAQ can be seen in Fig. 78.

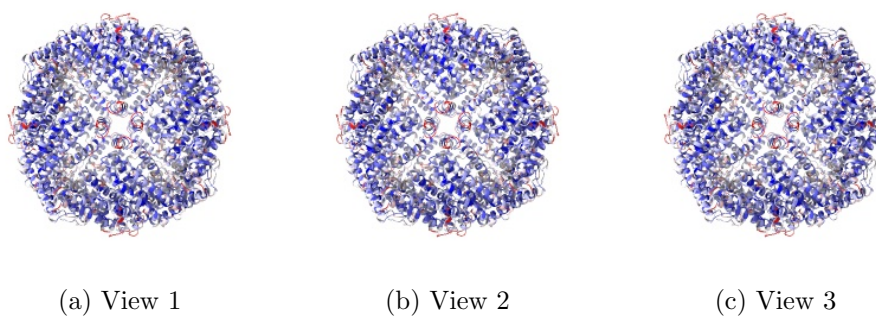


Figure 78: Atomic model colored by DAQ Views generated by ChimeraX at the following X, Y, Z angles: View 1 (0,0,0), View 2 (90, 0, 0), View 3 (0, 90, 0).

Automatic criteria: The validation is OK if the average DAQ score is larger than 0.5.

WARNINGS: 1 warnings

1. **The average DAQ is smaller than 0.5.**

14 Workflow

Workflow file: <http://nolan.cnb.csic.es/cryoemworkflowviewer/workflow/637ca2bbcd57e45e88f6fabb7f6b1095a3ca0de6>

SHA256 hash: 5d8c5ff8948f4ac986f5d43f819515e25668bfdcd954b8fb8c41d15cdf00fda2

Fig. 79 shows the image processing workflow followed in Scipion to achieve these results.

Explanation:

The method in [Jiménez et al., 2019] compares the expected energy profile from the reconstructed map to the one obtained by a SAXS experiment.

Results:

The radius of gyration was 51.0 Å. The χ^2 between the simulated curve and the experimental one was 27.6. Fig. 80 shows the two SAXS profiles for comparison.

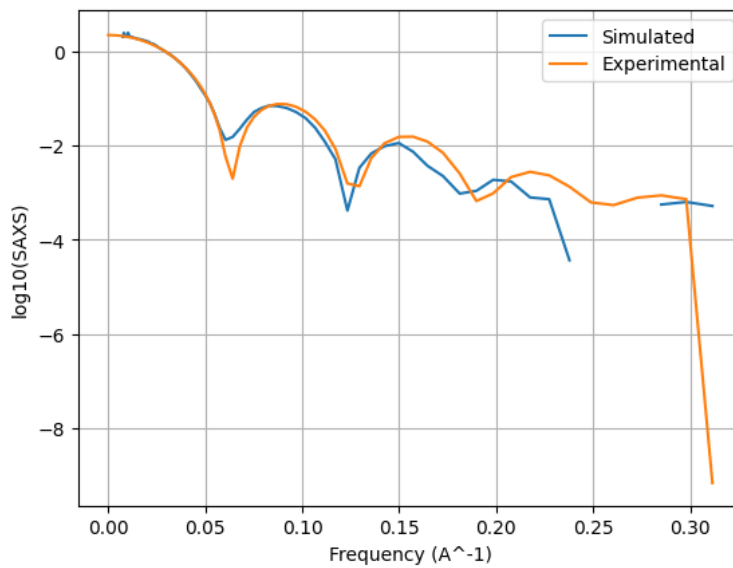


Figure 80: Simulated and experimental SAXS curves.

STATUS: Cannot be automatically evaluated

References

[Rosenthal and Henderson, 2003] Rosenthal, P. B. and Henderson, R. (2003). Optimal determination of particle orientation, absolute hand, and contrast loss in single particle electron-cryomicroscopy. *J. Molecular Biology*, 333:721–745.

- [Kaur et al., 2021] Kaur, S., Gomez-Blanco, J., Khalifa, A. A., Adinarayanan, S., Sanchez-Garcia, R., Wrapp, D., McLellan, J. S., Bui, K. H., and Vargas, J. (2021). Local computational methods to improve the interpretability and analysis of cryo-EM maps. *Nature Communications*, 12(1):1–12.
- [Ramírez-Aportela et al., 2019] Ramírez-Aportela, E., Mota, J., Conesa, P., Carazo, J. M., and Sorzano, C. O. S. (2019). DeepRes: a new deep-learning- and aspect-based local resolution method for electron-microscopy maps. *IUCRj*, 6:1054–1063.
- [Sorzano et al., 2017] Sorzano, C. O. S., Vargas, J., Oton, J., Abrishami, V., de la Rosa-Trevin, J. M., Gomez-Blanco, J., Vilas, J. L., Marabini, R., and Carazo, J. M. (2017). A review of resolution measures and related aspects in 3D electron microscopy. *Progress in biophysics and molecular biology*, 124:1–30.
- [Beckers and Sachse, 2020] Beckers, M. and Sachse, C. (2020). Permutation testing of fourier shell correlation for resolution estimation of cryo-em maps. *J. Structural Biology*, 212(1):107579.
- [Cardone et al., 2013] Cardone, G., Heymann, J. B., and Steven, A. C. (2013). One number does not fit all: Mapping local variations in resolution in cryo-em reconstructions. *J. Structural Biology*, 184:226–236.
- [Kucukelbir et al., 2014] Kucukelbir, A., Sigworth, F. J., and Tagare, H. D. (2014). Quantifying the local resolution of cryo-EM density maps. *Nature Methods*, 11:63–65.
- [Vilas et al., 2018] Vilas, J. L., Gómez-Blanco, J., Conesa, P., Melero, R., de la Rosa Trevín, J. M., Otón, J., Cuenca, J., Marabini, R., Carazo, J. M., Vargas, J., and Sorzano, C. O. S. (2018). MonoRes: automatic and unbiased estimation of local resolution for electron microscopy maps. *Structure*, 26:337–344.
- [Vilas et al., 2020] Vilas, J. L., Tagare, H. D., Vargas, J., Carazo, J. M., and Sorzano, C. O. S. (2020). Measuring local-directional resolution and local anisotropy in cryo-EM maps. *Nature communications*, 11:55.

- [Sorzano et al., 2014] Sorzano, C. O. S., Vargas, J., de la Rosa-Trevín, J. M., Zaldívar-Peraza, A., Otón, J., Abrishami, V., Foche, I., Marabini, R., Caffarena, G., and Carazo, J. M. (2014). Outlier detection for single particle analysis in electron microscopy. In *Proc. Intl. Work-Conference on Bioinformatics and Biomedical Engineering, IWBBIO*, page 950.
- [Punjani et al., 2017] Punjani, A., Brubaker, M. A., and Fleet, D. J. (2017). Building proteins in a day: Efficient 3D molecular structure estimation with electron cryomicroscopy. *IEEE Trans. Pattern Analysis & Machine Intelligence*, 39:706–718.
- [Sorzano et al., 2015] Sorzano, C. O. S., Vargas, J., de la Rosa-Trevín, J. M., Otón, J., Álvarez-Cabrera, A. L., Abrishami, V., Sesmero, E., Marabini, R., and Carazo, J. M. (2015). A statistical approach to the initial volume problem in single particle analysis by electron microscopy. *J. Structural Biology*, 189:213–219.
- [Méndez et al., 2021] Méndez, J., Garduño, E., Carazo, J. M., and Sorzano, C. O. S. (2021). Identification of incorrectly oriented particles in Cryo-EM single particle analysis. *J. Structural Biology*, 213:107771.
- [Vargas et al., 2017] Vargas, J., Melero, R., Gómez-Blanco, J., Carazo, J. M., and Sorzano, C. O. S. (2017). Quantitative analysis of 3D alignment quality: its impact on soft-validation, particle pruning and homogeneity analysis. *Scientific Reports*, 7:6307.
- [Vargas et al., 2016] Vargas, J., Otón, J., Marabini, R., Carazo, J. M., and Sorzano, C. O. S. (2016). Particle alignment reliability in single particle electron cryomicroscopy: a general approach. *Scientific Reports*, 6:21626.
- [Scheres, 2012] Scheres, S. H. W. (2012). A Bayesian view on cryo-EM structure determination. *J. Molecular Biology*, 415:406–418.
- [Punjani et al., 2020] Punjani, A., Zhang, H., and Fleet, D. J. (2020). Non-uniform refinement: adaptive regularization improves single-particle cryo-EM reconstruction. *Nature Methods*, 17(12):1214–1221.
- [Heymann, 2015] Heymann, B. (2015). Validation of 3DEM reconstructions: The phantom in the noise. *AIMS Biophysics*, 2:21–35.

- [Naydenova and Russo, 2017] Naydenova, K. and Russo, C. J. (2017). Measuring the effects of particle orientation to improve the efficiency of electron cryomicroscopy. *Nature communications*, 8:629.
- [Baldwin and Lyumkis, 2020] Baldwin, P. R. and Lyumkis, D. (2020). Non-uniformity of projection distributions attenuates resolution in Cryo-EM. *Progress in Biophysics and Molecular Biology*, 150:160–183.
- [Sanchez-Garcia et al., 2020] Sanchez-Garcia, R., Segura, J., Maluenda, D., Sorzano, C. O. S., and Carazo, J. M. (2020). MicrographCleaner: A python package for cryo-EM micrograph cleaning using deep learning. *J. Structural Biology*, 210:107498.
- [Pintilie et al., 2020] Pintilie, G., Zhang, K., Su, Z., Li, S., Schmid, M. F., and Chiu, W. (2020). Measurement of atom resolvability in cryo-em maps with q-scores. *Nature methods*, 17(3):328–334.
- [Ramírez-Aportela et al., 2021] Ramírez-Aportela, E., Maluenda, D., Fonseca, Y. C., Conesa, P., Marabini, R., Heymann, J. B., Carazo, J. M., and Sorzano, C. O. S. (2021). Fsc-q: A cryoem map-to-atomic model quality validation based on the local fourier shell correlation. *Nature Communications*, 12(1):1–7.
- [Herzik et al., 2019] Herzik, M. A., Fraser, J. S., and Lander, G. C. (2019). A multi-model approach to assessing local and global cryo-EM map quality. *Structure*, 27(2):344–358.e3.
- [Afonine et al., 2018] Afonine, P. V., Klaholz, B. P., Moriarty, N. W., Poon, B. K., Sobolev, O. V., Terwilliger, T. C., Adams, P. D., and Urzhumtsev, A. (2018). New tools for the analysis and validation of cryo-EM maps and atomic models. *Acta Crystallographica D, Struct. Biol.*, 74:814–840.
- [Barad et al., 2015] Barad, B. A., Echols, N., Wang, R. Y.-R., Cheng, Y., DiMaio, F., Adams, P. D., and Fraser, J. S. (2015). EMRinger: side chain-directed model and map validation for 3D cryo-electron microscopy. *Nature Methods*, 12(10):943–946.
- [Terashi et al., 2022] Terashi, G., Wang, X., Subramaniya, S.R.M.V., Tesmer, J.J.G. and Kihara, D. (2022). Residue-Wise Local Quality Estimation for Protein Models from Cryo-EM Maps. (submitted).

- [Jiménez et al., 2019] Jiménez, A., Jonic, S., Majtner, T., Oón, J., Vilas, J. L., Maluenda, D., Mota, J., Ramírez-Aportela, E., Martínez, M., Rancel, Y., Segura, J., Sánchez-García, R., Melero, R., Del Caño, L., Conesa, P., Skjaerven, L., Marabini, R., Carazo, J. M., and Sorzano, C. O. S. (2019). Validation of electron microscopy initial models via small angle X-ray scattering curves. *Bioinformatics*, 35:2427–2433.
- [Henderson et al., 2011] Henderson, R., Chen, S., Chen, J. Z., Grigorieff, N., Passmore, L. A., Ciccarelli, L., Rubinstein, J. L., Crowther, R. A., Stewart, P. L., and Rosenthal, P. B. (2011). Tilt-pair analysis of images from a range of different specimens in single-particle electron cryomicroscopy. *J. Molecular Biology*, 413(5):1028–1046.